OPTICAL MICROMANIPULATION OF AEROSOLS

Michael David Summers

A Thesis Submitted for the Degree of PhD
at the
University of St. Andrews

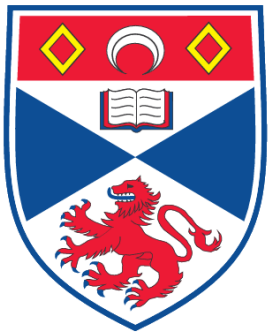

2009

OPTICAL MICROMANIPULATION OF AEROSOLS

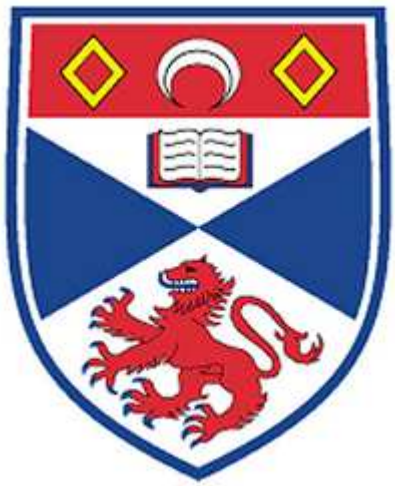

by

Michael David Summers

2009

A thesis submitted to the School of Physics and Astronomy, at the University of St Andrews, for the degree of Doctor of Philosophy

Optical Micromanipulation of Aerosols

Michael David Summers

Abstract

This thesis describes my work on the development of optical trapping techniques for manipulating airborne particles. Although many of the basic principles are similar to those used in more conventional colloidal experiments, there are many differences which have been described and investigated in detail in this work.

Basic characterisation measurements are made, such as axial Q and sample size selectivity, for a number of sample liquids in a basic optical tweezers setup. Performance at 532nm and 1064nm were compared and shown to be very similar, despite increased absorption in the infrared. A successful method was developed for the optical trapping of solid aerosol particles, allowing a direct comparison between similar particles suspended in both the gas and liquid phase.

A single beam levitation trap was developed for transporting liquid aerosols to allow multiple chemical measurements to be made on a single droplet. Performance between Gaussian and Bessel beams was compared for various liquids, with guiding distances of several millimetres being achieved with the Bessel beam geometry.

An experiment to demonstrate lasing within an optically tweezed droplet was also performed and spectra were taken. Although strong resonance modes were evident, the data was not conclusive. However, it is likely that a redesign of the experiment would be successful.

These techniques have extended research capabilities in the areas of both optical trapping and atmospheric chemistry, allowing the detailed study of single aerosol particles in the 1-10 μm range.

Contents

Declarations

I, Michael David Summers hereby certify that this thesis, which is approximately 40000 words in length, has been written by me, that it is the record of work carried out by me and that it has not been submitted in any previous application for a higher degree.

I was admitted as a research student in October 2004 and as a candidate for the degree of PhD in October 2005; the higher study for which this is a record was carried out in the University of St Andrews between 2004 and 2008.

Date ……. Signature of candidate ……..……...

I hereby certify that the candidate has fulfilled the conditions of the Resolution and Regulations appropriate for the degree of PhD in the University of St Andrews and that the candidate is qualified to submit this thesis in application for that degree.

Date …..…… Signature of supervisor ……...……

In submitting this thesis to the University of St Andrews we understand that we are giving permission for it to be made available for use in accordance with the regulations of the University Library for the time being in force, subject to any copyright vested in the work not being affected thereby. We also understand that the title and the abstract will be published, and that a copy of the work may be made and supplied to any bona fide library or research worker, that my thesis will be electronically accessible for personal or research use unless exempt by award of an embargo as requested below, and that the library has the right to migrate my thesis into new electronic forms as required to ensure continued access to the thesis. We have obtained any third-party copyright permissions that may be required in order to allow such access and migration, or have requested the appropriate embargo below.

The following is an agreed request by candidate and supervisor regarding the electronic publication of this thesis: Access to Printed copy and electronic publication of thesis through the University of St Andrews.

Date ……..… Signature of candidate ……..…

Signature of supervisor ……...…….……

Acknowledgements

Firstly, I would like to thank David McGloin for the opportunity to work with him over the last few years. His input, advice and patience over the course of my PhD work have been invaluable and will be sorely missed. I would also like to thank my lab mates Dan Burnham, Dan Rudd and Carlos López-Mariscal for sharing a great many fun and productive days in the lab. Keep pushing back the boundaries of aerosol trapping dudes! My thanks also go to Kishan Dholakia and the Dream Team for getting me interested in optical trapping in the first place and for their friendship, advice and endless banter stretching all the way back to my senior honours project in 2003. I was also glad for the opportunity to work with Jonathan Reid's group at the University of Bristol and to get to know another friendly and gifted group of people.

On a personal note, I dedicate this thesis to my friends and family; to Mum, Dad and Nicola for their love and support; Dave, Chris and Dimi for being my family away from home; and especially to my wife, Maggie, who has put up with me, my late nights and my stressing for the last few years. Thank you.

List of Constants and Variables

a	Radius	q	Mode number
A	Absorbance	Q_{cavity}	Cavity Q-factor
A(z)	Cross-sectional area	Q_{axial}	Axial trapping efficiency
B	Mass transfer number	r	Angle of reflection
c	Speed of light	R_s	Reflectivity (s-polarised light)
c_p	Specific heat	R_p	Reflectivity (p-polarised light)
d	Diameter	R	Reflectivity
E	Electric field	S	Mode separation
F	Force	T	Temperature
F_{scat}	Scattering force	T	Transmission (1-R)
F_{grad}	Gradient force	v	Velocity
F_d	Linear drag	V_x	Volume of object x
f_b	Cavity build-up factor	w	Gaussian beam radius
g	Acceleration due to gravity	x	Size factor of a spherical cavity
i	Angle of incident ray	z_R	Rayleigh range
I	Intensity	z	Distance along beam propagation
k_z	Longitudinal wavevector	α	Polarizability
k_r	Radial wavevector	β	Detector sensitivity
k_b	Boltzmann’s constant	γ	Axicon opening angle
l	Path length	γ_0	Stoke’s constant
m	Mass	ς	Stochastic force
M_{air}	Mass fraction of atmosphere	η	Viscosity
M_s	Mass fraction of sample	θ_i	Angle of incidence
n_x	Refractive index of material x	θ_t	Angle of transmission
NA	Numerical aperture	θ_a	Acceptance angle
p	Refractive index ratio	κ	Trap stiffness
P	Power		
P_{atm}	Atmospheric pressure		
P_s	Surface partial pressure		

λ Wavelength

λ_L Thermal conductivity

μ_a Absorption coefficient

μ_0 Permeability of free space

ζ_s Surface vapour concentration

ζ_∞ Environmental vapour concentration

ρ_x Density of material x

σ Scattering cross-section

τ Angle of refracted ray

ω Angular frequency

ω_c Corner frequency

Chapter 1

Introduction

1.1 Background and Motivation

Lasers are undoubtedly one of the most widespread technological developments of the twentieth century. Since the first demonstration of an "optical maser" in 1960 by Maiman [1, 2], the evolution of laser physics was impressively rapid. Less than 50 years later, lasers are present in a staggering range of everyday appliances. Of the many practical applications of lasers developed since these pioneering experiments, the ability to physically manipulate matter at a microscopic level is particularly exciting.

From initial experiments in pushing microscopic particles about using radiation pressure from a laser [3], the field of optical trapping developed. The realisation that a 3-dimensional gradient force could be generated by tightly focussing the beam [4] led to the first optical "tweezers", capable of capturing and manipulating individual particles in 3 dimensions. An interesting means to probe the properties of small particles and moving them about had now become a truly useful tool. Over the following 20 years, this non-invasive method for capturing and manipulating microscopic particles has been refined and a fascinating range of applications have been found. Of course, with continuing research into the applications and miniaturisation of optical trapping experiments, the optical lab-on-a-chip may one day become as ubiquitous as the common household CD player.

Although optical trapping has matured, there are still many interesting unexplored areas in the field. There has been little development in the trapping of airborne particles since some initial experiments conducted by Ashkin [3, 5]. Although the study of aerosols is a major focus of atmospheric chemistry, typical experiments use techniques which analyse the bulk properties of

atmospheric species, such as LIDAR [6] or photochemistry [7]. The effects governing the initial formation, or aggregation of atmospheric particles are less well known. Optical trapping techniques allow us to observe droplet growth or evaporation [8], particle-particle interactions [9], core-shell particles [10] and to perform spectroscopic analysis on individual droplets [11]. Although the field of atmospheric chemistry includes vitally important areas of study such as cloud formation, pollution monitoring and climate change, it is not the only subject to benefit from aerosol research. Fields as diverse as respiratory medicine and the automotive industry depend on accurate data of aerosol characteristics for their own studies and designs of nebulisers and combustion engines. This thesis will describe my recent work in the optical manipulation of such aerosols in detail.

1.2 Thesis Structure

The body of this thesis will begin with a chapter detailing the state of the art and the physical theory behind optical trapping. This will include an overview of the development of the field, a description of a typical optical tweezers system, much of the theoretical groundwork in the characterisation of optical traps, as well as an overview of more recent developments in technique and application.

Chapter 3 will build on the previous chapter by discussing the features particular to the trapping of aerosols. Previous work will be examined as well as the application of optical droplet studies, particularly in spectroscopy. Many of the experimental techniques developed during the course of my work to deal with aerosols are covered in this chapter, particularly with respect to sample generation, conditioning and dealing with evaporation effects.

In Chapter 4, many of the basic measurements and initial experiments will be described. These were designed to provide experience in the optical trapping of aerosols and to characterise some of the tweezing characteristics of droplets. The diameter of captured droplets, the effect of using different liquids and

practical measurements of evaporation are explored. A linear relationship between the diameter of tweezed droplets and the optical power in the trap is found for various liquid samples with an observed increase in gradient with refractive index. 1064 nm sources are shown to be as effective at typical tweezing powers as more expensive 532 nm lasers for aerosol tweezing, despite increased absorption by most liquids in the infrared, with Q_{axial} values as high as 0.42 obtained with dodecane droplets.

This work will be extended into Chapter 5 which will describe a method for generating and tweezing solid aerosol particles. The ability to tweeze silica spheres in air allows the direct comparison of the damping forces between trapping identical samples in different media. This is achieved using the power spectra of silica spheres trapped in air and water by the same tweezers. Trap stiffness was found to be approximately three times greater for aerosols compared with identical colloidal spheres.

Chapter 6 will move away from optical tweezers and examine my work on the optical guiding of aerosols. The principle was tested using a loosely focussed Gaussian beam to replicate the early experiments conducted by Ashkin on single beam levitation of particles. These results could then be compared to an improved design incorporating an axicon to generate a Bessel beam and allowing droplet samples to be guided over distances spanning millimetres. There is an improvement of more than five times when compared to the best achieved with a Gaussian beam.

The application of the work detailed in Chapter 6 will form the basis of Chapter 7, which aims to demonstrate the direct application of optical manipulation in atmospheric chemistry. This ‘lab-in-a-box’ experiment combines optical guiding techniques coupled with two different droplet sizing techniques. Comparing the droplet diameters obtained from scattering and from spectroscopy using the same sample is a useful result, as well as an interesting demonstration of a lab-in-a-box using a Bessel beam as an optical conveyor belt. As a further demonstration of applications of physics in the realm of chemistry, Chapter 7 also describes my work in creating a “laser in a raindrop”. Although droplets have been made to lase in the work of others,

notably Chang [12], using optical tweezers to hold the droplet was a way to gain experience with spectroscopy and making practical measurements on captured droplets.

The body of the thesis will conclude with the final chapter, which summarises my work and findings, as well as highlighting possible future avenues of research in the optical trapping of airborne particles.

1.3 References

1. Maiman, T.H., “Stimulated Optical Radiation in Ruby,” Nature **4736**, 493. (1960)

2. Schalow, A.L. and Townes, C.H., “Infrared and optical masers,” C.H., Phys. Rev. **112**, 1940 (1958)

3. Ashkin, A., “Acceleration and Trapping of Particles by Radiation Pressure,” Phys. Rev. Lett. **24**, 156 (1970)

4. Ashkin, A. and Dziedzic, J.M., "Feedback stabilization of optically levitated particles," Appl. Phys. Lett. **30**, 202 (1977)

5. Ashkin, A.; Dziedzic, J.M.; Bjorkholm, J.E. and Chu, S., "Observation of a Single-Beam Gradient Force Optical Trap for Dielectric Particles." Opt. Lett. **11,** 288 (1986)

6. Ansmann, A.; Riebesell, M. and Weitkamp, C., "Measurement of atmospheric aerosol extinction profiles with a Raman lidar," Opt. Lett. **15**, 746. (1990)

7. O'Dowd, C.D.; Smith, M.H.; Consterdine, I.E. and Lowe, J.A., “Marine aerosol, sea-salt, and the marine sulphur cycle: a short review,” Atmospheric Environment **31**, 73 (1996)

8. Magome, N. *et al*, “Optical Trapping of a Growing Water Droplet in Air”. J. Phys. Chem. B **107**, 3988 (2003)

9. Burnham, D.R. and McGloin, D., "Holographic optical trapping of aerosol droplets," Opt. Express **14**, 4176 (2006)

10. Signorell, R. and Jetzki, M., “Vibrational exciton coupling in pure and composite sulfur dioxide aerosols,” Faraday Discuss. **137**, 51 (2008)

11. Sayer, R.M.; Gatherer, R.D.B. and Reid, J.P., “A laser induced fluorescence technique for determining the pH of water droplets and probing uptake dynamics,” Phys. Chem. Chem. Phys. **5**, 3740 (2003)

12. Tzeng, M.; Wall, K.F.; Long, M.B. and Chang, R.K., “Laser emission from individual droplets at wavelengths corresponding to morphology-dependent resonances,” Opt. Lett. **9**, 499 (1984)

Chapter 2

Optical Trapping

2.1 Introduction to Optical Trapping

Arthur Ashkin and colleagues pioneered the field of optical trapping, starting in 1970 at Bell Labs and continuing until his retirement from research there in the early 1990s [1]. The early work of this "father of optical trapping" will hopefully put my own work in the field into the proper context. This remainder of the chapter will focus on the physics, experimental design and engineering issues involved in the construction of optical traps. This will include a description of how to build a basic optical tweezers system. Many of the elements described are common to all the systems used in my work, so I felt that a detailed description at this point would avoid later repetition and tedium.

2.2 Development of Optical Trapping

2.2.1 The birth of optical trapping

The first optical trap was built by Ashkin [2] and successfully trapped latex spheres of the order of 1μm diameter suspended in water. Using an argon laser beam focussed into a cell containing a colloidal solution of latex spheres, he showed particles being drawn into the centre of the beam and accelerated in the propagation direction until stopped by the cell wall. He reasoned that a force was exerted due to the refraction of rays at the sphere-liquid interface. The

resulting change in the radial component of the rays resulted in a net change in force acting towards the region of highest intensity.

He likened his spheres to converging lenses using this geometric optics approach and predicted air bubbles would act as diverging lenses due to the negative refractive index contrast between the bubbles and the medium. Indeed, bubbles were shown to always be pushed out of the laser beam.

Ashkin then proceeded to generate a stable "optical potential well" using two counter-propagating Gaussian beams focussed into a glass cell to hold spheres at an equilibrium point. He went on to discuss tuning lasers to atomic transitions in order to provide relatively large driving forces in atoms. These forces were experimentally proven by him and published later that year [3]. This work formed the basis of the field of atom trapping, for which his colleague, Steven Chu, won the Nobel Prize in 1997.

He also mentioned thermal effects in his paper and ensured they were as limited as possible. By choosing particles and a medium that was highly transparent at the laser wavelength, thermal gradients caused by the radiation (photophoresis) were small enough so as not to obscure the optical effects he was attempting to observe. He found that even at relatively high intensities, thermal effects were negligible. More detailed calculations of photophoresis in optical traps were published later [4], showing that heating of a typical silica or polymer sphere by a trapping laser only becomes an issue at low pressures approaching 25 mbar and demonstrated trapping in a high vacuum environment.

The trap was also tested on 5 µm diameter water droplets in air, which was the first mention of the optical trapping of aerosols. For clarity, studies conducted by Ashkin specifically on aerosols (of which there were disappointingly few) will be described in detail in Chapter 3.

2.2.2 Development of Optical Trapping (1970-1986)

In this early trapping work, a ray optics approach was used to describe the forces acting on a trapped droplet. The radiation pressure is what pushes the

latex spheres in the direction of beam propagation and is a consequence of reflection at the particle/medium interface. The magnitude of this scattering force acting on the particle of propagation can be calculated using the Fresnel equations i.e. it is governed by the difference in refractive index between the particle and the medium. When a photon is absorbed or reflected at a surface, the momentum is transferred to that particle [5]. For light entering the interface between two media at an angle, the more general Fresnel equations,

$$R_s = \left[\frac{n_1 \cos(\theta_i) - n_2 \cos(\theta_t)}{n_1 \cos(\theta_i) + n_2 \cos(\theta_t)} \right]^2 \qquad [2.1]$$

and

$$R_p = \left[\frac{n_1 \cos(\theta_t) - n_2 \cos(\theta_i)}{n_1 \cos(\theta_t) + n_2 \cos(\theta_i)} \right]^2 \qquad [2.2]$$

must be used [6], which take account of polarisation as well as angle. Circularly or unpolarised light is treated simply as an equal mix of s and p-polarised light.

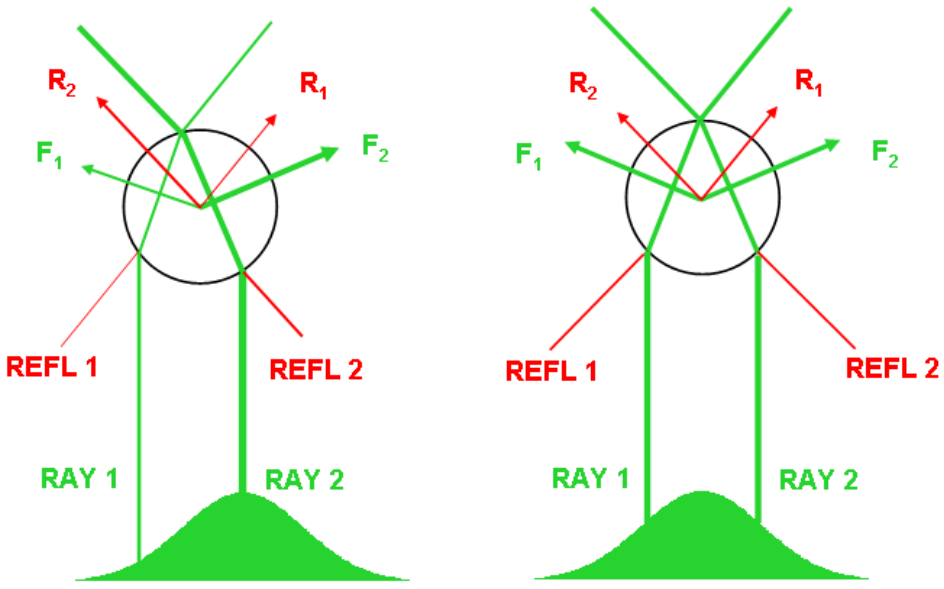

Figure 2.1: Ray optics diagram for a spherical particle in a Gaussian beam. The particle on the left is off-centre (F_2>F_1), and so experiences a force acting towards the region of highest intensity. On the right hand side, the particle is centred and so the forces are balanced.

The other force acting on the spheres in Ashkin's early trapping experiments is the gradient force (see figure 2.1). For a dielectric particle with a higher refractive index than the surrounding medium, any light is refracted at the interface according to Snell's Law. Light carries momentum in the direction of propagation, proportional to its energy. The change in the direction of light at the particle interface results in a change of the momentum of the light. In an interesting example of the conservation of momentum, the particle will move in such a way as to oppose any net momentum change. If the beam is more intense on one side of the particle than the other, the net change in momentum causes the particle to move towards the region of highest intensity in the beam. Likewise, for a particle with a refractive index lower than the medium, the particle is repelled from regions of high intensity.

The forces in the ray optics regime can be calculated using a ray-tracing approach [7, 8]. The force contribution of each ray is then summed over the range of angles light is incident on the particle. The force due to a single ray is

$$F_{ray} = \frac{n_1 P}{c}, \qquad [2.3]$$

where n_1 is the refractive index of the medium, P is the incident power and c is the speed of light. For a TEM_{00} Gaussian mode, the scattering force (along the z-axis) summed across the entire sphere is given by

$$F_{scat} = \frac{n_1 P}{c}\left(1 + R\cos(2\theta) - \frac{T^2\left[\cos(2\theta - 2r) + R\cos(2\theta)\right]}{1 + R^2 + 2R\cos 2r}\right), \qquad [2.4]$$

where R and T are the Fresnel coefficients of reflection and transmission and θ and r are the angles of incidence and refraction. The formula sums over all scattered rays and is therefore exact. Similarly, the transverse gradient force is given by

$$F_{grad} = \frac{n_1 P}{c}\left(R\sin(2\theta) - \frac{T^2\left[\sin(2\theta - 2r) + R\sin(2\theta)\right]}{1 + R^2 + 2R\cos 2r}\right). \qquad [2.5]$$

A number of additional particle manipulation experiments were conducted by Ashkin in subsequent years. In 1974, he experimented with Laguerre-Gaussian beam profiles (TEM_{01}) and demonstrated stable optical levitation of hollow glass spheres measuring tens of μm diameter [9] which were repelled from

regions of high intensity and were therefore trapped in the region of zero intensity in the centre of the Laguerre-Gauss mode generated by the trapping laser.

Although much of the work conducted by Ashkin was focussed on the engineering of an optical toolkit to manipulate a range of different particles, he had some specific applications in mind [10]. In addition to the trapping of atoms using accurate frequency tuning, Ashkin was particularly interested in the nature of light scattering and using optically trapped spheres to measure forces. Force measurements were conducted using feedback stabilization [11] using a 2-element photodiode to detect vertical movement in the particles. The resulting error signal was then used to adjust the laser current to move the levitated particle back to the equilibrium position. He envisaged this technique being used for measuring electric forces and charges (such as an analogue to Millikan's Oil Drop Experiment) [12] and for measuring thermal effects in vacuum.

Experimentally, it was used to accurately measure the scattering forces acting on optically levitated spheres [11]. During this work, it was also found that the equilibrium position of a levitated particle shifted with the angle of the incoming light. When the beam waist decreased sufficiently (corresponding to an increased angle), the particle could be levitated stably below the focus. In this case, the beam diameter was smaller than the sphere and so the axial forces were weaker than at points where the entire particle was illuminated; the focus was essentially a local minima in force with maxima above and below [9].

Meanwhile, work continued in parallel on the optical trapping of atoms using the resonance technique mentioned previously [13]. By 1986, highly focussed beams were being used to confine both atoms [14] and larger dielectric particles of the sort normally levitated [15]. These traps used a single beam, focussed using a microscope objective lens to tightly confine particles in the focal region. These new class of single-beam gradient force optical trap became known as "optical tweezers".

2.3.1 Optical Tweezers

The development of the optical tweezers opened up a plethora of new applications and studies on the microscopic scale. In addition to the existing techniques developed by Ashkin, a vast range of experiments were to be performed by a global community of scientists interested in this new field of optical trapping.

In this new optical tweezers setup, the optical gradient force was stronger than the scattering force from the radiation pressure due to the high degree of focussing provided by the objective lens (see figure 2.2). A particle could therefore be trapped in 3-dimensions instead of merely guided and pushed along the beam path. This allowed microscopic objects to be manipulated with precision.

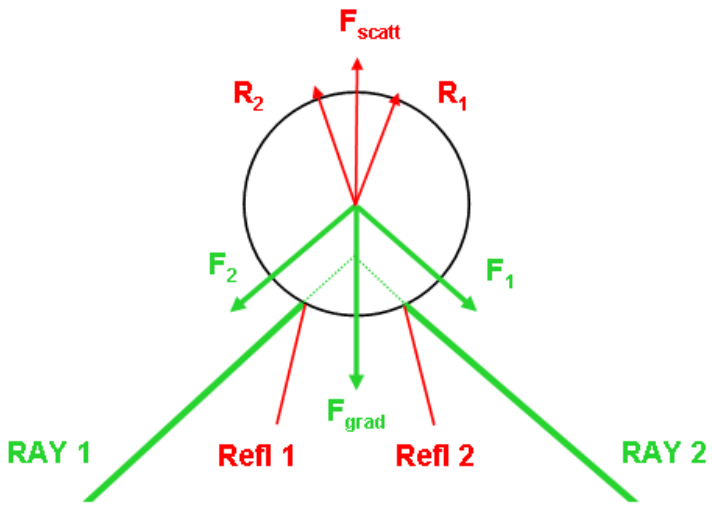

Figure 2.2: Z-trapping effect acting on a spherical particle trapped in a tightly focussed Gaussian beam. Incident rays are marked in green, generating corresponding gradient force in the z direction, F_{grad}. Reflections R1 and R2 in red, contribute to scattering force, F_{scatt}..

Again, the ray-optics model described for the levitation or dual beam traps can be used to describe optical tweezers [8] acting on particles significantly larger than the trapping wavelength (Mie particles). When a microscope objective with a high numerical aperture (NA) is used, rays enter the trapped particle

from a wide angle. When these rays refract, there is a significant change in the z component of the momentum (Figure 2.2 above). When the force due to this z-trapping effect is stronger than the scattering force acting in the propagation direction, the particle is drawn towards the focus. Close to the focus the optical gradient decreases and so a tweezed particle typically reaches an equilibrium position above the focus, where the scattering and z-component of the gradient forces are balanced [16]. If the particle is displaced from this point a restoring force draws it back, in much the same way as a Hookean mechanical spring, exhibiting a degree of damping according to the resistance provided by the local environment (see Section 2.2.3).

The z-trapping effect greatly increased the flexibility of the optical trap. Particles no longer required a wall, gravity, or a counter-propagating beam to hold them stationary. By moving the focus of the trapping laser (or the cell relative to the trapped particle), a sample could be moved easily in 3 dimensions through a cell. The simplest way to quantify the trapping of a particle is to measure the "trapping efficiency" (Q_{axial}) [17]. This quantity gives a measure of how well momentum is transferred to a trapped particle and is of the form

$$Q_{axial} = \frac{Fc}{nP}, \qquad [2.6]$$

where n is the refractive index of the particle, F is the trapping force, c is the speed of light and P is the power incident on the particle. Measuring the minimum axial trapping force required to levitate the particle is due to gravity gives

$$Q_{axial} = \frac{(\rho_s - \rho_m)V_s gc}{n_m P}, \qquad [2.7]$$

where Vs is the volume of the particle, g is the acceleration due to gravity, n_m is the refractive index of the medium and ρ_s and ρ_m are the density of the particle and the medium respectively. The Q values of colloidal traps are typically less than 0.1 [18]. One of the features of aerosol traps is that the axial trapping efficiency is often higher, due to the larger refractive index difference between the particle and the trapping medium.

In the transverse directions, the trapping force (F) can be calculated experimentally by a "drag and drop" method [19]. In other words, if the mass of the trapped particle is known, the force can be found by experimentally calculating the acceleration of the sample required in the transverse direction to break the trapping effect. However, this measurement is difficult to make in air, where the viscosity of the trapping medium is so low. The low velocity of particles in a typical optical trapping experiment allows us to work in the low Reynold's number regime, so we can ignore the effects of turbulence. The reduced viscosity reduces the linear drag, F_d, acting on the particle where

$$\mathbf{F}_d = -\gamma_0 \mathbf{v} \qquad [2.8]$$

γ_0 being the Stoke's constant,

$$\gamma_0 = 6\pi\eta a \qquad [2.9]$$

where a is the Stoke's radius, and η is the viscosity of the medium; 1.86×10^{-5} Pa.s in the case of air and 8.94×10^{-4} Pa.s for water (both at 25 degrees Celcius) [20]. By equating the drag force and the acceleration of the tweezed particle, the gradient force can be calculated.

However, in the case of particles which are smaller than the wavelength of the trapping light, the ray optics approach is no longer valid. In this Rayleigh scattering regime, particles can be treated as dipoles in an electromagnetic field. [21] The scattering force is still present in such a Rayleigh case and so the particles are still drawn to the region of highest intensity while being pushed away from the focus by the scattering. The forces acting on such nanoparticles are due to absorption and reradiation of light. Treating the particles as dipoles, the scattering force in the Rayleigh regime is expressed as

$$F_{scatt} = \frac{I_0 \sigma n_m}{c}, \qquad [2.10]$$

where I_0 is the intensity of the incident light, n_m is the refractive index of the medium and the scattering cross-section,

$$\sigma = \frac{128\pi^5 a^6}{3\lambda^4}\left(\frac{p^2-1}{p^2+2}\right)^2 \qquad [2.11]$$

where p is the refractive index ratio, (n_p/n_m), λ is the wavelength and a is the particle radius. As with the larger particles, the gradient force is due to the intensity gradient expressed as

$$F_{grad} = \frac{2\pi\alpha}{cn_m^2}\nabla I_0 \ , \qquad [2.12]$$

where the polarizability of the particle,

$$\alpha = n_m^2 a^3 \left(\frac{m^2 - 1}{m^2 + 2} \right) \qquad [2.13]$$

Unfortunately, much of the work conducted with optical tweezers is on objects close to the wavelength of the light used and does not fit clearly into the geometric Mie or Rayleigh models. In this regime, where the particles are approximately equal in size to the wavelength of the light used, the optical forces are difficult to calculate. Most attempts to more accurately model effects on this scale use a Generalised Lorenz-Mie theory (GLMT) [22, 23] or otherwise generalised treatments of the scattering of electromagnetic fields [24].

2.2.3 Particle Dynamics in Optical Tweezers

One of the most exciting basic applications is the use of optically trapped particles as microscopic probes. By measuring the forces acting on a bead with known physical properties, interactions can be quantified and potentials can be mapped. This can be achieved through particle tracking with CCD capture [25] for slow, or significant, particle motion or by a high resolution position detector for smaller displacements [26]. Some experimental designs have incorporated a faster and simpler Quadrant Photo-diode (QPD) for position detector [27]. This allows rapid changes in the position of a particle to be detected on a millisecond time-scale. Although particle tracking on short timescales is possible using a CCD, this was only achieved recently using a fast camera [28].

The QPD is a 4-element photodiode, each quadrant producing an independent voltage signal dependent on the incident light intensity. Signal processing,

usually in the form of an electronic circuit is used to create voltages equal to the difference in each axis. This signal is then relayed to a recording device, typically a Digital Acquisition card (DAQ) in a computer. A typical system consists of a quadrant photodiode illuminated by forward scattered light from a particle, usually using a condenser objective to magnify the light source. Light is projected onto the centre of the QPD from a stationary particle or a bead trapped at a very high power [29] in order to produce a null point for calibration. When the trap is less stiff, the motion of the particle is then tracked depending on the voltages output from the QPD system.

The dynamics of a trapped particle are usually compared in the form of a power spectrum. This is a plot of the frequency distribution of the particle's Brownian motion. Given that a tweezed particle is balanced above the focus of the trap due to the opposing scattering and z-trapping forces, the system is very much analogous to a mechanical spring. Optical traps can therefore be described in terms such as "stiffness" (where an intense trap suppresses the Brownian motion) and "damping" (where the environment surrounding the particle acts as a viscous dampener of the oscillations). A spring with a stiffness, κ, prevents the mass escaping due to the thermal fluctuations and acts to pull it back to the equilibrium position. The rate of oscillation is modified by the degree of damping in the system.

The position of such a damped harmonic oscillator can be described by the Langevin equation, which describes stochastic processes in constant potentials, in our case the Brownian motion of a particle in optical tweezers. The equation is of the form

$$m\ddot{x}(t) + \gamma_0 \dot{x}(t) + \kappa x(t) = \varsigma(t) \qquad [2.14]$$

where m = mass, $\gamma_0 = 6\pi\eta a$ (Stokes' law), κ = trap stiffness, ς = stochastic force, a = particle radius and η = dynamic viscosity of the medium. Re-arranging we have

$$\ddot{x}(t) + \Gamma_0 \dot{x}(t) + \Omega_0^2 x(t) = \xi(t), \qquad [2.15]$$

where

$$\xi(t) = \frac{\varsigma(t)}{m} \qquad [2.16]$$

Fourier transforming this and multiplying both sides by their complex conjugate we obtain the power spectrum of position fluctuations;

$$S_x(\omega) = \frac{k_b T}{\pi\kappa} \frac{\Omega_0^2 \Gamma_0}{\left(\omega^2 - \Omega_0^2\right)^2 + \Gamma_0^2 \omega^2} \qquad [2.17]$$

where

$$\Omega_0^2 = \frac{\kappa}{m} \qquad [2.18]$$

and

$$\Gamma_0 = \frac{\gamma_0}{m}. \qquad [2.19]$$

Rearranging again we can obtain a power spectrum;

$$S_x(\omega) = \frac{k_b T}{\pi} \frac{1}{\kappa^2} \frac{\omega_c^2 \gamma_0}{\left(\frac{m^2 \omega^4}{\gamma_0^2 - 2\kappa m}\right) + \omega_c^2 + \omega^2} \qquad [2.20]$$

with the corner frequency given by,

$$\omega_c = \sqrt{\frac{\kappa^2}{\gamma_0^2 - 2\kappa m}}. \qquad [2.21]$$

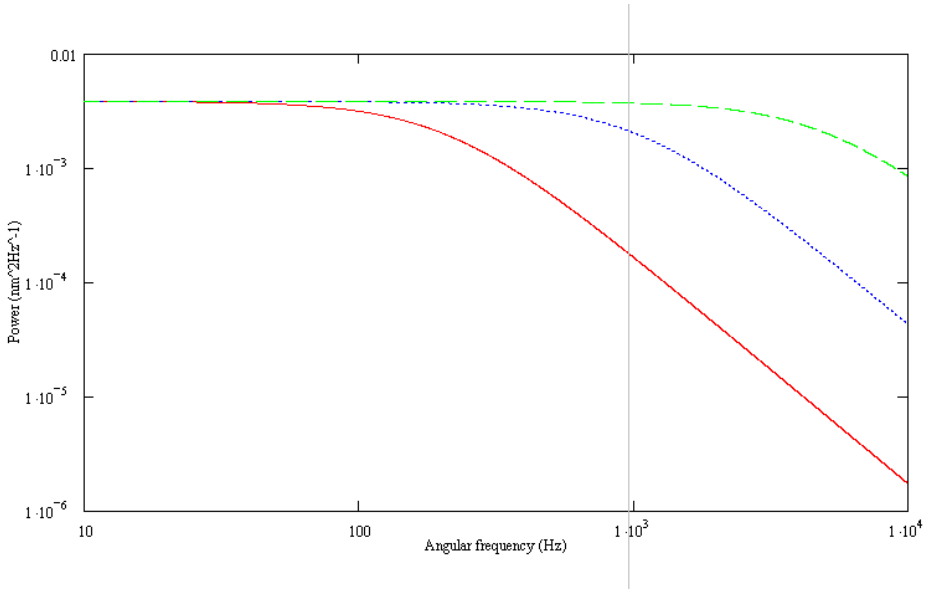

Figure 2.3. Theoretical power spectra plotting power $S_x(\omega)$ against angular frequency (ω) for a sphere tweezes in a liquid medium. The effect of increasing trap stiffness, κ, is illustrated from 0.2 $pN\mu m^{-1}mW^{-1}$ (red) to 1 $pN\mu m^{-1}mW^{-1}$ (blue) to 5 $pN\mu m^{-1}mW^{-1}$ (green).

The corner frequency term, which is equivalent to 3dB roll-off in electronics, allows us to measure the trap stiffness κ, experimentally. This is a useful quantity with which to characterise the trap quality (see figure 2.3). The gradient of high frequency tail of the power spectrum is an indicator of the damping in the system [30]. In the case of an underdamped system, typical of aerosols, this gradient varies with ω^{-4}. Colloidal particles are overdamped and the corresponding power spectra fall off with ω^{-2}. The size of the trapped particle may also play a part, modifying the inertial force and therefore the dynamic viscosity of the system.

2.2.4 Building Optical Tweezers

As the majority of experiments described in the later chapters of this thesis use optical tweezers as their basis, this section aims to help the reader to visualise these experimental designs more easily (see figure 2.4) and give an insight into why certain features are used.

The first consideration in optical trap is obviously the laser itself. Ideally, the laser used has a stable output power, a good mode with a low M^2, and good spatial (Poynting) stability. If the aim is to make precise measurements of particle dynamics, then constant power and directionality are essential. Heating and vibration are another important issue, so fibre delivery of the output is common, with the laser itself removed from the optical table. For delicate measurements and stability, the tables themselves tend to be vibrationally isolated, "floating" on legs filled with pressurised nitrogen gas.

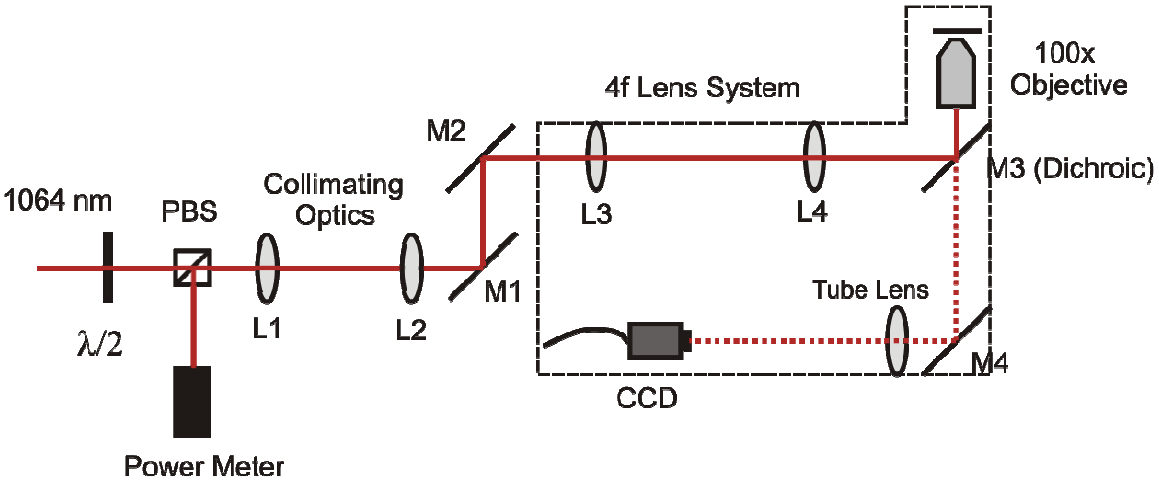

Figure 2.4: A typical optical tweezers arrangement with lenses to adjust the beam diameter for over-filling (L1 and L2) and for controlling the focal height or the tweezers and ensuring M1 is in a conjugate plane (L3 and L4).

The other main consideration is the microscope objective lens. For tweezers work, a 100x oil-immersion objective with a numerical aperture (NA) greater than 1.2 is typical. These are ideal for work with colloidal samples with a simple glass-water interface. Their behaviour is less well known for glass-air interfaces, such as those found in our aerosol studies, but they are still the best that are commercially available.

A pair of steering mirrors are used together to give control over both the angle and the displacement of the beam relative to subsequent optics. Ideally, the beam should pass straight through the centre of the optics to reduce any aberrations in the beam. The microscope imaging plane can be made conjugate

to a steering mirror by using lenses in a 4f telescope arrangement with the microscope back aperture at one end and the mirror at the other. This means that a generated trap can be moved directly along the sample plane with minimal distortion using the mirror mount.

The other parameter to consider is the diameter of the beam entering the objective lens. As mentioned previously, the rays focussed from the edge of the objective provide more gradient force because they are entering the focus at a steeper angle. For a Gaussian beam, the intensity falls off rapidly towards the edge. Common practice is therefore to slightly overfill the back aperture of the objective [16] so there is proportionally more light coming in from the edge of the objective [31]. The beam collimation and diameter at the back aperture can be controlled using a pair of lenses on a rail mount. When the beam is properly aligned and collimated, a small diffraction-limited spot forms in the focal plane of the microscope objective.

Throughout the experiments described in this thesis, the laser sources used for trapping have an output power of at least 1 W in continuous wave operation. In general, this is far in excess of the power required to tweeze or levitate small aerosol particles. Therefore optical losses are not a critical concern, but measuring them allows the power to be calculated at various points in the beam. Three main sources of power loss are present in an optical tweezers set-up.

Firstly, the reflection losses in the collimation and steering optics must be measured. This is straightforward and just involves measuring the power at the source and just before the microscope objective. These can be reduced by ensuring optics are coated with anti-reflection dielectric coatings at the appropriate wavelengths.

Secondly, the degree of overfilling at the objective back aperture must be taken into account. Assuming a Gaussian beam profile, this can be done simply by measuring the diameter of the back aperture and of the illuminating beam. As was mentioned previously, overfilling of the back aperture is common in tweezing in order to increase the average momentum change (angle of attack) of the tweezing photons, increasing the resulting gradient force.

The third and most difficult to measure source of loss is the microscope objective including the coverslip and immersion oil. Microscope objectives are designed to provide clear imaging of white light and are usually not specifically designed or tested at infrared wavelengths. Good and consistent results were achieved using Nikon E-Plan (NA=1.25) objectives at both visible and near-infrared wavelengths up to 1064 nm. A direct comparison of the input and output power levels through an objective with a high numerical aperture tends not to yield an accurate measurement. The divergence makes it difficult to get a detector close enough to the coverslip to capture all the transmitted light. Instead, the most common approach involves using two identical objectives facing one another [32]. A double-sided sample slide is prepared, containing twice the number of optical interfaces present in the experiment being conducted and placed between the dual objectives. Both objectives have to be accurately positioned in three dimensions to ensure perfect alignment, so they typically are mounted on xyz translation stages with micrometer screws. A laser at the appropriate wavelength is used and the output collimated with a diameter to exactly fill the back aperture of the first objective. Both objectives are adjusted to generate a collimated output from the back aperture of the second objective and the power measured. The total loss for the dual objective system is equal to the loss for a single objective and coverslip squared, therefore the square root of the total power loss is taken.

An alternative way to calculate the optical loss from a microscope objective is the micro-bolometer method [33]. This involves heating a known mass of mercury in a water sample in the focus of the tweezers. As the mercury reaches the boiling point of water, it can be observed to jump. However, this method assumes a liquid trapping medium and is therefore unsuitable for aerosol tweezers. By having an accurate measurement of these losses, the power at the trap site can be estimated accurately during experiments.

To control the output power of the laser, it is usual to use a half-wave plate and polarising beam-splitter in tandem, rotating the wave plate to adjust the power going into each direction. This avoids making changes to the laser itself, such as driving current, which may cause unwanted fluctuations in the emission. It

also allows a single laser to be used in two experiments simultaneously, or for a power meter to be used in the other arm from the beam splitter for real-time power measurements.
For a comprehensive description of optical tweezers construction, I recommend a recent protocol by Woei Ming Lee *et al* [34].

2.2.5 Counter-propagating beam traps

In one of his earliest optical trapping experiments Ashkin trapped a particle between two counter-propagating beams [1]. As expected, spheres would settle in an equilibrium position between the two beams and could be moved along the axis of propagation by blocking the appropriate beam. Although this optical potential approach to trapping particles is relatively simple, similar dual beam traps have been used in a number of optical trapping experiments [35]. Optical fibres are ideal for this technique, as it does not require focussing of the trapping light and precise alignment can be achieved using standard fibre alignment tools.
The dual beam fibre trap was first described in detail by Constable *et al* in 1993 [36]. Infrared diode lasers were coupled into two single-mode optical fibres and the fibre ends aligned to within a fraction of the beam waist in a cell consisting of glass capillaries and microscope coverslips. The experiment was also repeated using a He-Ne and an Ar laser as the light sources. The gradient force in this counter-propagating arrangement allowed the manipulation of polystyrene spheres in the 0.1 to 10 µm range. The effect of fibre separation from 20-280 µm was examined and a power range of 3-100 mW was used for trapping. This dual fibre technique is key to many experiments, where the precise placement of a fibre pair either side of a channel allows samples flowing through the channel to be captured easily. These will be described in more detail in Section 2.5.
The phenomenon of optical binding is another area of interest making use of counter-propagating optical traps [37,38,39]. Optical binding involves the

interaction between particles when exposed to an electromagnetic field. Particles are observed to distribute themselves in counter-propagating evanescent or free-space fields according to the attractive or repulsive forces generated. The ability to make crystal analogues in this way is of particular interest soft condensed matter research.

2.3 Tailored Optical Potentials

2.3.1 Tweezers and Momentum

Although Gaussian beams are common in optical trapping, a number of more complex trapping geometries have been demonstrated. Many of these exhibit interesting and useful properties that together form a varied "toolkit" available to the scientist. As well as providing linear motion via scattering and gradient forces, tweezers can also be designed to provide rotational and even orbital angular momentum. Birefringent particles, such as calcite, can be rotated in optical tweezers by rotating a linearly polarized source with a half-wave plate, or by ensuring the light is circularly polarised [35].

This was first demonstrated in a tweezers analogue [40] of an experiment conducted by R. A. Beth in the 1930s [41]. The original experiment involved measuring the torque applied to a birefringent half-wave plate by incident circularly polarized light, thus demonstrating the conservation of angular momentum. The modern equivalent used a standard tweezers setup with an additional quarter-wave plate to rotate optically trapped particles of calcite. As would be expected, changing the angle of the wave-plate by 90 degrees reversed the direction of rotation.

As first demonstrated by Ashkin [1], perhaps one of the most obvious modifications that can be made is to generate a Laguerre-Gaussian mode with an orbital angular momentum component [42]. This can be achieved using a hologram [43] rather than modifying the laser output. Laguerre-Gaussian beams such as these have a clear central minimum surrounded by a ring of high

intensity. As with Gaussian tweezers, particles of a higher refractive index than the trapping medium are attracted to this region of high intensity, allowing multiple particles to be trapped simultaneously in the ring. In addition, objects with a refractive index lower than that of the medium can be confined in the centre of the ring. The spiral "cork-screw" nature of the phase means that particles trapped in the ring can be made to orbit [44] due to a form of orbital angular momentum. These phase modifying techniques can be further extended to create still more tools for the tweezers toolkit.

2.3.2 Bessel Beams

One of the most intriguing forms of beam used in recent experiments is the Bessel beam. Theorised and demonstrated by Durnin in 1987 [45,46], this solution of the Helmholz equation consists of a circularly symmetric light distribution determined by the Bessel function. The zero-order (J_0) Bessel beam that has a bright spot in the centre, and the high-order Bessel beam (HOBB) with a central minimum and which has been shown to transfer angular momentum[47].

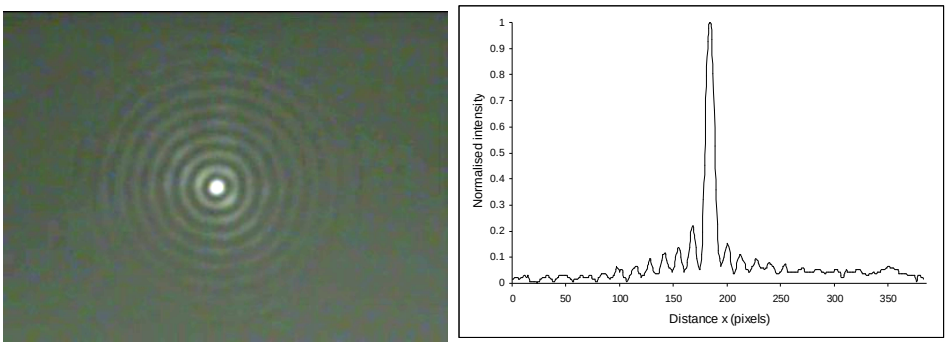

Figure 2.5: Example of a zeroth-order Bessel beam and cross-sectional intensity profile (left) and a corresponding line profile (right).

Durnin showed that there was a propagation-invariant solution for the free space wave equation

$$\left(\nabla^2 - \frac{1}{c^2}\frac{\partial^2}{\partial t^2}\right)E(x,y,z,t) = 0\,. \qquad [2.22]$$

The electric field amplitude of the theoretical non-diffracting Bessel beam is described by

$$E(r,\phi,z) = A_0 \exp(ik_z z) J_n(k_r r) \exp(\pm in\phi)\,. \qquad [2.23]$$

Where J_n is a Bessel function of order n and r, φ and z are the radial, azimuthal and longitudinal components of the beam. k_z and k_r are the wavevectors in the longitudinal and radial directions respectively. These wavevector components can be expressed in terms of k where

$$k = \sqrt{k_z^2 + k_r^2} = \frac{2\pi}{\lambda} \qquad [2.24]$$

with λ as the wavelength of the light forming the Bessel beam. A_0 represents the Gaussian wave of the form

$$E(r,z) = E_0 \frac{w_0}{w(z)} \exp(-\frac{r^2}{w^2(z)})\,. \qquad [2.25]$$

For a zeroth order (n=0) Bessel beam generated by illuminating the axicon with a simple Gaussian beam (of radius w_0), the phase factor exp(±inφ) simply becomes equal to 1 and the intensity can be expressed as

$$I(r,z) = 2\pi k_r w_0 \frac{2P_0 z}{\pi w_0^2 z_{\max}} J_0^2(k_r r) \exp(\frac{-2z^2}{z_{\max}^2}) \qquad [2.26]$$

where P_0 is the power incident on the axicon (z=0), $k_r = k(n-1)\gamma$ where γ is the opening angle of the axicon with refractive index n in the paraxial approximation and

$$z_{\max} = \frac{kw_0}{k_r}\,. \qquad [2.27]$$

Durnin originally created the zero-order Bessel beam with the use of an annulus illuminated by a collimated Gaussian laser beam. The resulting annular profile was then passed through a lens to form its Fourier transform, the Bessel beam. However, the technique was found to be inefficient as the majority of the beam is blocked by the obstruction. The use of a conical lens, or axicon [48] is now preferred as it allows the majority of the incident light to be transmitted. In order to generate high-order Bessel beams, a hologram is

usually used to transform the Gaussian beam to a Laguerre-Gaussian beam before it passes through the axicon.

The majority of the interest in Bessel beams lies with their pseudo non-diffracting nature. It is well known that a Gaussian beam diverges when it is focused and that this is usually expressed in terms of the Rayleigh range. This is the distance from the beam waist at which the beam cross-sectional area has expanded by a factor of 2, given by

$$z_R = \frac{\pi w_0^{\,2}}{\lambda} \qquad [2.28]$$

where w_0 is the beam diameter at the focus and λ is the wavelength of light.
In an ideal Bessel beam, there would be no such divergence present in the central region of the beam. Unfortunately, such an ideal beam is physically unattainable (requiring an infinitely large cross-sectional area), so a pseudo non-diffracting approximation is all that can be achieved. However, the central maximum of Bessel tweezers can propagate without diverging over a distance 100 times that of a Gaussian beam Rayleigh range using the correct parameters. This can be expressed as

$$z_{\max} \approx \frac{w_0}{(n-1)\gamma}, \qquad [2.29]$$

where z_{max} [49] is the maximum propagation distance of the Bessel beam, n is the refractive index of the axicon and γ is its opening angle. The drawback is that the lower the divergence of the beam, the less the power contained in the central maximum and the more distributed throughout the rings. So the design of such tweezers involves a payoff between range and efficiency.

Another effect that is characteristic of Bessel beams is referred to as reconstruction [50]. This is a consequence of the conical wavefronts produced by the axicon. Any point of light that passes the edge of an obstruction in the beam can overlap with the rays from the other points around the obstruction. In other words, if the central region of the beam is blocked, the beam profile is regenerated a set distance from the obstruction in the direction of propagation. In this manner, the beam can pass through multiple such obstructions. Therefore, Bessel beams not only have a large trapping range but can even

"stack" multiple particles in one-dimensional arrays [51] (see figure 2.5). In the case of high-order Bessel beams, particles can also be given angular momentum, allowing them to move in orbits around the rings.

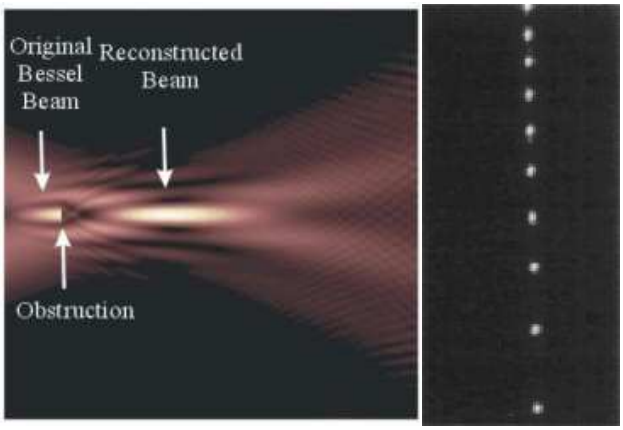

Figure 2.5: Schematic of Bessel reconstruction (left) and creation of vertically levitated 1-D array of particles in water using a Bessel beam (right) [51].

2.3.3 Spatial Light Modulators

A more recent development in optical micromanipulation is the widespread use of spatial light modulators (SLMs) [52]. These devices are capable of modulating an incident collimated light-source in terms of amplitude or phase. The surface of an SLM is typically divided into an array of elements/pixels up to megapixel resolutions [53]. By manipulating the individual elements through modulation in reflectance or transmission, an image can be created in a similar manner to other optical computing systems. In essence, the SLM operates as a dynamic diffractive optical element (DOE) [54], placed in the Fourier plane of the optical system. The image being generated in the trapping plane can be updated according to the frame rate of the device, allowing trapped particles to be moved at discrete intervals.

A lot of effort has been put into computational methods used to shape the beam. Iterative computer algorithms are used to calculate the appropriate phase hologram to create the desired beam profile in the focal plane of the objective lens [55]. Traps can be manipulated in 3-dimensions using this technique by controlling the divergence of the light entering the objective to

change the height above the lens at which the trap forms [56]. Of course, dynamic holography is not limited to generating distinct traps, but can be used to generate a wide range of "optical landscapes". These have been particularly useful for optical sorting experiments where particles react differently to optical fields depending on their size or composition [57]. Some specific applications using SLMs are reviewed in Section 2.5 below.

There has also been considerable success in generating Bessel beams [58] and arrays of optical traps with SLMs [54,59,60] using modified input beam profiles, such as Laguerre-Gaussian modes. Although these experiments were conducted on colloidal samples and there was no previous record of the trapping of aerosols with an array of optical traps, our group successfully mastered this feat [61]. This SLM-based system was used for some of our basic optical trapping experiments outlined in Chapter 4. This technology can be used to observe the merging of individual droplets and potentially to observe chemical reactions between microscopic liquid samples. Both of these areas are of interest to the chemistry community.

2.3.4 Acousto-optic Modulators

Acousto-optic modulators provide an alternative means to create multiple optical traps [62]. These devices use acousto-electric transducers (often piezo-electric crystals) to create standing sound waves in a transparent material [63]. The standing wave acts as a diffraction grating for light passing through, with the diffraction angle determined by the wavelength of the acoustic standing wave. Combining two such Bragg deflectors at right-angles provides a means of scanning a beam in both transverse directions, controlled via the driving voltage applied to the piezos.

This system provides continuous movement of individual particles [64], without the trap refresh rates associated with SLMs. However, while an SLM device can generate a hologram consisting of an array of traps simultaneously, AOMs cannot. Instead, the beam must be shared across of all of the required trap sites with the beam scanning between each point at a rate governed by the

device. This makes it less suitable for generating complex optical landscapes but very useful for controlled positioning of conventional Gaussian traps. AOM-based traps were not used in the experiments detailed in this thesis, but are still an important modern development in trapping which may play a part in future work in this area.

2.4 Applications of Optical Trapping

2.4.1 Optical Tweezers in Biology

Shortly after the development of optical tweezers [15], Ashkin was quick to implement his new technique in the investigation of biological cells [65]. Although the initial tweezers demonstration at 514nm was unsuitable for manipulating biological samples due to absorption and subsequent cell death, 1064 nm was highly successful. This opened the way for a wide range of biological experiments utilising optical tweezers as a non-invasive tool for manipulation and force measurement in biology, while maintaining sterility in a sample. Due to the use of a microscope objective in the tweezers design, the ability to integrate optical traps with existing microscope systems was also an advantage.

On the micrometer level, tweezers have been used to determine forces governing the motion of cells. The initial biological studies by Ashkin and Dziedzic involved investigating the physical mechanisms by which bacteria attach themselves to objects. Bacterial flagella allow bacteria to move and are essentially a small molecular motor with a filament which is used to tether the bacterium to objects, such as microscope coverslips. The main body of a bacterium can be manipulated by optical tweezers and the effect on the flagella observed. This allowed the physical properties to be studied in detail, particularly the effect of torque applied by twisting the bacterium [66]. The motility of sperm cells [67, 68] is a typical measurement to which optical

tweezers are suited, with considerable interest in applications to *in vitro* fertilisation [69].

By combining tweezers with a cutting laser as a "micro scalpel" [70], chromosomes within a cell can be manipulated. This technique typically employs a pulsed UV cutting laser to cut the organic matter. This can be used to study cell fusion, where two neighbouring cells are cut at their common interface [71]. The division of cells can be affected by optical manipulation of the chromosomes [72].

Optical trapping techniques have been applied to even smaller size scales than the cell or chromosome. This includes the study of proteins such as kinesin [73], which carries biological material within cells. The binding forces in processes involving these motor proteins are measured using optical tweezers and beads coated in the protein of interest. By chemically binding DNA to coated spheres, DNA molecules can be manipulated optically and even tied in knots [74]. With precise tuning of the wavelength of trapping light, such molecules can be cut optically [70].

An excellent example of a biological application of dual beam fibre trapping (See Section 2.2.5) is the optical stretcher [75]. In addition to trapping cells in a dual fibre trap, cells were also seen to deform to due to the surface forces. The degree of deformation between cells was found to vary between various cell types, as well as between malignant and non-malignant cells of the same type. This technique is ideal for detecting cancer cells in biological samples flowing past the trap.

2.4.2 Optical Trapping in Microfluidics

Combining optical traps with a flowing sample has become an area of recent interest. Such microfluidic systems are touted as a means of producing an optical "lab-on-a-chip", eventually leading to tiny, inexpensive, mass-produced diagnostic tools driven optically. Using a silicon-based polymer called polydimethylsiloxane (PDMS), microfluidic channels can be made easily via lithographic techniques [76]. These channels can then be bonded to a

microscope coverslip and used in conventional optical traps, with the sample liquid confined by the PDMS. Syringes can be used to supply a microfluidic chip with samples and the flow rates can be controlled using syringe pumps.

This technology becomes particularly powerful when combined with optical manipulation techniques. Birefringent elements [77] can be rotated by adjusting the polarisation of light, creating miniature pumps for small channels. Trapped particles can be used as force probes, to map the fluid dynamic forces [78]. Biological cells can be pumped through the system and analysed [79] or sorted optically [80] using appropriate optical landscapes.

The field of optical sorting was pioneered by Grier's group at the University of Chicago (now at New York University). Their first study involved rotating a flow of colloidal particles relative to an SLM-generated array of traps [81,82]. They observed a "kinetic locking" effect whereby particles were directed by the trap array depending on the direction of flow relative to the 2-dimensional crystal analogue. This effect was dependent on the particle size and this led to optical fractionation in which the trap array was tilted an angle which deflected particles of one size while permitting smaller particles to pass through. However, care had to be taken to run the experiment at a low enough power in order to avoid trapping the particles instead of merely deflecting them.

This technique has been further refined by Grier [83], as well as other research groups. McDonald *et al* [84] demonstrated efficient optical sorting using a 3-dimensional optical lattice. The traps were modified to allow greater flow rates at a range of different deflection angles, resulting in a throughput of around 35 particles per second. This system has obvious application in biological samples where different species must be separated, such as red and white blood cells [80].

The creation of such biophotonic devices is an area of great interest in the optical trapping community. With an aim of creating microscope-based "lab-on-a-chip" systems, this is a high-profile area in the field. However, less interest has been shown in the application of these principles in chemistry and in studying atmospheric particles. Many of the techniques developed for the manipulation of colloidal particles can be applied to the relatively unexplored

realm of aerosols. Therefore, I shall review previous work conducted in the optical study of aerosols in the next chapter.

2.5 References

1. http://www.aps.org/programs/honors/recipients.cfm.html

2. Ashkin, A., "Acceleration and trapping of particles by radiation pressure", Phys. Rev. Lett. **24**, 156 (1970)

3. Ashkin, A., "Atomic-beam deflection by resonance-radiation pressure", Phys. Rev. Lett. **25**, 1321 (1970)

4. Ashkin, A. and Dziedzic, J.M., "Optical levitation in high vacuum," Appl. Phys. Lett. **28**, 333 (1976)

5. Hecht, Eugene, "Optics", 3rd ed., pg. 55

6. Hecht, Eugene, "Optics", 3rd ed, pg. 113

7. Roosen G**.**, "Optical levitation of spheres," Can. J. Phys. **57**, 1260 (1979)

8. Ashkin, A, "Forces of a single-beam, gradient laser trap on a dielectric sphere in the ray optics regime," Biophysical Journal **61**, 569 (1992)

9. Ashkin, A and Dziedzic, J.M., "Stability of optical levitation by radiation pressure," Appl. Phys. Lett. 24, 586 (1974)

10. Ashkin, A., "Applications of laser radiation pressure," Science **210**, 1081 (1980)

11. Ashkin, A and Dziedzic, J.M, "Feedback stabilization of optically levitated particles," Appl. Phys. Lett. 30, 202 (1977)

12. Millikan, R.A., "On the Elementary Electric charge and the Avogadro Constant," Phys. Rev. II **2**, 109 (1913)

13. Ashkin, A., "Trapping of atoms by resonance radiation pressure," Phys. Rev. Lett. **40**, 729 (1978)

14. Chu, S.; Bjorkholm, J.E., Ashkin, A. and Cable, A. "Experimental observation of optically trapped atoms," Phys. Rev. Lett. **57**, 314 (1986)

15. Ashkin, A.; Dziedzic, J.M.; Bjorkholm, J. E. and Chu, S., "Observation of a single-beam gradient force optical trap for dielectric particles," Opt. Lett. **11**, 288 (1986)

16. Neuman, K.C. and Block, S.M., “Optical trapping review,” Review of Scientific Instruments **75**, 2787 (2004)

17. Wright W.H.; Sonek G.J. and Berns M.W., “Parametric study of the forces on microspheres held by optical tweezers,” Appl. Opt. **33,** 1735 (1994)

18. O’Neil, A.T. and Padgett, M.J. “Axial and Lateral trapping efficiency of Laguerre–Gaussian modes in inverted optical tweezers,” Optics Communications **193**, 45 (2001)

19. Muller, O.; Schliwa, M. and Felgner, H., "Calibration of light forces in optical tweezers," Appl. Opt. **34**, 977 (1995)

20. Lide, D.R., “CRC Handbook of Chemistry and Physics”, 88th Edition (2007)

21. Gordon J.P., "Radiation Forces and Momenta in Dielectric Media", Physical Review A **8**, 14 (1973)

22. Ren, K.F.; Greha, G. and Gouesbet, G., “Radiation pressure forces exerted on a particle located arbitrarily located in a Gaussian beam by using the generalized Lorenz-Mie theory and associated resonance effects,” Opt. Commun. **108**, 343 (1994)

23. Zemanek, P.; Jonas, A. and Liska, M., “Simplified description of optical forces acting on a nanoparticle in the Gaussian standing wave,” J. Opt. Soc. Am. A Opt. Image Sci. Vis **19**, 1025 (2002)

24. Barton, J.P., “Expansion of an arbitrarily oriented, located, and shaped beam in spheroidal coordinates,” J. Appl. Phys. **64**, 1632 (1988)

25. Milne, G.; Dholakia, K.; McGloin, D; Volke-Sepulveda, K. and Zemánek, P., "Transverse particle dynamics in a Bessel beam," Opt. Express **15**, 13972 (2007)

26. Ghislain, L.; Switz, N. and Webb, W., “Measurement of small forces using an optical trap,” Rev. Sci. Instrum. **65**, 2762 (1994)

27. Friese, M.E.J.; Rubinsztein-Dunlop, H.; Heckenberg, N.R. and Dearden, E.W., “Determination of the force constant of a single-beam gradient trap by measurement of backscattered light,” Appl. Opt. **35**, 7112 (1996).

28. Keen, S.; Leach, J.; Gibson, G. and Padgett, M., "Comparison of a high-speed camera and a quadrant detector for measuring displacements in optical tweezers," J. Opt. A-Pure Appl. Opt. **9**, S264-S266 (2007)

29. Berg-Sørensen, K.; Flyvbjerg, H., "Power spectrum analysis for optical tweezers," Rev. Sci. Instrum. **75**, 594 (2004)

30. Di Leonardo, R. *et al*, "Parametric Resonance of Optically Trapped Aerosols," Phys. Rev. Lett. **99**, 010601 (2007)

31. Simpson, N. B.; McGloin, D.; Dholakia, K.; Allen, L. and Padgett, M.J., "Optical tweezers with increased axial trapping efficiency," Journal of Modern Optics **45** 1943 (1998)

32. Svoboda, K. and Block, S.M., "Biological Applications of Optical Forces," Annual Review of Biophysics and Biomolecular Structure **23,** 247 (1994)

33. Viana, N.B.; Rocha, M.S. and Mesquita, O.N., "In situ laser power measurement at the focus of microscope objectives used in optical tweezers," Appl. Phys. Lett. **81**, 1765 (2002)

34. Lee, W.M.; Reece, P.; Marchington, R.; Metzger, N.K. and Dholakia, K., "Construction and calibration of an optical trap on a fluorescence optical microscope," Nature Protocols **2**, 3226 (2007)

35. Jess, P.R.T.; Garcés-Chávez, V.; Smith, D.; Mazilu, M.; Paterson, L.; Riches, A.; Herrington, C.S.; Sibbett, W. and Dholakia, K., "Dual beam fibre trap for Raman micro-spectroscopy of single cells," Opt. Express **14**, 5779 (2006)

36. Constable, A.; Kim, J.; Mervis, J.; Zarinetchi, F. and Prentiss, M., "Demonstration of a fiber-optical light-force trap," Opt. Lett. **18**, 1867 (1993)

37. Mellor, C.D. and Bain, C.D., "Array Formation in Evanescent Waves," ChemPhysChem **7**, 329 (2006)

38. Reece, P.J.; Garces-Chavez, V. and Dholakia, K., "Near-field optical micromanipulation with cavity enhanced evanescent waves," Appl. Phys. Lett. **88**, 221116 (2006)

39. Metzger, N.K.; Dholakia, K. and Wright, E.M., “Observation of bistability and hysteresis in optical binding of two dielectric spheres,” Physical Review Letters **96**, 068102. (2006)

40. Moothoo, D.N.; Arlt, J.; Conroy, R.S.; Akerboom, F.; Voit, A. and Dholakia, K., “Beth's experiment using optical tweezers,” Amer. J. Phys. **69**, 271 (2001)

41. Beth, R.A., ‘‘Mechanical Detection and Measurement of the Angular Momentum of Light,’’ Phys. Rev. **50**, 115 (1936)

42. Allen, L.; Beijersbergen, M.W.; Spreeuw, R.J. and Woerdman J.P., “Orbital angular momentum of light and the transformation of Laguerre-Gaussian laser modes”. Phys. Rev. A **45**, 8185 (1992).

43. Arlt, J. *et al*, “Spatial transformation of Laguerre-Gaussian laser modes”. Journal of Modern Optics **48,** 783 (2001)

44. Garces-Chavez, V. *et al*, “The reconstruction of optical angular momentum after distortion in amplitude, phase and polarization”. J. Opt. A: Pure Appl. Opt. **6**, S235–S238 (2004)

45. Durnin, J., "Exact solutions for nondiffracting beams. I. The scalar theory," J. Opt. Soc. Am. A **4**, 651 (1987)

46. Durnin, J.; Meceli, J.J. and Eberly, J.H., “Diffraction-Free Beams”, Phys. Rev. Lett. **58**, 1499 (1987)

47. Volke-Sepulveda, K. *et al*, “Orbital angular momentum of a high-order Bessel light beam”. J. Opt. B: Quantum Semiclass. Opt. **4**, S82–S89 (2002)

48. Herman, R.M. and Wiggins, T.A., "Production and uses of diffractionless beams," J. Opt. Soc. Am. A **8**, 932 (1991)

49. Arlt, J.; Garces-Chavez, V; Sibbett, W. Dholakia, K., “Optical micro-manipulation using a Bessel light beam,” Optics Communications **197**, 239 (2001)

50. Bouchal Z.; Wagner J.; Chlup M.,” Self-reconstruction of a distorted nondiffracting beam,” Optics Communications **151**, 207 (1998)

51. Garcés-Chávez, V. *et al*, “Optical Levitation in a Bessel Light Beam”. Appl. Phys. Lett. **85,** 4001 (2004)

52. Curtis, J.E.; Koss, B.A. and Grier, D.G., “Dynamic holographic optical tweezers,” Opt. Commun. **207**, 169 (2002)

53. Holoeye (website). http://www.holoeye.com/spatial_light_modulators_pluto.html

54. Dufresne, E.R. and Grier, D.G., “Optical tweezer arrays and optical substrates created with diffractive optics”, Review of Scientific Instruments **69**, 1974. (1998)

55. Soifer, V.; Kotlyar, V. and Doskolovich, L., “Iterative Methods for Diffractive Optical Elements Computations”. Taylor and Francis, (1997)

56. Rodrigo, P.J.; Daria, V.R. and Gluckstad, J., “Four-dimensional optical manipulation of colloidal particles,” Appl. Phys. Lett. **86**, 074103 (2005)

57. Chapin, S.C.; Germain, V. and Dufresne, E.R., "Automated trapping, assembly, and sorting with holographic optical tweezers," Opt. Express **14**, 13095 (2006)

58. Chattrapiban, N. *et al*, “Generation of nondiffracting Bessel beams by use of a spatial light modulartor,” Optics Letters **28**, 2183 (2003)

59. Tao, S.H. *et al*, “The generation of an array of nondiffracting beams by a single composite computer generated hologram”. J Opt. A: Pure Appl. Opt. **7**, 40 (2005).

60. Melville, H. *et al*, “Optical Trapping of three-dimensional structures using dynamic holograms”. Optics Express **11**, 3562 (2003)

61. Burnham, D.R. and McGloin, D., "Holographic optical trapping of aerosol droplets," Opt. Express **14**, 4176 (2006)

62. Milne, G.; Rhodes, D.; MacDonald, M. and Dholakia, K., "Fractionation of polydisperse colloid with acousto-optically generated potential energy landscapes," Opt. Lett. **32**, 1144 (2007)

63. http://www.rp-photonics.com/acousto_optic_modulators.html

64. Perch-Nielsen, I.; Rodrigo, P. and Glückstad, J., "Real-time interactive 3D manipulation of particles viewed in two orthogonal observation planes," Opt. Express **13**, 2852 (2005)

65. Ashkin, A. and J.M. Dziedzic, “Optical trapping and manipulation of viruses and bacteria,” Science **235**, 1517 (1987)

66. Block, S.M.; Blair, D.F. and Berg, H.C., “Compliance of bacterial polyhooks measured with optical tweezers,” Cytometry **12**, 492 (1991)

67. Tadir, Y. ; Wright, W.H. ; Vafa, O. ; Ord, T. ; Asch, R.H. ; Berns, M.W. , “Micromanipulation of sperm by a laser generated optical trap ,” Fertility and sterility **52**, 870 (1989)

68. Konig, K.; Liang, H.; Berns, M.W. and Tromberg, B.J., "Cell damage in near-infrared multimode optical traps as a result of multiphoton absorption," Opt. Lett. **21**, 1090 (1996)

69. Tadir, Y.; Wright, W.H.; Vafa, O.; Liaw, L.H.; Asch, R. and Berns, M.W., “Micromanipulation of gametes using laser microbeams,” Hum. Reprod. **6**, 1011 (1991)

70. Liang, H.; Wright, W.H.; Cheng, S.; He, W. and Berns M.W., “Micromanipulation of chromosomes in PTK2 cells using laser microsurgery (optical scalpel) in combination with laser-induced optical force (optical tweezers),” Exp Cell Res. **204,** 110 (1993)

71. Steubing, R.W.; Chang, S.; Wright, W.H.; Namajiri, Y. and Berns, M.W., “Laser induced cell fusion in combination with optical tweezers: The laser cell fusion trap,” Cytometry **12**, 505 (1991)

72. Berns, M.W., “Laser scissors and tweezers,” Sci. Am. **278**, 62 (1998)

73. Block, S.M.; Goldstein, L.S.B. and Schnapp, B.J., “Bead movement by single kinesin molecules studied with optical tweezers,” Nature **348**, 348 (1990).

74. Arai, Y.; Yasuda, R.; Akashi, K.; Harada, Y.; Miyata, H.; Kinosita, K. and Itoh, H., “Tying a molecular knot with optical tweezers,” Nature **399**, 446 (1999)

75. Guck, J.; Ananthakrishnan, R.; Mahmood, H.; Moon, T.J.; Cunningham, C.C. and Käs, J., “The optical stretcher: a novel laser tool to micromanipulate cells,” Biophys J. **81**, 767 (2001)

76. Sia, S.K. and Whitesides, G.M., “Microfluidic devices fabricated in poly(dimethylsiloxane) for biological studies,” Electrophoresis **24**, 3563 (2003)

77. Friese, M. E. J., Rubinsztein-Dunlop, H. , Gold, J. , Hagberg, P. & Hanstorp, D., “Optically driven micromachine elements,” Appl. Phys. Lett. **78**, 547 (2001)

78. Ghislain, L.P. and Webb, W.W., "Scanning-force microscope based on an optical trap," Opt. Lett. **18**, 1678 (1993)

79. Ozkan, M. *et al*, “Optical manipulation of objects and biological cells in microfluidic devices,” Biomed Microdevices **5**, 61 (2003)

80. Paterson, L.; Papagiakoumou, E.; Milne, G.; Garcés-Chávez, V.; Tatarkova, S.A.; Sibbett, W.; Gunn Moore, F.J.; Bryant, P.E.; Riches, A.C. and Dholakia, K., “Light-induced cell separation in a tailored optical landscape,” Appl. Phys. Lett. **87**, 123901-1 (2005)

81. Ladavac, K.; Kasza, K. and Grier**,** D.G., "Sorting by periodic potential energy landscapes: optical fractionation," Phys. Rev. E **70**, 010901(R) (2004)

82. Korda, P.T.; Taylor, M.B. and Grier, D.G., "Kinetically locked-in colloidal transport in an array of optical tweezers," Phys. Rev. Lett. **89**, 128301 (2002)

83. Koss, B.A. and Grier, D.G., “Optical peristalsis,” Appl. Phys. Lett. **82**, 3985 (2003)

84. MacDonald, M.P.; Spalding G.C. and Dholakia, K., “Microfluidic sorting in an optical lattice,” Nature **426**, 421 (2003)

Chapter 3

Aerosols and Optics

3.1 Introduction

The aim of this section is to describe the discoveries and methods related to the optical trapping of aerosols, developed since the early work by Ashkin and his contemporaries. Much of the modern work in the field involves spectroscopy and other chemical techniques, as opposed to the mostly biological flavour of optical trapping in colloids outlined in the previous chapter. To that end, some of the key techniques and developments relevant to this thesis will be described in some detail.

Modifications to basic colloidal trapping systems for work with aerosols will be covered here, as will specific techniques and methods developed for optically trapping airborne particles. In addition, a portion of this chapter will be dedicated to the engineering and design issues governing the generation of aerosol samples themselves. I feel that the variety of models used, tested and modified during the course of my work is worthy of mention. For many of the experiments, the balance of flow rate, droplet size and environmental conditions were crucial to success and consistency.

3.2 Development of the Optical Manipulation of Aerosols

3.2.1 Liquid Aerosol Trapping

As with other areas of study with optical trapping, Ashkin was the one to pioneer aerosol manipulation with lasers. In his first optical trapping paper [1],

Ashkin observed atomised droplets of water in a single 50mW beam. He recorded the droplets being pushed by the beam at a velocity of approximately 0.25cm/sec. Although it was not specifically mentioned in his first paper, this approach would also have been capable of levitating particles. By balancing the radiation pressure against the gravitational force acting on the particle, a particle can be held at a desired point [2].

Transparent particles were also levitated in a beam with the purpose of acting as a sensitive force probe in a technique dubbed "force spectroscopy" [3]. By using a tuneable dye laser, Ashkin and Dziedzic levitated silicone oil droplets and some other more volatile oils in air. It was known that the droplets would form highly regular spheres and with the specific oils selected, a range of refractive indices from 1.4 to 1.53 and radii from 4 to 30μm was possible. The aim of the experiment was to examine the radiation-pressure force as a function of a size factor x, where

$$x = \frac{2\pi a}{\lambda}, \qquad [3.1]$$

a is the particle radius and λ is the wavelength of the incident light.

It was shown that Ashkin's levitation trap could be used as a sensitive force probe to investigate the effects of light scattering theories in detail. By devising an electronic feedback system, a levitated droplet could be locked at a constant height, and the required laser power measured. Assuming any change in the laser power was made to counteract a net change in force acting on the particle, the radiation pressure force (dependent on the voltage applied to the laser) could be monitored as the size function was altered. Although the specifics of the experimental setup were not described, it is assumed that the radiation pressure from the levitating laser was balanced by the weight of the droplet. As the Debye-Mie theory being investigated described plane-waves, the droplets were balanced at a point away from the focus of a loosely focussed Gaussian beam. The size factor was altered both by gradually changing the wavelength of the levitating beam (change in λ) and by taking the evaporation of the particle into account (change in a).

As the droplet size factor was varied sharp dips in the required levitating power were observed at specific values of size factor, x. The theory predicted that these force resonances were a surface-wave effect, suggesting that the droplet was acting as an optical cavity. To prove this was the case, Ashkin moved the droplets towards the focus of the trapping beam to a point where the beam radius was smaller than that of the particle. When there was no light passing through the edge of the particle, the resonances were no longer evident. This supported the idea of the light being coupled into a cavity. To quantify the coupling of light into such micro-resonator, the term Q_{cavity} is used. Analogous to a finesse value for a conventional optical cavity, it is a measure of the energy stored in the droplet where

$$Q_{cavity} = \frac{2\pi \ x \ Energy \ stored}{Energy \ lost \ \ per \ cycle}. \qquad [3.2]$$

Such droplet-based "Whispering Gallery Mode" (WGM) cavities have demonstrated Q_{cavity} values in excess of 10^6 [4].

The ability of liquid droplets to form very high-Q cavities is of particular interest to researchers in physical chemistry. A number of spectroscopic techniques can be modified to make use of coupling into a resonating mode, leading to improvements in the resolution of the measurements. This method, known as Cavity Enhanced Droplet Spectroscopy (CEDS), is the current focus of Jonathan Reid at the University of Bristol [5]. My own work in the manipulation of aerosols is to aid the work towards the final goal of constructing a working system that can trap and transport droplets through a number of probes. In other words, the ultimate goal is the creation of a "lab-in-a-box" for aerosols, in collaboration with Jonathan Reid's group.

The group at Bristol has been building on the work of Ashkin and many others in quantifying the WGMs in droplets and other particles and examining their potential in the field of spectroscopy. The properties of the elastic light scattering investigated by Ashkin and Dzeidzic [6] had already provided a method for determining the size, shape and refractive index of particles from observed resonances. The particle characteristics have a direct effect on the observed properties of the constituent molecules. The high-Q resonance

possible in a droplet equates to a path length in the order of metres or a photon lifetime of many nanoseconds. The low loss has allowed non-linear optical processes to be observed using relatively low intensities. Although the most useful of these for the purposes of the project is Stimulated Raman Scattering (SRS), processes such as lasing [7] and sum-frequency generation [8] have also been demonstrated in levitated spheres.

A more recent set of experiments at Kyoto University [9] has achieved an axial trapping efficiency (Q_{axial}) of 0.46 using 5mW at 1064nm to trap a 5.7μm radius droplet of water. This was in part achieved through the use of a 100x objective lens with a convergence angle of 120 degrees at the focus to produce optical tweezers, as opposed to Ashkin's early aerosol work with levitation traps. However, an interesting feature of the experiment was the means of the droplet generation. The droplets were formed in a sealed cell containing ammonium chloride particles and supersaturated with water vapour. The sub-micron sized particles of ammonium chloride acted as nucleation sites, encouraging the growth of water droplets from the surrounding vapour. These could then be trapped by the vertical beam and observed as they continued to grow. Once the droplets grew to a critical size (dependent on the laser power), they would fall out of the trap.

This is an interesting approach and allowed the Kyoto group to analyse a wide range of particle sizes easily. They could rapidly determine the maximum droplet size supported by a trap of a given power. The high numerical aperture of the objective lens allowed them to achieve far higher trapping efficiencies than previous experiments. This experimental design may also have a use in the process of deliquescence [10]. This is the process of a solid dissolving into a solution and is of interest to chemists. Understandably, it is a difficult process to monitor from start to finish. Growing a droplet around a solute and gradually diluting it could provide a useful approach in this area of chemistry.

The high trapping efficiencies achieved by the group at Kyoto University suggest that the droplets as large as 1mm in radius may be trapped in the future using laser powers no greater than 1 W, albeit in the absence of a strong gravitational force. This may seem a little extreme, but more recent

experiments by the same group [11] have taken place on board a jet aircraft on trajectories designed to alter the gravitational forces acting on an optical levitation trap. This work could eventually lead to Ashkin's original optical tweezers design making it onto the International Space Station. It may be safe to say that Ashkin's tweezers design has probably been taken further than he originally envisaged!

3.2.2 Solid Aerosol Trapping

Although the majority of aerosol trapping work has focussed on liquid droplets, solid aerosols are of course also of interest. Atmospheric solid aerosols tend to be comprised of dust (if continental) or salt (if marine) [12]. They can also comprise of solid cores, surrounded by a liquid shell due either to nucleation or freezing. Atmospheric chemists typically use LIDAR techniques to detect species in the atmosphere in bulk [13]. The ability to study such atmospheric particles and their interactions in small numbers is something that optical trapping can potentially deliver.

As with the majority of optical trapping, Ashkin was the first to optically trap solid aerosol particles[14]. He then examined the stable optical levitation of glass beads measuring 30-60 µm across in a TEM_{01} mode [15]. Solid particles were launched into the beams through the use of an acoustically agitated glass plate. These techniques were later extended to the study of a range of nonspherical particles in optical levitation traps [16]. This work was further explored by Thurn *et al* and combined with Raman spectroscopy [17].

However, the optical tweezing of solid aerosols was not automatically achieved until 1997 [18], 11 years after the first tweezers paper. The method employed by Omori *et al* was similar to Ashkin's approach, using a piezoelectric element to vibrate a microscope slide covered with silica spheres. Particle oscillation forced the particles into a trap, using a non-inverted optical tweezers, focused just above the sample plane.

3.2.3 Alternative Aerosol Trapping Techniques

It must be noted that optical trapping is not the only technique available for the capture, confinement and analysis of aerosol particles. In fact, many interesting aerosol droplet experiments have been conducted simply by optically probing a steady stream of falling droplets [19,20,21] This work was important in the characterisation of droplets and Whispering Gallery Modes cavity enhancements in particular. Such falling aerosols were made to lase by doping them with laser dyes such a Rhodamine 6G [22]. Stimulated Raman scattering experiments were successfully conducted on water and ethanol droplets [23].

For charged aerosol particles, confinement can be achieved by using electric fields. Quadrupole ion traps have been used for this purpose [24], especially for solid aerosols. [25]. Combined with light scattering measurements, this technique is useful for measuring particle size and therefore also evaporation and condensation rates as well as crystallisation phenomena [26] these studies focussed on aerosol particles measuring as small as 10μm, but have the obvious limitation of requiring the aerosols to be charged before entering the trap.

Ultrasonic levitation is another competitor to optical trapping for the study of aerosols [27]. Ultrasonic transducers can be used to produce standing waves which effectively trap aerosol particles in the nodes. In this manner, regularly spaced 1-D arrays of droplets have been shown. However, the size range of droplets which can be trapped by this method is larger than that achieved by optical trapping (typically around 1mm) [28].

Another interesting approach to aerosol confinement involves trapping and guiding particles within a hollow-core optical fibre [29]. This method is largely undeveloped and the measurement and observation of such a particle is difficult. However, it provides a potential means to transport aerosol particles and perhaps a way to load other optical traps in a controlled manner.

However, the advantages afforded by optical tweezers are numerous. Firstly, the particles can be viewed through the same microscope objective used for tweezing. By adding a position detector (QPD or a CCD), the forces acting on

the particle can be accurately measured. In addition, the particles can be confined to a much higher degree than the alternatives. Using multiple trapping techniques, small numbers of aerosols can be controlled and particle-particle interactions studied in detail.

3.3 Chemical Techniques with Aerosols

3.3.1 Introduction

In Raman scattering [30], some of the light from an incident monochromatic light source is absorbed by the medium. Some of the light is simply scattered by the material and reradiated at the same wavelength by the process of Rayleigh scattering [31]. Usually, there is a weak component of the light that undergoes inelastic scattering. This light gets absorbed, and due to interactions with the molecules in the medium, gets reradiated at a wavelengths shifted from that of the original radiation. If energy is lost, the new spectral lines are known as Stokes lines (shifted to longer wavelengths). Anti-stokes lines are created by transitions with a higher energy, but are usually a much weaker non-linear effect [32]. The theory behind the process describes the transition energies being shifted due to phonon interactions (vibrational transitions). These are characteristic of a particular substance, so an energy pulse above a specific threshold can result in a molecular "fingerprint" which can be detected in the spectrum of the scattered light.

With regards to this project, the interest in SRS lies with its ability to give particle size measurements to nanometre accuracy. By tuning over a $6x10^{-4}$ nm bandwidth around the resonance point of a WGM, a radius change of 0.1nm has been observed in 10μm particles [33]. With this level of accuracy, the effects of evaporation and even refractive index dispersion are factors in the measurement. Thermal gradients in the particle can be inferred from the quality of the spectra obtained from a sample. Measurements of both the size and composition of sample mixtures have been made, although the accuracy of

the radius calculation was somewhat reduced from those achieved with pure droplets [34]. Although SRS is useful for determining droplet sizes, the threshold power density required for detecting trace concentrations of impurities is greater than is practical in many cases. However, the enhancement provided by the cavity nature of the droplets still provides an improvement over the strength of the Raman Scattering signal expected from such a small sample [19].

3.3.2 Droplets as Microcavities

Extending the description of the resonances demonstrated by Ashkin [35], one can view the resonant radiation field within the droplet as any other cavity mode. Light rays travelling inside a spherical particle undergo total internal reflection at the interface between the outer circumference and the surrounding medium. Resonance occurs when a standing wave exists with an integer number of wavelengths of the illuminating light guided around the circumference.

The mode number, q, can be expressed as

$$q = \frac{2\pi na}{\lambda}, \qquad [3.3]$$

where n is the refractive index of the particle, a is the particle radius and λ is the wavelength of the light. A WGM also consists of a radial mode order, l, which defines the mode intensity from the outside of the droplet towards the centre (see figure 3.1). There is a fall-off in intensity of the WGM with distance from the edge and an evanescent component which extends beyond the outer surface [36].

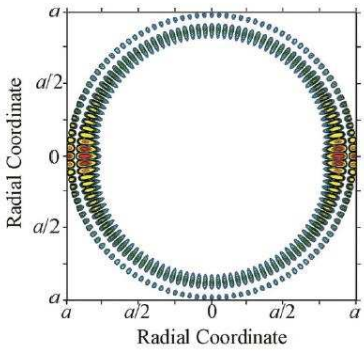

Figure 3.1: Model of WGM (mode number 60, mode order 2) propagating in a droplet produced by the Reid group at the University of Bristol

Each mode number consists of both a TE and a TM mode, resulting in a total mode degeneracy of 2n+l. This has a polarisation dependent effect on the scattered radiation. Both modes are evident in the forward and backward directions, but not at 90 degrees. The TM mode is scattered in the plane parallel to the plane of the incident polarisation and the TE mode is scattered in a perpendicular plane [37].

Understanding the nature of WGMs has been useful in determining the most effective way to couple light into a droplet. The illumination geometry determines both the intensity and shape of the spectral fingerprint obtained from a spherical cavity. The intensity is affected by the quantity of light coupled into the droplet. Altering both the position and the strength of the focus can modify these coupling characteristics. The other somewhat obvious factor in droplet illumination is whether the wavelength is on resonance with a WGM. Of course, for illumination sources with a broad fluorescence spectrum (such as dyes) many resonance wavelengths can be excited simultaneously. However, there is also some interest in off-resonance edge illumination of microcavities and the phenomenon of photonic nanojets in microcavities [38].

For a non-resonant, loosely focussed illuminating beam, SRS enhancements of 300 times have been demonstrated in areas of overlap between the WGM and the pump intensity. The efficiency of the process has been found to increase with droplet size. In the case of an illuminating plane wave that is on resonance, the relative linewidths of the laser and the WGM have an effect on

the coupling efficiency. One useful measurement for characterising energy coupling into a droplet is the cavity build-up factor

$$f_b = \frac{3n^2_{\lambda_{WGM}} \lambda^2_{WGM} Q_{cavity}}{4\pi^2 a^2}, \qquad [3.4]$$

where N_{WGM} is the refractive index at the WGM wavelength $\lambda_{WGM.}$

A number of experiments have been conducted with pulsed illuminating lasers and the decay in intensity observed [39,40], allowing these factors to be more accurately determined. Finally, it has been found that if the illuminating beam is tightly focussed, care must be taken to match the wavevectors of the incident beam and the coupled mode [41,42].

3.3.3 Cavity Enhanced Droplet Spectroscopy (CEDS)

The use of cavity feedback to enhance signal strength is a common technique in spectroscopy [43]. Similarly, the spectra generated from droplets differ from those obtained in bulk samples. The WGM resonances result in distinct features not present in many other resonance enhanced techniques [40] and more akin to the modes produced in single mode fibre [44]. The separation between modes is evenly spaced [45]. Assuming the refractive index is invariant with wavelength, the mode separation, S(a) can be expressed as

$$S(a) = \frac{\lambda^2 \tan^{-1}\sqrt{(p^2 - 1)}}{2\pi a\sqrt{(p^2 - 1)}} \qquad [3.5]$$

where $p=(n_l/n_m)$, λ is the wavelength and a is the radius of the sphere, as defined previously. This allows the measurement of droplet radius from the wavelengths of WGMs [46]. It is also clear that the mode spacing increases with decreasing radius, which provides a useful means of measuring a change in the diameter of liquid droplets due to evaporation [47].

However, the accuracy in any measurement of a spherical particle by spectroscopy is also dependent on refractive index dispersion [48]. In the case of trapping liquid droplets, cooling due to evaporation and heating due to

absorption of laser radiation and thermal gradients are important considerations [49,50]. With an appropriate experimental design droplet size can be measured to sub-nanometer accuracy. [51]

Cavity enhancement has consequences in both fluorescent and Raman spectroscopy. Fluorescence spectroscopy, with respect to CEDS, deals with dye droplets and dye doped spheres, usually excited with plane wave continuous-wave sources [52,53]. In the fluorescent spectra of droplets, cavity resonances are obvious and used to determine particle size and evaporation rates [54]. If round trip gain exceeds loss, then lasing takes place, resulting in stimulated emission at WGM wavelengths [55,56].

Raman spectroscopy studies on droplets typically involve falling droplets or levitated spheres [44]. With a low pump intensity the resulting spontaneous Raman signal is typically used for sizing and aerosol dynamics measurements [19]. The majority of work in Raman CEDS takes place at higher intensities, above the stimulated Raman signal threshold. In this regime the signal strength increases exponentially with pump intensity. Although spontaneous Raman can be used to detect concentrations of one tenth that of stimulated Raman [57] due to the threshold requirement of SRS [58], SRS allows combined size and composition measurements [59,60,61]. It has been shown that the detection limit of SRS measurements can be lowered by using a seed pump for producing 1st order SRS signals [62].

3.4 Features of Aerosol Tweezers

3.4.1 Changes to Tweezers Design and Operation

Although the basic aerosol optical tweezers design is no different to that used in colloidal trapping experiments, there are features particular to aerosol tweezers. The most obvious difference is the effect of having a glass:air interface above the objective instead of glass:water. The increased refractive index difference between the coverslip and the trapping medium; 1 to 1.53 in

the case of silica glass, reduces the critical angle at the interface. Any rays approaching the interface at an angle greater than the critical angle are reflected, removing them from the tweezers. In the case of an objective with an NA of 1.25, using air as a trapping medium results in an effective NA of close to 1. Eliminating rays with a large horizontal momentum component reduces the gradient force provided by the trap.

When working with liquid aerosols, another problem is having the sample deposited on the coverslip. Any particles present on the coverslip distort the light passing through. The effect is particularly pronounced for liquids like water with a high surface tension which produce puddles with a pronounced curvature. In the case of experiments involving water droplets, the coverslips are pre-treated with the surfactant Sodium Dodecyl-Sulphate (SDS). This reduces the surface tension of water on the surface, creating large flat puddles or uniform layers of water, minimising the distortion to the light for trapping and imaging.

3.4.2 Tweezers Characteristics for Aerosols

Perhaps the most obvious difference between trapping particles in air and trapping in a liquid is the increase in refractive index contrast. This increases both the gradient and scattering forces acting on the particle, reducing the minimum power required for trapping. The other obvious effect is the difference in the mechanical properties of the respective trapping media. As mentioned in section 2.2.2, the drag force acting on a particle is dependent on the viscosity (η) of the surrounding fluid, where the values for η are 1.86×10^{-5} Pa.s in the case of air and 8.94×10^{-4} Pa.s for water at 25°C.

The effect of this is that trapped particles in air will generally oscillate more than equivalent particles in a liquid medium. The difference between a tweezed droplet and a sphere in a liquid suspension was described in work conducted with the University of Glasgow [63], exploring the underdamped oscillations of tweezed droplets. The damping effects described refer to the interaction between a particle and the optical field of the tweezers, and aren't to

be confused with the effect of convection and airflow in sample cells. Although airflow and convection ain the medium are important and problematic at best, they are an issue of fluid dynamics and engineering rather than something specific to optical tweezers.

3.5 Generation of Aerosol Samples for Trapping

3.5.1 Nebuliser Designs

The most crucial component in the generation of aerosol samples is the nebuliser. The devices turn a liquid sample into a cloud of droplets, usually by forcing the liquid through a small hole or mesh. Several different nebuliser types were used in these experiments, depending on the requirements.

Figure 3.2: Omron U-22 Nebuliser used for generating aerosol samples in the majority of the experiments described.

For general aerosol trapping applications, a commercial medical handheld nebuliser was used (see figure 3.2). The Omron U22 Microair nebuliser consists of a mesh with 3 µm holes which is vibrated using an ultrasonic transducer. It produces a consistent, constant flow of droplets, with a mass median aerodynamic diameter (MMAD) of between 3.4µm and 6 µm. It can be used to nebulise water, dilute glycerol solutions and ethanol. However it is unsuitable for nebulising solvents, such as dodecane, as they soften some of the plastics used in the mesh cap. Generally, nozzles are used with this nebuliser to channel the flow into a cell.

The most basic nebuliser design used consists of a small glass nozzle located above a sample chamber. The liquid sample is driven through the nozzle using compressed air at pressure between 2 and 4.5 bar, depending on the aerosol characteristics required. Higher pressures usually produce clouds consisting of smaller droplets. The pressurised gas is provided by either a canister with a flow controller or a compressor unit. The directional airflow resulting from the pressurised air in this style of system makes it useful for optical levitation experiments with a weak trap. This allows more power to be used to confine a droplet in the transverse (x and y) directions, while maintaining balance in the direction of beam propagation (z).

The other nebuliser design used (Omron Aerosonic) generates ultrasonic waves to drive liquid samples from a deliberately shaped sample cup, through a nozzle. This system generates dense clouds of droplets with a mmad of 3.5 µm at a constant rate. This is ideal for studies of aerosols in bulk, or for creating larger droplets by appropriate conditioning of the flow to increase the rate of collisions between droplets.

3.5.2 Flow conditioning and cell design

Depending on the experiment and trap design, the basic aerosol flow required conditioning to control flow rate, velocity and droplet size to improve the chance of successful trapping events. The simplest method involves using additional nozzles to direct and to constrict (speed up) or expand (slow down) the flow (see figure 3.3).

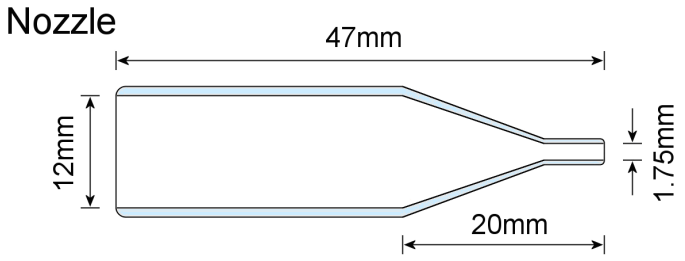

Figure 3.3: Typical glass nozzle used with the Omron U-22 nebuliser..

The aerosol sample then flows into a sample cell containing and surrounding the trapping volume. These sample cells also require designing, specific to the demands of a particular experiment. The cells used for trapping aerosols usually use cuvettes, microscope slides or transparent substrates as their basis (see figure 3.4). This provides optical windows, either for side-imaging with a microscope objective with a long working distance, or to allow probe or pump light to reach an aerosol sample from outside. The sample cell is normally placed on top of a coverslip, usually placed above an oil-immersion microscope objective.

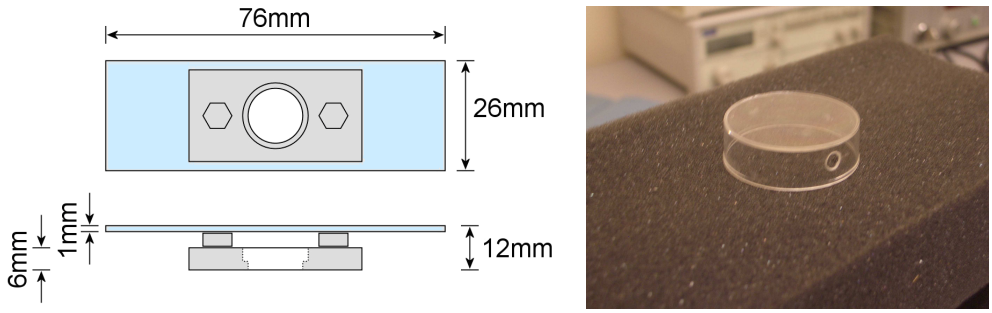

Figure 3.4: Some sample cell designs (high evaporation rate cell (left), modified Petri dish cell (right)).

Given the nature of optical trapping in air, our samples are particularly sensitive to air flow within the cell. To that end, baffles or small enclosures (typically a washer) are placed within the cell to shield the trapping region from stray airflows or disturbances caused by the flow of aerosol into the cell. If a nozzle is being used, then the flow is often directed slightly away from the trap to adjust the volume and velocity of the incoming aerosol, further reducing the disturbance. In addition, convection currents tend to be greater in cells of a greater volume, so smaller sample cell designs tend to be more successful, especially with basic tweezers experiments.

For greater consistency, funnels can be used to hold larger volumes of aerosol cloud, with any airflows generated from the nebuliser isolated from the sample cell below. This has the additional effect of increasing droplet size by increasing the period droplets have to coagulate before entering the trapping

region. Apertures or inverted nozzles can be used to create a steadily falling stream of droplets of a desired density.

3.5.3 Management of Droplet Evaporation

Given that the droplet samples used in our experiments are small, with diameters of less than 10 µm, evaporation is a major factor. Evaporation takes place when molecules near the surface of the droplet have sufficient kinetic energy to leave the droplet [64]. These molecules form a vapour in the environment surrounding the liquid. Likewise, molecules from the surrounding vapour can enter the droplet. The equation

$$\left(\frac{d}{d_0}\right) = 1 - \frac{8\lambda_L}{\rho_{liquid} c_p d_0^2} \ln(1+B)t, \qquad [3.6]$$

as derived by Renz [65] is used in this thesis to quantify the effect of evaporation where λ_L is the thermal conductivity of the liquid, c_p is the specific heat of the sample, d_0 is the initial droplet diameter, t is time and B is a "mass transfer number"

The mass transfer number is the rate at which molecules from the vapour return to the liquid and depends on the pressure and density of the vapour in the medium. If the rate of evaporation is equal to the rate of molecules entering the droplet, the atmosphere is said to be saturated with the vapour and the droplet remains at a constant diameter. In the case of water, this can also be expressed as a humidity of 100 %. There will be a more detailed examination of droplet evaporation in Section 4.3.

However, the sample cells used in our experiments are not perfectly sealed environments. There is usually some loss of vapour from the cell either through the aerosol inlet, or from any gaps between the sample cell and the coverslip. These leaks reduce the vapour pressure inside the cell, bringing the atmosphere below the saturation point and disrupting the equilibrium with the liquid droplet. This makes it important to reduce the leakage of vapour from the sample cell by keeping the inlet hole small and ensuring the bottom of the

cell forms a seal with the coverslip. This can be achieved with sealant materials, or in many cases simply a layer of the sample liquid itself.

Another relatively simple method for maintaining a constant droplet diameter within the sample cell is to add reservoirs of the sample liquid within the cell. These can either take the form of paper soaked in the liquid, or a vessel filled with the sample when appropriate. This provides an additional source of vapour to replenish any lost from the sample chamber, maintaining the equilibrium between droplet and atmosphere for longer.

In addition to maintaining a saturated environment, steps can also be taken to reduce the required vapour pressure. This is achieved by adding an impurity to the liquid. In the case of water, adding sodium chloride has the effect of reducing the vapour pressure. If the vapour concentration in the cell drops below saturation, the droplet shrinks. As the volume of the droplet decreases, there is a corresponding increase in the salt concentration, further reducing the required vapour pressure. Using this technique, a salt water droplet can remain trapped indefinitely, provided the atmosphere is sufficiently humid to prevent the salt crystallising out of solution. This is generally not a problem with the prevailing weather conditions in St Andrews.

3.6 Cameras, Objectives and Particle Sizing

Although Cavity Enhanced Droplet Spectroscopy (CEDS) [5] can give very accurate droplet sizing, this technique requires the use of a spectrometer. A more straightforward but less accurate method involves measuring droplet diameters from images captured from a CCD. A calibration slide is used in the focal plane of the microscope objective to get the correct scaling factor between camera pixels and the corresponding distance at the focal plane of the objective.

For video and frame capture, three different camera models were used depending on the specifics of the experiment. A Watec colour camera (WAT-250D) was used with visible samples where colour viewing was useful, such as

the trapping and excitation of dyes. A Watec (WAT-902H) is sensitive to infrared wavelengths and so was used for work at 1064 nm. A camera based on a CMOS chip (Basler A601Firewire) was used for rapid measurements due to its high frame rate and adjustable region of interest, as well as being used in the spatial light modulator (SLM) tweezers.

After camera selection, the next consideration for producing a good image for droplet sizing is generating a good level of contrast. This is achieved in our experiments by using a variable fibre-delivered white light source (Thorlabs OSL1) in conjunction with Kohler illumination optics [66]. This system allows for good adjustment of the brightness and illumination to give the required image contrast. The resulting sharp images reduce the uncertainty in the position of edges in the features in the imaging plane.

To ensure particles are in the focal plane and being illuminated correctly, a standard sample side is used. The sample can be moved using an xyz translation mount in the same way as during tweezing experiments. The illumination source can be seen in the centre of the particle being imaged on the camera as a bright spot in the centre. By adjusting the sample height above the objective, the bright spot can be brought into focus on the camera. When the particle is in focus, the diameter of the particle is measured as the diameter of the outermost dark ring in the image [67,68,69].

This same method is used to ensure that the trapping plane for the tweezers is the same as that being imaged. By adjusting the collimation lenses in the tweezers, the light entering the back aperture of the objective can be slightly focussed or de-focussed to adjust the position of the trap above the coverslip. When a trapped particle is in focus, with the bright spot from the illumination in the centre, the trap site is known to be in focus. Any deviation of a trapped particle out of the focal plane of the objective leads to blurring in the image and usually an overestimation in the particle size, assuming the stage micrometer was precisely in focus when calibration took place.

Clearly, optical tweezers are a very useful addition to aerosol analysis with a great deal of potential for novel and detailed studies. With the particulars of aerosol generation and measurement worked out, the characterisation of optical

tweezers for aerosols could take place. These early forays into the optical tweezing of liquid droplets are the subject of the next chapter.

3.8 References

1. Ashkin, A., “Acceleration and Trapping of Particles by Radiation Pressure,” Phys. Rev. Lett. **24**, 156 (1970)

2. Ashkin, A. and Dziedzic, J.M., “Observation of Resonances in the Radiation Pressure on Dielectric Spheres” Phys. Rev. Lett. **38**, 1351. (1977).

3. Ashkin, A. and Dziedzic, J.M., "Feedback stabilization of optically levitated particles," Appl. Phys. Lett. **30**, 202 (1977)

4. Hopkins, R.J. *et al*, “Determination of the size and composition of multicomponent ethanol/water droplets by enhanced raman scattering”, Chemical Physics Letters **380**, 665. (2003)

5. Symes, R. *et al*, “Cavity enhanced droplet spectroscopy: Principles, perspectives and prospects”, Phys. Chem. Chem. Phys. **6**, 474 (2004)

6. Chylek, P. *et al*, “Simultaneous determination of refractive index and size of spherical dielectric particles from light scattering data.” Applied Optics **22**, 2302. (1983)

7. Sandoghar, V. *et al*., “Very low threshold whispering-gallery mode microsphere laser,” Phys. Rev. A. **54**, 1777. (1996)

8. Leach, D.H. *et al*, “Third-order sum-frequency generation in droplets: experimental results,” J. Opt. Soc. Am. B **10**, 34. (1993)

9. Magome, N. *et al*, “Optical Trapping of a Growing Water Droplet in Air”. J. Phys. Chem. B **107**, 3988 (2003)

10. Brooks, S.D. *et al*, “Delequescence Behavior of organic/ammonium sulphate aerosol”, Geophysical Research Letters **29**, 1917 (2002).

11. Kohira, M.I. *et al*, “Optical Levitation of a Droplet under Linear Increase of Gravitational Acceleration,” Chem. Phys. Lett. **414**, 389 (2005)

12. O'Dowd, C.D.; Smith, M.H.; Consterdine, I.E. and Lowe, J.A., “Marine aerosol, sea-salt, and the marine sulphur cycle: a short review,” Atmospheric Environment **31**, 73 (1996)

13. Ansmann, A.; Riebesell, M. and Weitkamp, C., "Measurement of atmospheric aerosol extinction profiles with a Raman lidar," Opt. Lett. **15**, 746. (1990)

14. Ashkin, A. and Dziedzic, J.M**.,** **"**Optical Levitation by Radiation Pressure," Appl. Phys. Lett **19**, 283 (1971)

15. Ashkin, A. and Dziedzic, J.M**.,** **"**Stability of optical levitation by radiation pressure," Appl. Phys. Lett. **24**, 586 (1974)

16. Ashkin, A. and Dziedzic, J.M., "Observation of light scattering from nonspherical particles using optical levitation," Appl. Opt. **19**, 660 (1980)

17. Thurn, R. and Kiefer, W., "Raman-Microsampling Technique Applying Optical Levitation by Radiation Pressure," Appl. Spectrosc. **38**, 78 (1984)

18. Omori, R.; Kobayashi, T. and Suzuki, A., "Observation of a single-beam gradient-force optical trap for dielectric particles in air." Optics Letters **22**, 816 (1997)

19. Qian, S.X.; Snow, J.B.; Tzeng, H.M. and Chang R.K., "Lasing Droplets: Highlighting the Liquid-Air Interface by Laser Emission Science," Science, **231**, 486 (1986)

20. Moon, H.J.; Kim, G.H.; Lim, Y.S.; Go, C.S.; Lee, J.H. and Chang, J.S., "Lasing images from two merging ink-doped liquid droplets," Opt. Lett. **21**, 913 (1996)

21. Acker, W.P.; Leach, D.H. and Chang, R.K., "Third-order optical sum-frequency generation in micrometer-sized liquid droplets," Opt. Lett. **14**, 402 (1989)

22. Tzeng, H.M.; Wall, K.F. and Long, M.B., "Laser emission from individual droplets at wavelengths corresponding to morphology-dependent resonances," Opt. Lett. **9**, 499 (1984)

23. Snow, J.B.; Qian, S.X. and Chang, R.K., "Stimulated Raman scattering from individual water and ethanol droplets at morphology-dependent resonances," Opt. Lett. **10**, 37 (1985)

24. Steiner, B.; Berge, B.; Gausmann, R.; Rohmann, J. and Rühl, E., "Fast in-situ Sizing Technique for Single Levitated Liquid Aerosols," Appl. Opt. **38**, 1523 (1999)

25. Berge, B; Sudholz, K.; Steiner, B.; Rohmann, J. and Rühl, E., “Fast in-situ of single leviated solid aerosols,” Phys. Chem. Chem. Phys. **1**, 5485 (1999)

26. Carleton, K. L.; Sonnenfroh, D. M.; Rawlins, W. T.; Wyslouzil, B. E. and Arnold, S., “Freezing behavior of single sulfuric acid aerosols suspended in a quadrupole trap,” Journal of Geophysical Research **102**, 6025 (1997)

27. Mason, N.J.; Drage, E.A.; Webb, S.M.; Dawes, A; McPheat, R. and Hayes, G., “The spectroscopy and chemical dynamics of microparticles explored using an ultrasonic trap,” Faraday Discuss. **137**, 367 (2008)

28. Azzouz, H.; Alkhafadiji, L.; Balslev, S.; Johansson, J.; Mortensen, N.A.; Nilsson, S. and Kristensen, A., "Levitated droplet dye laser," Opt. Express **14**, 4374 (2006)

29. Renn, M.J.l Pastel, R. and Lewandowski, H.J., “Laser Guidance and Trapping of Mesoscale Particles in Hollow-Core Optical Fibers,” Phys. Rev. Lett. **82**, 1574 (1999)

30. Raman, C.V. and Krishnan, K.S., “A New Type of Secondary Radiation,” Nature **121**, 501 (1928)

31. Twersky, V., "Rayleigh Scattering," Appl. Opt. **3**, 1150 (1964)

32. Cheng, J.X. and Xie, X. S. **,** “Coherent Anti-Stokes Raman Scattering Microscopy: Instrumentation, Theory, and Applications,” J. Phys. Chem. B **108**, 827 (2004)

33. Ray, A.K. *et al*, “Precision of light scattering techniques for measuring optical parameters of microspheres”, Applied Optics **30**, 3974 (1991).

34. Hopkins, R.J.; Symes, R.; Sayer, R.M. and Reid, J.P., “Determination of the size and composition of multicomponent ethanol/water droplets by cavity-enhanced Raman scattering,” Chem Phys. Lett. **380**, 665. (2003)

35. Ashkin A. and Dziedzic, J.M., “Stability of optical levitation by radiation pressure,” Appl. Phys. Lett. **24**, 586 (1974)

36. Hill, S.C. and Benner, R.E. "Morphology-dependent resonances associated with stimulated processes in microspheres," J. Opt. Soc. Am. B **3**, 1509 (1986)

37. Huckaby, J.L.; Ray, A.K. and Das, B., “Determination of size, refractive index, and dispersion of single droplets from wavelength-dependent scattering spectra,” Appl. Opt. **33**, 7112 (1994).

38. Chen, Z.; Taflove, A. and Backman, V., "Highly efficient optical coupling and transport phenomena in chains of dielectric microspheres," Opt. Lett. **31**, 389 (2006)

39. Wolf, J.-P..; Pan, Y.-L.; Turner, G.M.; Beard, M.C..; Schmuttenmaer, C.A.; Holler, S. and Chang, R.K., “Ballistic trajectories of optical wave packets within microcavities,” Physical Review A **64**, 023808 (2001)

40. Garrett, C. G. B.; Kaiser, W. and Bond, W.L., “Stimulated emission into optical whispering modes of spheres,” Phys. Rev. **124**, 1807 (1961)

41. Khaled, E.E.M.; Hill, S.C. and Barber, P.W., “Internal electric energy in a spherical particle illuminated with a plane wave or off-axis Gaussian beam,” Appl. Opt. **33**, 524 (1994)

42. Khaled, E.E.M.; Hill, S.C.; Barber, P.W. and Chowdhury, D.Q., “Near-resonance excitation of dielectric spheres with plane waves and off-axis Gaussian beams,” Appl. Opt. **31**, 1166 (1992)

43. Lin, H.-B. and Campillo, A.J., "Radial profiling of microdroplets using cavity-enhanced Raman spectroscopy," Opt. Lett. **20**, 1589 (1995)

44. Qian, S. and Chang, R.K., “Multiorder Stokes Emission from Micrometer-Size Droplets,” Phys. Rev. Lett. **56**, 926 (1986)

45. Benner, R.E.; Barber, P.W.; Owen, J.F. and Chang, R.K., “Observation of Structure Resonances in the Fluorescence Spectra from Microspheres,” Phys. Rev. Lett. **44**, 475 (1980)

46. Sayer, R.M.; Gatherer, R.D.B., Gilham, J.J. and Reid, J.P., “Determination and validation of water droplet size distributions probed by cavity enhanced Raman scattering ,” Phys. Chem. Chem. Phys. **5**, 3732 (2003)

47. Hopkins, R.J.; Mitchem, L.; Ward, A.D. and Reid, J.P., “Control and characterisation of a single aerosol droplet in a single-beam gradient-force optical trap,” Phys. Chem. Chem. Phys. **6**, 4924 (2004)

48. Eversole, J.D.; Lin, H.B.; Huston, A.L.; Campillo, A.J.; Leung, P.T.; Liu, S.Y. and Young, K., "High-precision identification of morphology-dependent resonances in optical processes in microdroplets," J. Opt. Soc. Am. B **10**, 1955 (1993)

49. Hopkins, R.J.; Howle, C.R. and Reid, J.P., "Measuring temperature gradients in evaporating multicomponent alcohol/water droplets ," Phys. Chem. Chem. Phys. **8**, 2879, (2006)

50. Sageev, G. and Seinfeld, J.H., "Laser heating of an aqueous aerosol particle," Appl. Opt. **23**, 4368 (1984)

51. Tzeng, H.M., Wall, K.F., Long, M.B. and Chang, R.K., "Evaporation and condensation rates of liquid droplets deduced from structure resonances in the fluorescence spectra," Opt. Lett. **9**, 273 (1984)

52. Choi, M.Y.; Chan, C.K. and Zhang, Y.-H., "Application of Fluorescence Spectroscopy To Study the State of Water in Aerosols," J. Phys. Chem. A **108**, 1133 (2004)

53. Sayer, R.M.; Gatherer, R.D.B. and Reid, J.P., "A laser induced fluorescence technique for determining the pH of water droplets and probing uptake dynamics," Phys. Chem. Chem. Phys. **5**, 3740 (2003)

54. Kiraz, A.; Kurt, A.; Dündar, M.A.; Yüce, M.Y. and Demirel, A.L., "Volume stabilization of single, dye-doped water microdroplets with femtoliter resolution," J. Opt. Soc. Am. B **24**, 1824 (2007)

55. Eversole, J.D.; Lin, H. and Campillo, A.J., "Input/output resonance correlation in laser-induced emission from microdroplets," J. Opt. Soc. Am. B **12**, 287 (1995)

56. H Tzeng, H.M., Wall, K.F., Long, M.B. and Chang, R.K., "Laser emission from individual droplets at wavelengths corresponding to morphology-dependent resonances," Opt. Lett., **9**, 499 (1984)

57. Walrafen, G.E.; Fisher, M.R.; Hokmabadi, M.S. and Yang, W.-H., "Temperature dependence of the low- and high-frequency Raman scattering from liquid water," J. Chem. Phys. **85**, 6970 (1986)

58. Lin, H.B. and Campillo, A.J., "cw Nonlinear Optics in Droplet Microcavities Displaying Enhanced Gain," Phys. Rev. Lett **73**, 2440 (1994)

59. Serpenguzel, A.; Chen, G. and Chang, R.K., “Stimulated Raman scattering of aqueous droplets containing ions: concentration and size determination,” Part. Sci. Technol. **8**, 179 (1990).

60. Thurn, R. and Kiefer, W., "Structural resonances observed in the Raman spectra of optically levitated liquid droplets," Appl. Opt. **24**, 1515-1519 (1985)

61. Preston, R.E.; Lettieri, T.R. and Semerjian, H.G., “Characterization of single levitated droplets by Raman spectroscopy,” Langmuir **1**, 365 (1985)

62. Pasternack, L; Fleming, J.W. and Owrutsky, J.C., “Optically seeded stimulated Raman scattering of aqueous sulfate microdroplets,” J. Opt. Soc. Am. B **13**, 1510 (1996)

63. Di Leonardo, R. *et al*, “Parametric Resonance of Optically Trapped Aerosols,” Phys. Rev. Lett. **99**, 010601 (2007)

64. Fieberg, C., “Experimental Investigation of Droplet Evaporation Under Hot Temperature and High Pressure Conditions,” Thesis. (2003)

65. Renz, U., 2001. Vorlesungsumdruck Technische Verbrennung. Lehrstuhl für Wärmebertragung und Klimatechnik, RWTH Aachen

66. Schulz, G.; Schwider, J.; Hiller, C. and Kicker, B., "Establishing an Optical Flatness Standard," Appl. Opt. **10**, 929 (1971)

67. Malot, H. and Blaisot, J.-B., “Droplet Size Distribution and Sphericity Measurements of Low-Density Sprays Through Image Analysis,” Particle & Particle Systems Characterization **17**, 146 (2000)

68. Glover, A.R.; Skippon, S.M. and Boyle, R.D., "Interferometric laser imaging for droplet sizing: a method for droplet-size measurement in sparse spray systems," Appl. Opt. **34**, 8409 (1995)

69. Barnes, M.D.; Lermer, N.; Whitten, W.B. and Ramsey, J.M., “A CCD based approach to high-precision size and refractive index determination of levitated microdroplets using Fraunhofer diffraction,” Rev. Sci. Instrum. **68**, 2287 (1997)

Chapter 4

Tweezing of Liquid Aerosols

4.1 Introduction

Optical trapping [1] has found use in a wide range of research including manipulation of biological samples [2] and particle dynamics [3]. Although the majority of these involve the trapping of colloidal samples, there has been a recent interest in the ability to optically trap aerosol particles. The analysis of individual droplets in air is of specific interest to atmospheric chemistry, respiratory medicine and analytical chemistry in general. Although the characteristics of clouds have been analysed in bulk [4], there has been difficulty in obtaining samples of individual or small ensembles of atmospheric particles. Optical tweezers are ideally suited to this task, and with the use of dynamic tweezers created with Spatial Light Modulators (SLMs) [5] or Acousto-Optic Modulators (AOMs) [6], the physical interactions between particles can be observed in detail.

Although the optical tweezing of liquid droplets had been described by our colleagues in Bristol [7], the emphasis of these experiments was on spectroscopy [8]. Some of the physical properties of aerosol traps were still undocumented, including the effect of using infrared light. A comparison between tweezing at 532 nm and 1064 nm was of interest due to the availability of inexpensive suitable sources at infrared wavelengths. There were concerns that the increased absorption of water at 1064 nm would make it unsuitable for tweezing droplets. If successful, 1064 nm would be available as a cheaper alternative to 532 nm for our aerosol experiments, as well as reducing the cost of tweezers systems in the future

4.2 Considerations for Aerosol Tweezing

Our 1064nm tweezers consisted of a single beam passed through a 100x Nikon oil immersion microscope objective in an inverted configuration. The optical loss through the objective was found to be 0.27 using the dual objective method [9]. In our tweezers, the objective formed a focus approximately 30 µm above the coverslip. A glass sample chamber was placed above the coverslip to confine the aerosol sample which was sprayed in through a small hole in the chamber. An xyz translation stage was used to adjust the position of the coverslip and the height of the trap focus.

To reduce the effects of evaporation of the sample to the outside atmosphere, small pieces of paper were soaked in the sample liquid and placed in the cell. These reservoirs maintained the environment around the trap at a high humidity, increasing the droplet lifetime in the cell. The four different liquid samples were used in the trap characterisations were 2 % salt water solution, ethanol, dodecane and 20 % glycerol solution. These gave a good range in refractive index, density and evaporation rate, but with similar viscosities which could be nebulised successfully.

Our aerosol samples were created using a nebuliser consisting of an ultrasonic vibrating membrane, generating droplets in the 2-10 µm diameter range at the trapping site, with a mean diameter of approximately 5 µm as stated by the manufacturer [10]. However, the output varies significantly with any particular unit [11], so our nebuliser had to be tested. A distribution of droplet sizes was estimated by measuring droplet diameters in the focal plane of our setup with the CCD and white light illumination as described below (see figure 2.4).

Imaging of the aerosol samples were achieved using the same microscope objective as the trap. A dichroic mirror was used to reflect the laser light at 45 degrees, but allow the visible light from the backlight to pass to a CCD camera. When determining the size of a trapped droplet, the diameter was measured from an image capture. When the droplets are in focus, the backlight is imaged as a bright spot in the centre. The droplet diameter is then measured as the diameter of the outer dark ring [12] of the droplet image (see figure 4.1).

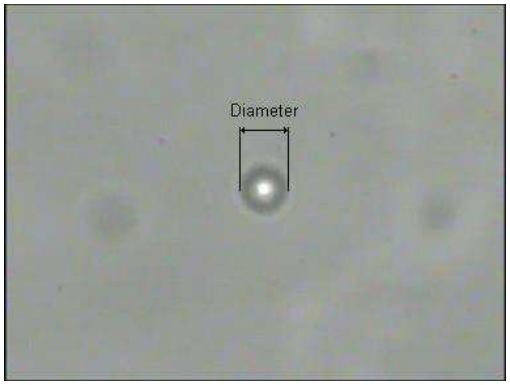

Figure 4.1 Image of a typical trapped droplet in the focal plane of the microscope objective, imaged onto a CCD.

One of the concerns raised in the optical trapping of liquid aerosol particles was the potential effect of heating due to absorption at the trapping wavelength. Absorption spectra of liquid samples were taken on a Perkin Elmer Lambda 35 UV/VIS spectrometer. For water, an absorbance value (A) of 0.07 was found at 1064 nm. This wavelength is at a well documented, but nevertheless fortuitous trough in the spectrum (see graph 4.2).

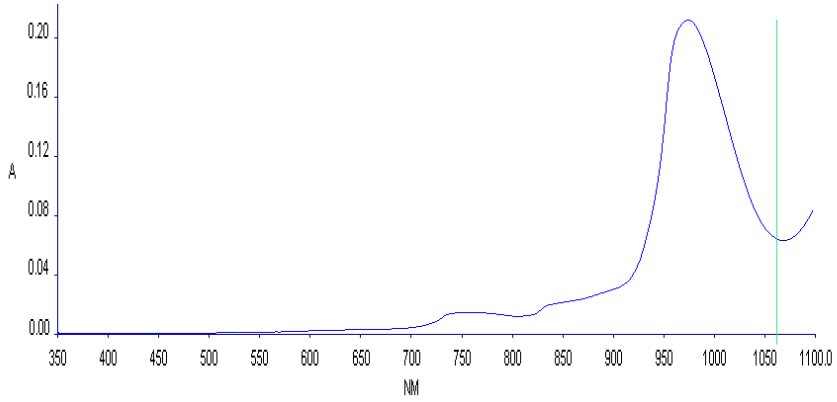

Graph 4.2: Graph of absorbance (A) with wavelength (in nm) for water, clearly showing a dip in absorbance for wavelengths near 1064 nm.

An excellent current resource discussing the spectroscopic absorption of water is provided by Martin Chaplin at the London South Bank University [13]. Absorption at a given wavelength is measured in terms of an absorption coefficient, $\mu_a(\lambda)$, in units cm^{-1}, given by

$$\frac{I}{I_0} = e^{-\mu_a(\lambda)l}, \qquad [4.1]$$

where I_0 is the incident light intensity, I is the transmitted intensity and l is the path length through the sample in cm. The absorbance is given by

$$A = -Log_{10}(\frac{I}{I_0}) \qquad [4.2]$$

and rearranging gives

$$\mu_a(\lambda) = \frac{\ln(10^A)}{l}. \qquad [4.3]$$

Suggesting that the absorbance of 0.07 measured for the water sample at 1064 nm, with a path length of 1 cm, is equivalent to an absorption coefficient, μ_a at 1064 nm of 0.16 cm^{-1}. This value is in reasonable agreement with the literature, which gives a value of 0.12 cm^{-1} at 1060 nm [14, 15].

Another experimental concern was the build up of the sample liquid on the coverslip. Any droplets which land on the coverslip near the trapping region can distort the trap site formed above. In the case of water, Sodium Dodecyl Sulphate (SDS) was used as a surfactant to reduce the surface tension. This had the effect of causing the surface water to form a uniform layer below the trap, reducing the distortion. This allowed the coverslip to be used for longer periods without the need for drying or replacing. The lack of a surfactant for the other sample liquids meant that dry spots had to be found and the coverslip had to be replaced more often. However, the majority of the time consuming fine tuning of the apparatus and experimental technique was performed using salt water samples for this reason.

4.3 Evaporation

From our initial droplet trapping studies, it was evident that evaporation was taking place with in the cell. Droplets would rapidly adjust to an equilibrium size (see figures 4.3 and graph 4.4) after their initial capture, indicating that the humidity at

the trap site was slightly less than 100 % and that the salt added to the droplets was lowering the vapour pressure with increasing concentration as expected.

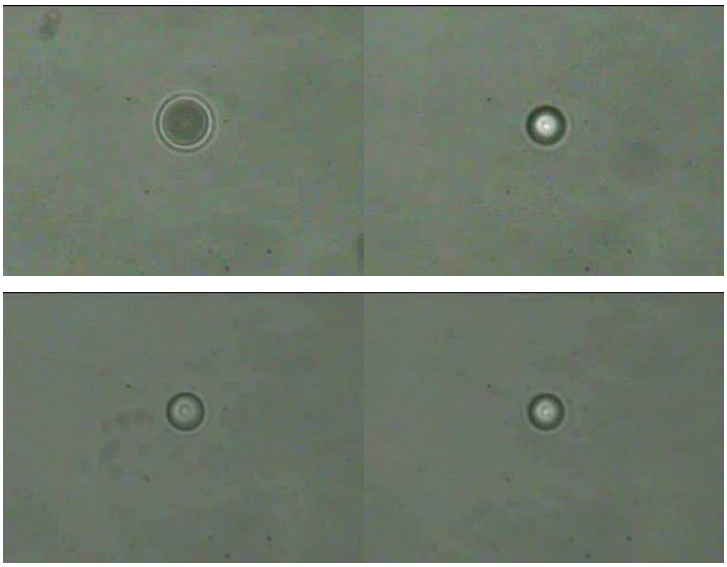

Figure 4.3: The evaporation of a droplet (see graph 4.5 below). From top left to bottom right: (a) At initial trapping 0 s, (b) After the initial equilibrium point (2 s), (c) After 80 s, (d) At 120 s.

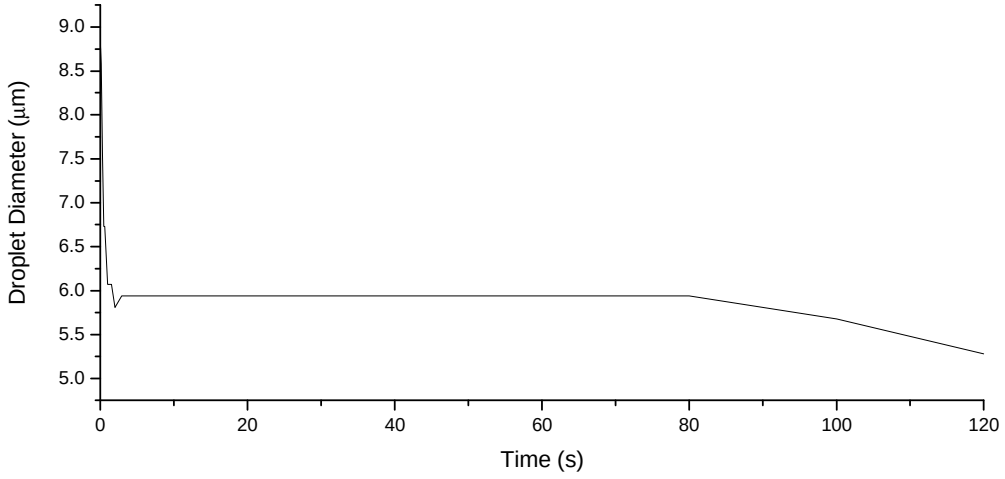

Graph 4.4: Evaporation of a 2% salt water solution in a poor sample cell with a reservoir. The droplet evaporates to equilibrium within the first 2 seconds and remains at a stable size until the reservoir runs out and the droplet begins evaporating again. The droplet leaves the trap after 120s.

The evaporation of the droplets could be estimated by comparing frames at different times after the initial capture. This visual method of measuring the changing droplet diameter could then be compared to the more accurate CERS measurements taking place in Bristol with the use of a spectrometer [7]. Bristol confirmed that measuring the droplet circumference using the outermost dark ring on the image is the correct visual method assuming the trapped particle is properly in focus. Getting a measure of the evaporation characteristics allowed cell designs to be tested, compared and optimised. Different liquids and initial salt concentrations could similarly be assessed.

The evaporation of the droplets in our aerosol samples is a major factor in many of the experiments described in this thesis. The basis of the modelling is the work of Renz, as translated by Fieberg [16]. This style of evaporation model is described as "film theory" and describes the surface of a droplet in terms of an energy and mass balance [17]. Under steady-state conditions, the change in droplet diameter can be described as

$$\left(\frac{d}{d_0}\right) = 1 - \frac{8\lambda_L}{\rho_{liquid} c_p d_0^2} \ln(1+B)t \qquad [4.4]$$

Where λ_L is the thermal conductivity of the liquid, c_p is the specific heat of the sample, d_0 is the initial droplet diameter, t is time and B is a "mass transfer number" given by

$$B = \frac{\xi_S - \xi_\infty}{1 - \xi_S} \qquad [4.5]$$

where ξ_S is the vapour concentration at the surface of the droplet and ξ_∞ is the vapour concentration "at infinity" (i.e. the environment). Under steady-state conditions, ξ_S is given as

$$\xi_S = \frac{1}{1 + \left(\frac{P_{atm}}{Ps} - 1\right)\frac{Mair}{Ms}} \qquad [4.6]$$

where P_{atm} is the atmospheric pressure and P_s is the partial pressure at the surface. In the case of water, the variation of the saturation vapour pressure with temperature near room temperature is well known and given by the Arden Buck Equation [18]

$$P_S = 6.1121 \exp\left(\frac{(18.678 - \left(\frac{T}{234.5}\right)T}{257.14 + T} \right) \qquad [4.7]$$

with T in degrees Celcius and Ps in hPa. Given that the environment surrounding the droplet can be considered saturated, this gives a value of Ps=23.373 hPa at a temperature of 20 °C (our room temperature). The effect of relative humidity is illustrated in graph 4.5 (below).

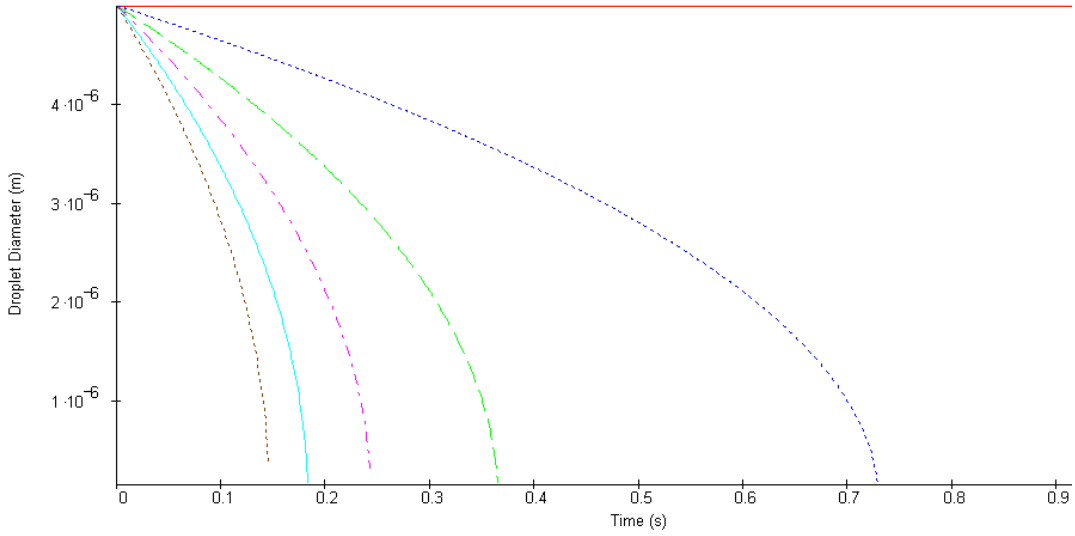

Graph 4.5: Water droplet diameter against time for various humidities.. From an initial diameter of 5µm, the individual plots show the evaporation for different relative humidity in the surrounding environment, from 100% (red) to 99% (brown) in steps of 0.2%.

The other issue of interest is the evaporation rate for different liquids. First of all, the addition of salt to our water droplets reduces the vapour pressure. We can model this effect by taking the salt concentration into account for the increased heat capacity (c_p) and the decrease in vapour pressure (modified Goff-Gratch Equation) of our droplet. The heat capacity for salt is 1.23 $Jg^{-1}K^{-1}$ compared to 4.186 $Jg^{-1}K^{-1}$ for water and so it cannot be neglected. As the droplet decreases in volume due to evaporation, the concentration of salt present increases. This allows the droplet to reach an equilibrium diameter which depends on the humidity of the local environment.

4.4 Measuring Captured Droplet Diameter with Trap Power

4.4.1 Experimental Method

After optimising the cell and trapping beam, the first experiment conducted with the aerosol tweezers was designed to gain experience in trapping aerosols while making some useful basic measurements. During initial testing with the aerosol tweezers, trapping was found to be more successful within specific laser power ranges. The aim was therefore to examine the diameter of droplets trapped at specific trapping powers (after optical losses were taken into consideration).

The aerosol sample consisted of salt water at a concentration of 20g/litre (2 % mass per unit volume). It was nebulised with the handheld Omron U22 nebuliser and delivered into the sample cell via a narrow nozzle. The most effective cell for this experiment was found to be a modified Petri dish with a drilled inlet hole. Pieces of paper soaked in water were used to maintain a high humidity within the cell.

A series of droplets were captured for a range of different trapping powers. A droplet was only counted as trapped if it remained trapped in the tweezers for longer than 10 seconds. The cell was kept in an over-saturated condition, and the diameter of each droplet was measured visually from screen captures. Because the aerosol conditioning (flow and nozzle) was kept the same for each measurement, the likelihood of successful trapping varied for each size due to the distribution of aerosol diameters. Viable samples were obtained frequently in the 5 µm range, but the process could take many minutes for significantly smaller and larger droplets. Under optimum trapping conditions, with an abundance of appropriately sized aerosols, stable trapping usually took place after a few short bursts from the nebuliser (within 30 s).

4.4.2 Experimental Results

For the purposes of this comparison of droplet size with trapping power, the initial droplet diameter was measured. This ignored any evaporative processes taking place within the sample. As was expected, initially larger droplets were more stable at higher trapping powers and could not be trapped at low powers. This is just a function of the intensity required for levitation of the droplet. Once trapped, droplets would then evaporate to an equilibrium diameter, which varied due to the concentration of salt in the droplet. A larger initial droplet contains more saltwater and therefore has a higher concentration of salt as the droplet diameter decreases towards the minimum.

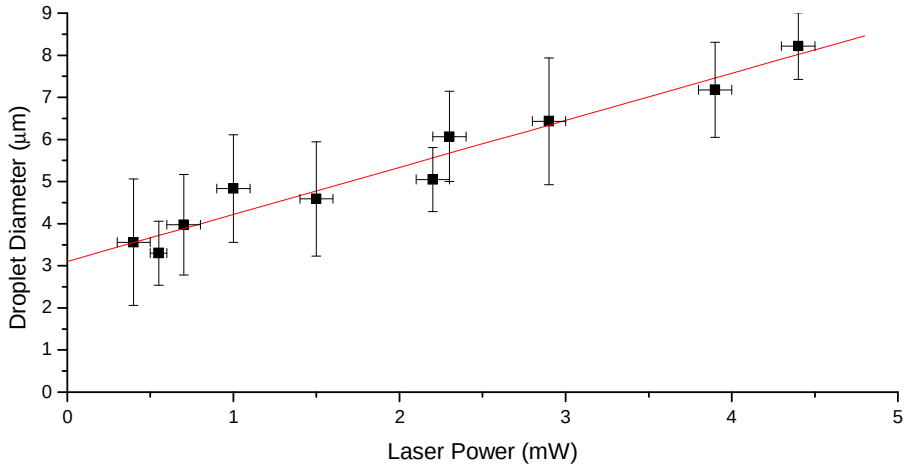

Graph 4.6. Initial diameter of captured 2 % salt water droplets with optical power at the trap site.

The increase of mean initial droplet size with trapping power is clear from graph 4.6. The error bars denote the standard error in the droplet diameters recorded for each data point. An unexpected result of this experiment was that the minimum size of trapped droplet also increased with trapping power. In other words, small particles could be trapped at low powers, but not at higher ones. The reason for this was not immediately obvious, although it may be a consequence of the relatively low effective NA of our traps in air. The difference in refractive index between the

coverslip (n≅1.5) and the trapping medium (n≅1) results in a critical angle at the interface of approximately 42 degrees, as opposed to approximately 62 degrees for a colloidal sample. Therefore, any photons arriving from a greater angle than 42 degrees are reflected at the boundary. This means that the effective NA of the microscope is approximately 1 when tweezing in air where

$$NA = n\sin\theta_a \qquad [4.7]$$

n is the refractive index of the glass optics in the objective lens and θ_a is the acceptance angle. This is compared to a potential NA of over 1.3 for liquid based tweezers with a suitable objective [13].

To get a quantitative measure of this effect, I have plotted the difference between the gradient force and scattering force below (see graph 4.7). This is based on calculations made by Ashkin in 1992 [19]. Although both the scattering and gradient forces increase with increasing objective NA, the gradient force increases at a faster rate up to an NA of about 1.35.

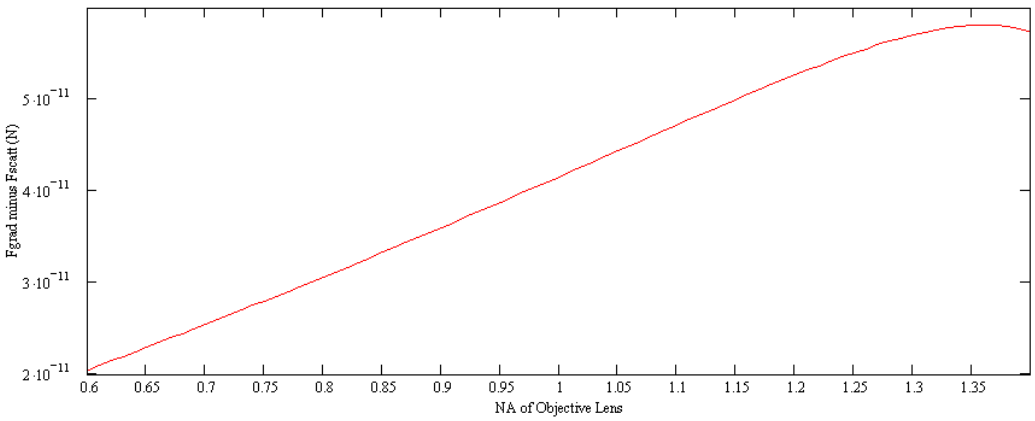

Graph 4.7 Graph of $F_{grad} - F_{scatt}$ (the difference between the gradient and scattering forces) acting on a 5µm colloidal polystyrene sphere versus the numerical aperture (NA) of the objective lens for an optical power of 5mW.

This reduced effective NA weakens the gradient force relative to the scattering force, pushing particles away unless they are already close to the focus. However, this effect becomes more difficult to quantify with the addition of a water layer of variable thickness above the coverslip. Experimental observation suggests that a

uniform water layer between the glass:air boundary improves trapping conditions. Although individual surface droplets distort the beam, the addition of surfactant to the coverslip results in a layer of water of uniform thickness across the surface. This layer of intermediate refractive index also decreases the height of the focus above the coverslip and water layer as the experiments progress. The buildup of water limits the lifetime of experiment and the layer must be removed when the layer becomes prohibitively thick (on the order of 10 µm).

4.4.3 Sample size selection

Although this experiment was designed to test different trapping conditions and gain familiarity with the tweezing of liquid aerosols, the results were somewhat surprising. The clear trend of an increasing minimum droplet size with trapping power provides a crude method for size selection of droplets. Although growing droplets [20] is an elegant way to provide droplets of a very specific size, the ability to select droplets within a size range from a random sample is of particular interest to atmospheric chemistry and would be a likely feature of any “lab-in-a-box” system.

Another experiment conducted to this end was an attempt at optically sorting falling droplets according to their diameter. Such optical sorting techniques have proven successful in the field of microfluidics [21] where optical fields can be used to direct particles according to size. In our case, a simple collimated beam was used to exert a constant optical force on a falling stream of droplets (see graph 4.8 and figure 4.9). Assuming a uniform light field, the number of photons impinging on a droplet scales with the cross-sectional area, or the radius squared. The mass of the droplet scales with the volume, or the radius cubed. Measuring the angle of droplet deflection in the optical field would therefore give a measure of the size of the droplet, with smaller droplets being deflected by a greater angle. Beyond the field, the droplets would ideally fall vertically, resulting in a grading of droplet size with horizontal displacement.

Although this optical fractionation of droplets with optical intensity appeared simple in theory, actual implementation was more difficult. Creating a uniform flow was

the first difficulty and even with cloud chambers and apertures, the collision of droplets with cell walls and each other made it difficult to ensure droplets remained at their selected diameter. Similarly, evaporation effects would vary depending on the environment local to a droplet, causing droplet diameters to vary through the cell. Convection currents were also visible in the cell, deflecting the droplet flow.

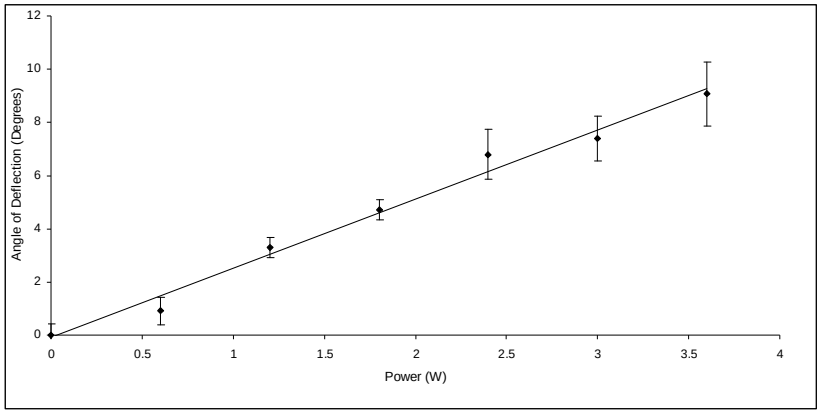

Graph 4.8 Deflection angle of water droplet flow with laser power incident in the horizontal direction.

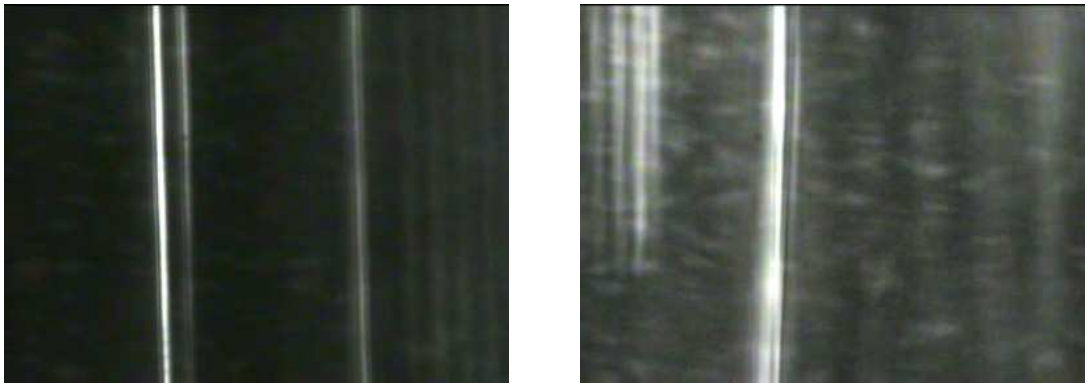

Figure 4.9 Falling droplets passing through the beam. Bright lines are droplets lying close to the focal plane of the imaging optics. Left: at 0.5 W, Right: at 3 W of optical power.

Perhaps with extensive engineering, this basic method could be used to separate droplets according to diameter. However, care would have to be taken to reduce evaporation, convection currents, maintain a uniform flow and find a way to prevent droplets from colliding and coagulating during fractionation. Slowing the droplet flow and increasing the interaction time between the droplets and the optical field would increase any fractionation effects. A more useful approach may be to generate

interference fringes in the same manner as microfluidic particle sorting techniques [21], but again, a more uniform flow would be required as well as a longer interaction time with the optical field. Again, precise engineering would be required to produce a sufficiently slow moving uniform flow through the cell. Therefore it did not appear to be an approach worth pursuing further and optical tweezers remain our most successful means to select droplets within specific size ranges.

4.5 Comparing 1064nm and 532nm Tweezers

To answer the question as to whether laser heating was a factor in the effectiveness of our aerosol traps, a direct comparison of tweezers performance at 532 nm and 1064 nm was made. From the spectrum of water taken previously (Graph 4.3), it was clear that the absorption at 1064 nm was significantly higher than at 532 nm. A direct comparison of the absorption coefficients gives a value of 0.00032 cm^{-1} at 525 nm and 0.12 cm^{-1} at 1060nm [14,15]. Later work by Querry established a value of 0.000647 cm^{-1} at 532.8 nm [22, 23].

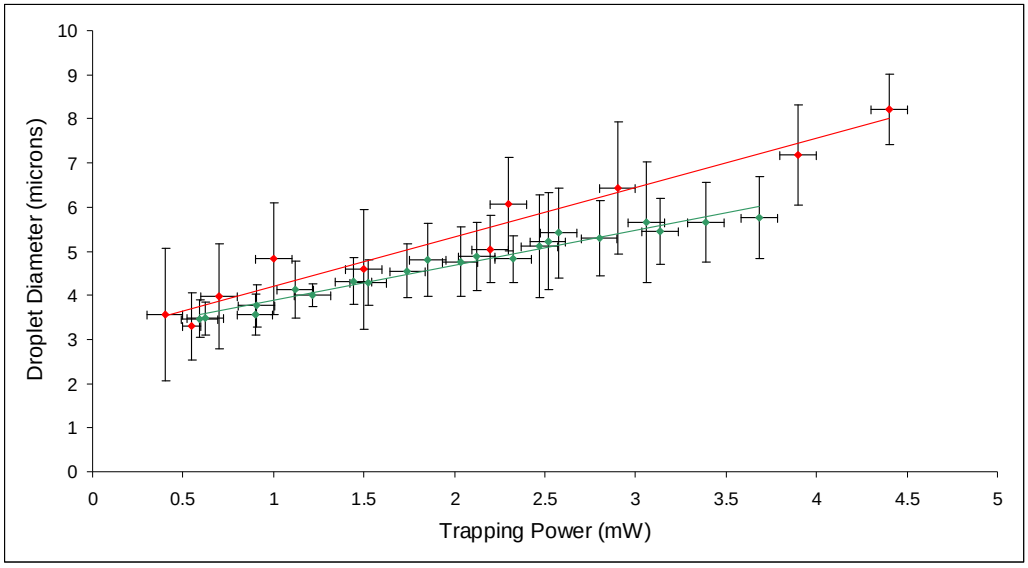

Graph 4.10: Comparison of initial droplet diameter with trapping power at 532 nm (green line) and 1064 nm (red line). The error bars indicate the range in diameter of droplet trapped at each trapping power sampled.

The measurement of the diameter of trapped droplets with trapping power was performed at 532 nm and compared to the data for 1064 nm (see graph 4.10). In this case, a spatial light modulator (SLM) was used to generate an array of trap sites, allowing multiple samples to be trapped in parallel. However, an identical microscope objective (Nikon E-plan NA=1.3) was used and the trapping power was measured at the trap site, so a direct comparison is valid. In addition, an identical Petri-dish cell with soaked paper reservoirs was used for both. The Q-values obtained for both traps were very similar with Q=0.22 for 532 nm and Q=0.25 for 1064 nm. This may account for the small difference between the two wavelengths in graph 4.10.

The other assumption made in both cases was that the humidity at the trap site was the same and slightly less than 100% so that the effects of additional heating could be observed. The rapid evaporation of droplets observed within the first second of trapping showed that this was the case. Using the absorption spectrum for water (graph 4.3 above), the coefficients of absorption, μ_a (see equation 4.3), are 0.16 cm^{-1} at 1064 nm and 0.0036 cm^{-1} at 532 nm.

Another possible factor in the difference between the 532 nm and 1064 nm case is the refractive index dispersion in water. These values are 1.336 and 1.325 respectively [24]. Similarly, although the objectives used were identical, they were designed for visible wavelengths and their performance at 1064 nm is likely to be different than at 532 nm. When additional sources are available, preferably one tunable over a large range, a more detailed investigation of these affects can take place. However, this experiment accomplished its main goal of studying the properties of aerosol tweezers at 1064 nm. Providing the sample cell is at a high humidity, the increase in vapour pressure associated with the additional laser heating of the sample in the near infrared is not prohibitive.

4.6 Trapping and Identification of Different Samples

4.6.1 Trapping Different Liquids

The aim of this experiment was to successfully trap different liquids and investigate the possibility of using aerosol tweezers as a means of differentiating between liquids according to refractive index. The method used was identical to that described in Section 4.4.1 for the optical tweezing of water aerosol, only the reservoirs contained the sample liquid instead of water. As with the water experiment, the absorption spectra for ethanol, dodecane and a 20 % glycerol solution were obtained to assess if heating due to the laser was likely to be a problem.

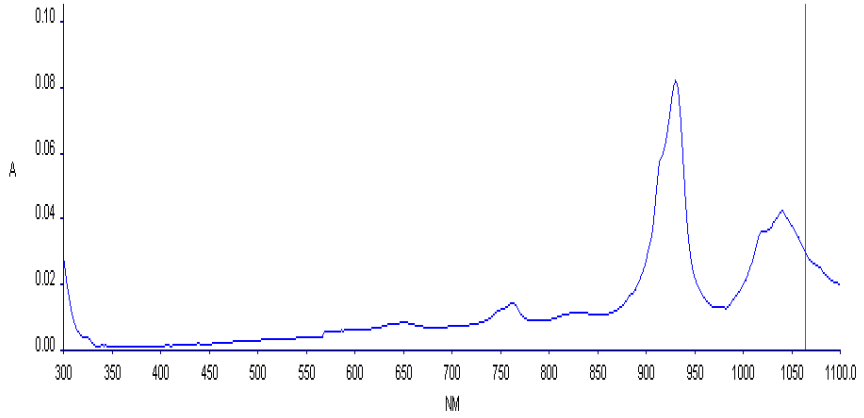

Graph 4.11: Absorbance with wavelength for dodecane with 1064 nm marked with a vertical line.

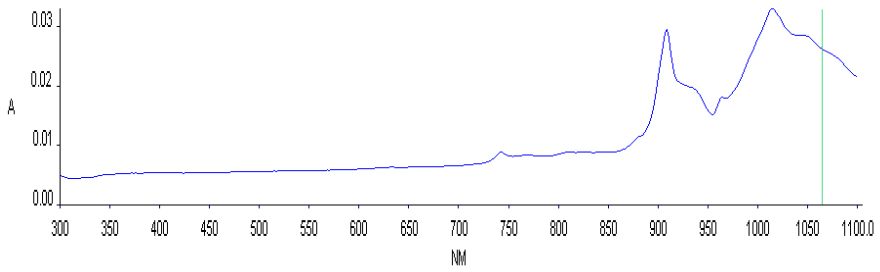

Graph 4.12: Absorbance with wavelength for ethanol with 1064 nm marked by a vertical line.

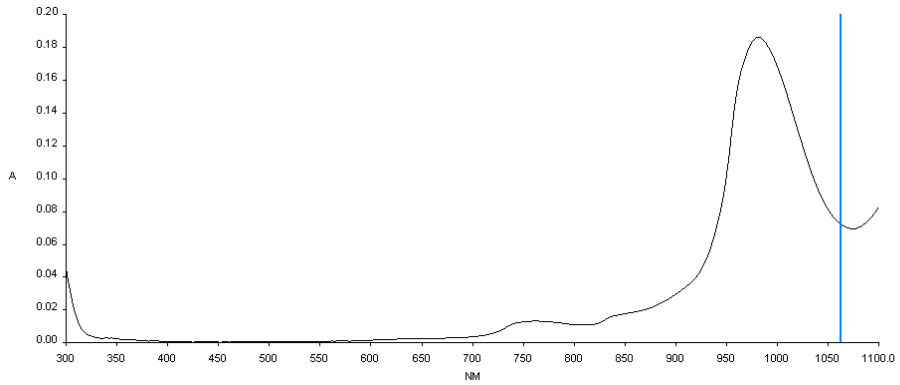

Graph 4.13: Absorbance with wavelength for 20 % glycerol, with 1064 nm marked by a vertical line.

The absorption at 1064 nm for dodecane (graph 4.11) and ethanol (graph 4.12) was found to be approximately the same (A=0.03), corresponding to an absorption coefficient, μ_a(1064 nm), of 0.07 cm^{-1}. The subsequent measurement of a 20 % glycerol solution (see graph 4.13) yielded a similar absorbance spectrum to pure water, with additional absorption in the UV, which was irrelevant to the experiment. Given the success of the previous water droplet trapping experiments in the infrared and the lower absorption in ethanol and dodecane, laser heating could be ruled out as a problem for these liquids.

The first set of experiments was conducted to compare the relationship between trapping power and initial droplet size for each liquid. The second series of experiments used a simple axial Q measurement to determine whether differences in refractive indices could be detected with aerosol tweezers.

Simultaneous measurements were made on the trap lifetimes for each sample liquid. All the liquids tested were stable in the optical trap, so evaporation was the main factor on droplet lifetime. Salt water droplets could remain in the trap for several hours using our sample cell and samples have been trapped overnight at Bristol in their sealed chamber. Pure water droplets evaporate at a rate dependent on the initial droplet size, how sealed the sample cell is and the size of the sample reservoir. If the trapping power is decreased as the droplet evaporates, lifetimes of approximately 20 minutes are attainable. Dodecane droplets can be trapped for up to 40 minutes and

ethanol for up to a minute if the aerosol cloud is dense, or up to 10 seconds for a typical short burst. Ethanol droplets can be trapped for longer periods by having a continuous aerosol flow, such as that provided by a pneumatic nebuliser, or by adding a salt which is soluble in ethanol. These techniques have the effect of reducing the rate of evaporation either by maintaining a supersaturated environment or by reducing the vapour pressure. Both of these techniques are used in other experiments covered later in this thesis.

4.6.2 Droplet Sizing with Trapping Power for Different Liquids

As with the optical trapping of water droplets, the initial droplet diameter was measured for each sample to reduce the effect of evaporation. Each point on the graph (see graphs 4.14 to 4.17) corresponds to a mean value measured for at least five separate trapped droplets. Droplet samples were more common in the 4-6 μm range, due to the size distribution of aerosol from the nebuliser. The error bars in the y-axis correspond to the standard error in the mean value obtained for each point. The error bars in the x-axis are from the reading error in the half wave-plate mount used to adjust the output power of the laser.

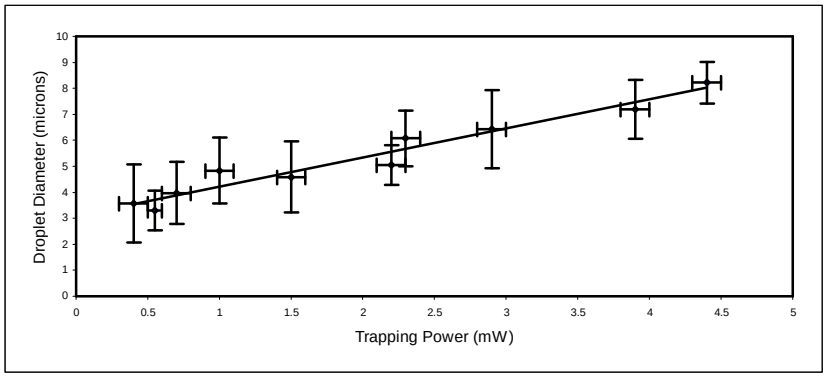

Graph 4.14: Initial diameter of captured water droplets with optical power at the trap site.

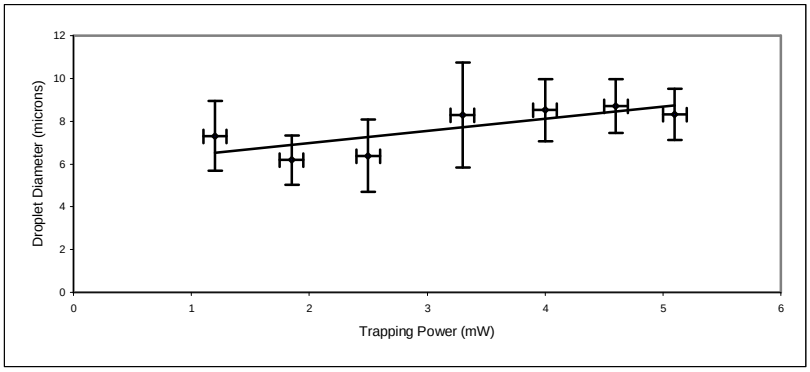

Graph 4.15: Initial diameter of captured droplets of ethanol with optical power at the trap site.

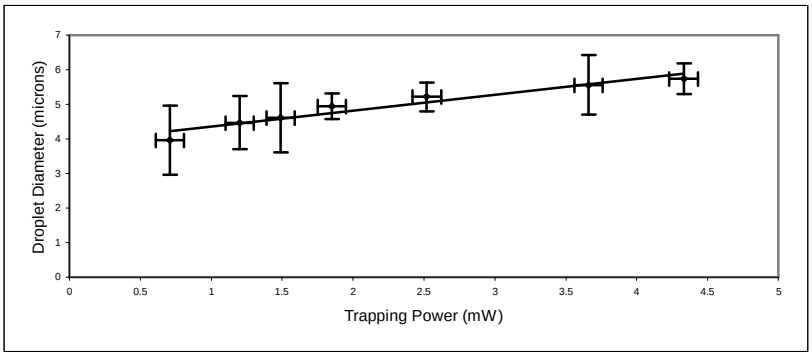

Graph 4.16: Initial diameter of captured droplets of 20 % glycerol solution with optical power at the trap site.

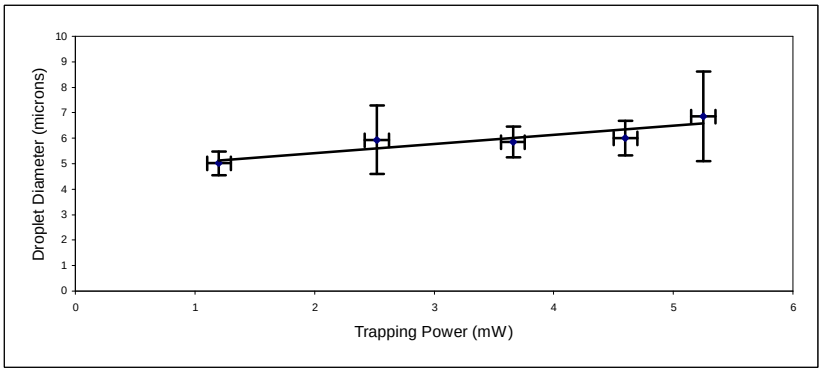

Graph 4.17: Initial diameter of captured droplets of dodecane with optical power at the trap site.

The data series obtained for the dodecane sample is smaller than for the other liquids. This is due to the samples damaging a soft plastic component in the nebuliser, rendering it inoperable. Again, there was a linear relationship between the trapping

power required and the mean diameter of trapped droplets. This makes sense given that the mass (contributing to downforce) increases with a^3 and the cross-sectional area of the droplet (contributing to upforce) with a^2. As before, initially larger droplets were more stable at higher trapping powers and could not be trapped at low powers for all the liquids tested. This is in agreement with work conducted by our colleagues at Bristol [7].

To remove the effect of the density of each liquid in the gradient, the graphs were plotted in terms of droplet mass against trapping power. The mass was obtained simply by multiplying the density of each sample by the volume of each droplet.

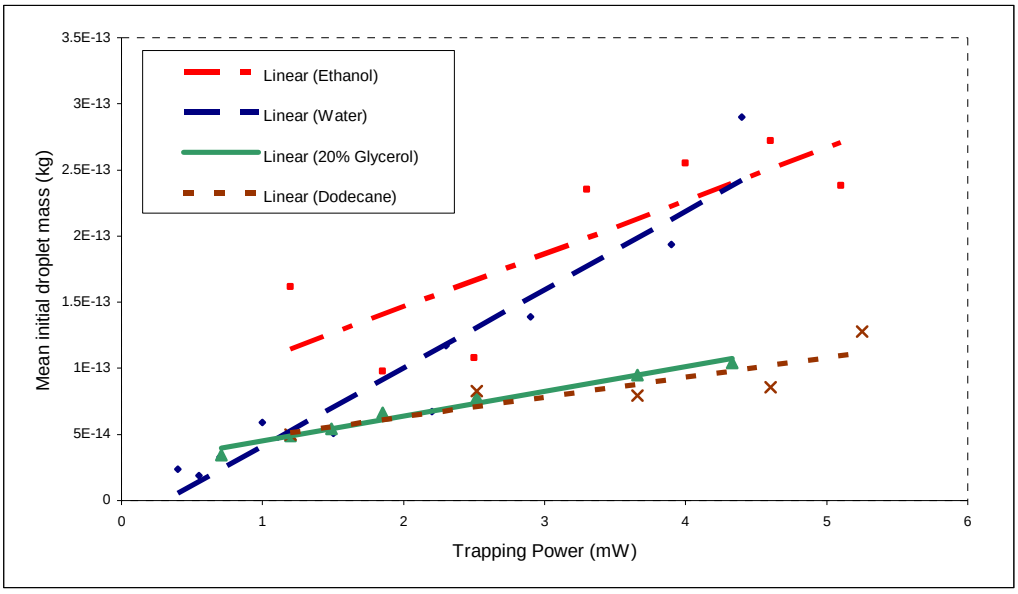

Graph 4.18: Initial mass versus trapping power of captured droplets for all samples.

Chemical Name	Refractive Index	Density (kg/m^3)	Viscosity (cP)
20% Glycerol	1.38	1050.8	1.12
Water	1.324	998.2	1.02
Ethanol	1.36	789.2	1.26
Dodecane	1.42	754.6	1.38

Table 4.19: Relevant properties of the liquids used in the droplet manipulation studies

Sample Details	Refractive Index	Gradient of mass versus power line
Water (1064 nm)	1.324	5.92×10^{-14}
Ethanol	1.36	4.00×10^{-14}
20% Glycerol Solution	1.38	1.87×10^{-14}
Dodecane	1.42	1.50×10^{-14}

Table 4.20 Gradients of mass versus power with refractive index for the different sample liquids

There is a trend of a decreasing gradient with increasing refractive index (see graph 4.18), as was found in the comparison of 532 nm and 1064 nm tweezers (Section 4.5). This suggests that with an increased refractive index (see tables 4.19 and 4.20), smaller droplets can be trapped even at higher trapping intensities. Using the same model as detailed earlier (see equations 2.4 and 2.5), the effect of refractive index on the gradient and scattering forces can be found. Assuming a droplet of 5 µm in diameter, the difference between gradient force and scattering force is as follows (graphs 4.21 and 4.22).

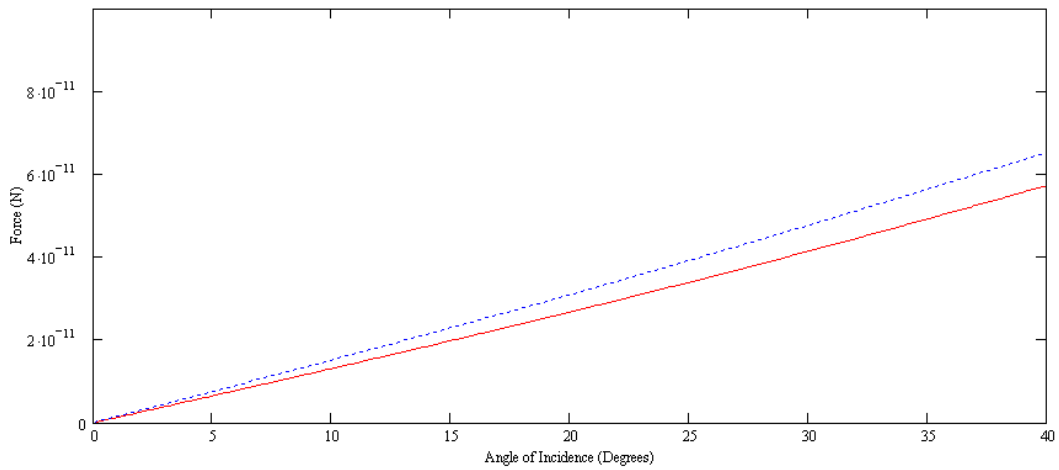

Graph 4.21 Plot of gradient force for 5 µm droplets in a 5 mW beam with the refractive index of water (solid red line) and dodecane (dotted blue line). There is a marked increase in gradient force with refractive index using this model.

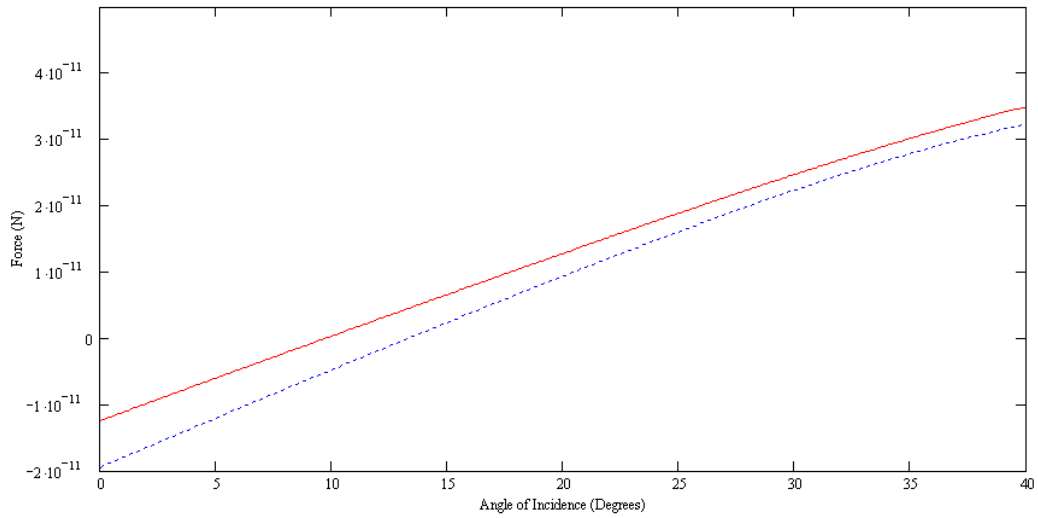

Graph 4.22 Plot of gradient force minus scattering force with angle of incidence for 5 µm droplets in a 5 mW beam with the refractive index of water (solid red line) and dodecane (dotted blue line). The gradient force only becomes stronger than the scattering force when light is focussed at an angle of more than 12° by the objective lens.

Therefore, increasing the refractive index of the droplet increases the scattering force more than the gradient force. While this explains why the droplets of higher refractive index require more optical power, it still doesn't explain the difference in gradients. In other words, why can't we trap smaller droplets of water at higher trapping intensities? The increased gradient force may allow smaller droplets to be tweezed at higher powers, although one would expect the corresponding increase in scattering force to make this more difficult.

Although the data set is limited, there is a trend here which is worth further investigation. Other potential samples with different refractive indices included chloronaphthalene (n=1.6), di-chloro methylbenzene (n=1.54) and pure glycerine (n=1.473). However, these liquids weren't compatible with our nebulisers, either due to high viscosity or a highly solvent nature. In addition, the output volume of the nebuliser varied slightly between liquids, with a decreased flow for ethanol. This, in addition to evaporation effects in the nebuliser nozzle, may have effected the size distribution of droplets in the sample cell.

Using a nebuliser constructed completely from glass and metal may solve the problem of generating aerosol samples of the more reactive chemicals and more viscous liquids with a large range of refractive indices. A specifically engineered sample cell with pneumatic inlets may provide more consistent results, allowing the characterisation of liquids. However, the need to make a large number of measurements to obtain the required data means that spectrometry remains a far more useful method of chemical identification.

4.6.3 Measuring Axial Trapping Efficiency, Q

In order to more directly compare the tweezers for different samples, the axial trapping efficiency for each liquid was measured. This involved trapping droplet samples in the tweezers and reducing the trapping power until the droplet fell out of the trap. Direct imaging with a CCD was used to measure the diameter of droplets in the trap. The trapping efficiency, Q_{axial} [25], is a measure of the momentum transferred from the beam to the trapped particle in the axial direction, as described in section 2.3.1 (see equation 2.7).

Multiple measurements over a range of droplet sizes were made (see table 4.23) and the uncertainty in Q is the standard error in each data set. The evaporation rate in ethanol droplets made it difficult to make a confident measure of the axial trapping efficiency. The uncertainty in the dodecane value is due to a smaller data set due to nebuliser damage, as described in the previous sub-section.

Chemical Name	Refractive Index	Q
2% Salt Water	1.324	0.28 ± 0.05
Ethanol	1.36	0.22 ± 0.11
20% Glycerol	1.38	0.27 ± 0.03
Dodecane	1.42	0.42 ± 0.08

Table 4.23 Table of axial trapping efficiency and refractive index for the different liquids tweezed.

The axial trapping efficiency for dodecane, with a Q of 0.42, was significantly higher than the other liquid samples. This value is also in agreement by work conducted at published by Ward, Longhurst and Quirke [26]. Although they used a microscope objective with an NA of 1.4, trapping in air would have limited the effective NA to a value of approximately 1 as with our system. However, the refractive index contrast between droplets and the air medium is greater than that of typical colloidal particles. This results in a higher trapping efficiency. The trapping efficiency for our salt water solution is significantly lower than that achieved by Magome *et al* [20]. However, their value of Q=0.46 was achieved using a more complex trapping cell, allowing the droplet to grow slowly to a maximum volume at the trap site. The 20 % glycerol solution gave a very similar result to the salt water droplets, despite having a slightly higher refractive index.

4.7 Conclusion

This chapter has described many of the initial aerosol tweezing experiments. These include the development of many of the experimental basics used and the characterisation of aerosol tweezers. Evaporation of droplet samples was considered in detail taking into account cell design, the use of sample liquid reservoirs and aerosol flow conditioning.

The effect of wavelength on the trapping of 2 % salt water droplets was investigated, measuring the mean diameter of droplets trapped over a range of laser powers in identical sample cells at 532 nm and 1064 nm. The performance was comparable between both wavelengths, despite stronger absorption in water droplets in the infrared. This confirmed that a relatively cheap laser source at 1064 nm could be used for much of the subsequent work. In addition, the size of droplets trapped in the tweezers was found to be dependent on the trapping power. This provides some control over the size of a captured droplet from a random environmental sample of aerosol.

The droplet size versus trapping power measurements were repeated for a range of liquids including ethanol, glycerol solution and dodecane. Other liquids were successfully trapped optically, but weren't suitable for long-term use or gave inconsistent aerosol flow when used with our nebulisers. The axial trapping efficiency of our basic tweezers setup was measured for each of our sample liquids and our result for dodecane agrees with that already published. This work refined our methods and techniques, allowing us to proceed to more ambitious experiments and break new ground. One of the major challenges for our work was the successful trapping of solid aerosol particles, the subject of the next chapter.

4.8 References

1. Ashkin, A.; Dziedzic, J.M.; Bjorkholm, J.E. and Chu, S., "Observation of a Single-Beam Gradient Force Optical Trap for Dielectric Particles." Opt. Lett. **11**, 288 (1986)

2. Ashkin, A. and Dziedzic, J.M., "Optical trapping and manipulation of viruses and bacteria," Science **235**, 1517 (1987)

3. Berg-Sørensen, K. and Flyvbjerg, H., "Power spectrum analysis for optical tweezers," Rev. Sci. Instrum. **75**, 594 (2004)

4. Ansmann, A.; Riebesell, M. and Weitkamp, C., "Measurement of atmospheric aerosol extinction profiles with a Raman lidar," Opt. Lett. **15**, 746. (1990)

5. Melville, H. *et al*, "Optical Trapping of three-dimensional structures using dynamic holograms". Optics Express **11**, 3562 (2003)

6. Perch-Nielsen, I.; Rodrigo, P. and Glückstad, J., "Real-time interactive 3D manipulation of particles viewed in two orthogonal observation planes," Opt. Express **13**, 2852 (2005)

7. Hopkins, R.J.; Mitchem, L.; Ward, A.D. and Reid, J.P., "Control and characterisation of a single aerosol droplet in a single-beam gradient-force optical trap," Phys. Chem. Chem. Phys. **6**, 4924 (2004)

8. Sayer, R.M.; Gatherer, R.D.B.; Gilham, R.J.J. and Reid, J.P., "Determination and validation of water droplet size distributions probed by cavity enhanced Raman scattering," Phys. Chem. Chem. Phys. **5**, 3732 (2003)

9. Svoboda, K. and Block, S.M., "Biological Applications of Optical Forces," Annual Review of Biophysics and Biomolecular Structure **23**, 247 (1994)

10. Omron U22 manual, available at http://www.medro.ro/manuals/U22.pdf

11. Dennis, J.H.; Pieron, C.A. and Asai, K., "Aerosol Output and Size from Omron NE-U22 MicroAir nebulizer," Poster at http://www.omronb2b.com/img/pdf/fil_427.pdf

12. Malot, H. and Blaisot, J.-B., “Droplet Size Distribution and Sphericity Measurements of Low-Density Sprays Through Image Analysis,” Particle & Particle Systems Characterization **17**, 146 (2000)

13. A useful website on water, “Water Structure and Science” maintained by Martin Chaplin at London South Bank University http://www.lsbu.ac.uk/water/vibrat.html

14. Hale, G.M., Querry, M.R., "Optical constants of water in the 200 nm to 200 µm wavelength region," Appl. Opt. **12**, 555 (1973)

15. http://omlc.ogi.edu/spectra/water/data/hale73.dat See Appendix B

16. Fieberg, C., “Experimental Investigation of Droplet Evaporation Under Hot Temperature and High Pressure Conditions,” (Diploma Thesis with translation of work reported in German by Renz, U. (2001).) (2003)

17. Kincaid, D.C., Langley, T.S., “A Water Droplet Evaporation and Temperature Model,” ASAE Transactions **32,** 457 (1969)

18. Buck, A. L., New equations for computing vapor pressure and enhancement factor, J. Appl. Meteorol. **20**, 1527 (1981)

19. Ashkin, A., “Forces of a single-beam gradient laser trap on a dielectric sphere in the ray optics regime,” Biophys. Journal **61**, 569 (1992)

20. Magome, N.; Kohira, M.I.; Hayata, E.; Mukai, S. and Yoshikawa, K., “Optical trapping of a growing water droplet in air,” J. Phys. Chem. B **107**, 3988 (2003)

21. MacDonald, M.P.; Spalding, G.C. and Dholakia, K., “Microfluidic sorting in an optical lattice,” Nature **426**, 421 (2003)

22. Querry, M.R.; Wieliczka, D.M. and Segelstein, D.J., "Water (H_2O),"Handbook of Optical Constants of Solids II,” 1059 (1991)

23. http://omlc.ogi.edu/spectra/water/data/querry91.dat See Appendix B

24. Harvey, A.H.; Gallagher, J.S. and Sengers, J.M.H.L., “Revised Formulation for the Refractive Index of Water and Steam as a Function of Wavelength, Temperature and Density,” J. Phys. Chem. Ref. Data **27**, 761 (1998)

25. Wright, W.H.; Sonek, G.J. and Berns, M.W., "Parametric study of the forces on microspheres held by optical tweezers," Appl. Opt. **33**, 1735 (1994)

26. Ward, A.D.; Longhurst, M. and Quirke, N., “Optical trapping of airborne hydrocarbon droplets from on oil mist,” Journal of Experimental Nanoscience **1**, 75 (2006)

Chapter 5

Tweezing of Solid Aerosols

5.1 Introduction

Since their creation in 1986 [1] optical tweezers have evolved to become an important tool in a wide range of different applications [2,3]. The ability to isolate single or multiple [4] aerosols and analyse their size and composition is of particular interest, especially in the field of atmospheric chemistry [5]. Until recently the study of the behaviour of solid aerosols has been neglected but is of obvious importance for such studies [6,7]. Optical tweezers provide not only the means to hold the particle but also the ability to precisely measure its displacement fluctuations due to the Brownian stochastic force of the surrounding fluid. Comparing the dynamics of identical particles trapped in the two very different media, air and water, allows differences between the two trapping regimes to be investigated.

5.2 Experimental Considerations for Solid Aerosols

The use of optical tweezers combined with a sensitive light detector as a means of precise measurement of force and position was initially an extension of laser differential interferometry [8]. Early work by Ghislain *et al* [9] utilized a photodiode to measure amplitude changes in the transmitted light from the trapping beam to monitor the motion of a tweezed particle, generating a power spectrum. Further work using this technique showed that sensitivities greater than 10 times that of a scanning force microscope could be achieved [10]. We

have chosen this back focal pane interferometry technique [11] to study the effect of trapping medium on the Brownian motion of a trapped silica sphere.

The basis of our position sensitive detector system is a quadrant silicon photo-diode (Hammamatsu S5980). The signal from each quadrant is amplified and processed electronically on a circuit based on previous work by Allersma *et al* [12] and outputted to a digital acquisition board (PCI-6014E). With proper calibration to an appropriate zero-point, the relative signals of the four separate photodiode elements provide an accurate displacement at a frequency of up to 25 MHz. The variance in the signal is then analysed in terms of angular frequency and then displayed as a power spectrum. However, thought must be given in order to find a suitable model for the dynamics of our tweezed sample.

Such a trapped particle can be treated as a damped harmonic oscillator whose position is described by the Langevin equation;

$$m\ddot{x}(t) + \gamma_0 \dot{x}(t) + \kappa x(t) = \sqrt{(2k_B T \gamma_0)}\eta(t) \qquad [5.1]$$

where m is particle mass, $\gamma_0 = 6\pi\eta a$ is the stokes drag, κ is the optical trap stiffness, η the medium's viscosity, a, the particle radius and $\sqrt{(2k_B T \gamma_0)}\eta(t)$, the Brownian stochastic force at temperature, T [13]. When trapping in air the inertial term is significant and must be included. The inertial effects can be observed to be

$$S_x^{inert}(\omega) = \frac{k_b T}{\pi\kappa} \frac{\Omega_0^2 \Gamma_0}{\left(\omega^2 - \Omega_0^2\right)^2 + \Gamma_0^2 \omega^2} \qquad [5.2]$$

where $\omega_0 = (\kappa/m)^{0.5}$ and $\Gamma_0 = \gamma_0/m$. The gradient of the power spectrum tail is characteristic of the degree of damping in the system, falling of with ω^{-4} for an underdamped system and ω^{-2} for an over damped system [14, 15]. A more complete description of the methods can be found in Section 2.2.3 of this thesis.

To make a direct comparison between the aerosol and colloidal cases, a simple means of loading the tweezers was required. Although Omori et al [16] succeeded in tweezing glass spheres; we have been unable to replicate their

results. Our attempts have included several versions of a vibrating coverslip method, similar to that of Omori and even earlier work by Ashkin used for loading levitation traps with solid particles. The technique involves using piezoelectric transducers placed underneath a coverslip and driven to varying degrees to force particles into an optical trap in the focal plane of a non-inverted microscope objective above. However given initial failure, the surface of the slide was imaged from the side using a long working-distance objective (Mitutoyo 50X LWD). This allowed us to gauge the effectiveness of our efforts. The most successful samples contained a large range of diameters, which may have prevented packing of spheres on the surface. This suggests that coating the surfaces in such a way as to limit Van de Waals forces may be a necessary

Another approach to this loading problem may be to have the optical axis and microscope objective arranged horizontally. However, this would result in gravity acting at right angles to the trap, resulting in forces which are non-symmetric around the optical axis. Instead, we suspend our sample in ethanol and use a commercial medical nebuliser unit to spray it into a glass chamber into which a standard inverted single beam gradient force trap is focused. Although the chamber decreases the evaporation rate of the residual ethanol, it helps to shield the trap from surrounding air currents, increasing stability.

5.3 Proof of Concept

Initial development of the sample cell, aerosol delivery and tweezing methods was conducted on a 1064 nm tweezers system (see figure 5.1), without the QPD and associated imaging system. The tweezing power in this case was provided by a 2 W CW ytterbium fibre laser, used in combination with a polarising beamsplitter and half-wave plate to adjust the power at the objective as well as neutral density filters to reduce the maximum output power to 100 mW.

The beam, which had been expanded using a telescope arrangement to ensure the back aperture of the microscope objective was slightly overfilled [16], passed through a 100x Nikon E Plan oil-immersion microscope objective (NA=1.25). The chamber was placed on a thickness one coverslip on top of the objective, with the focus forming approximately 10 microns above.

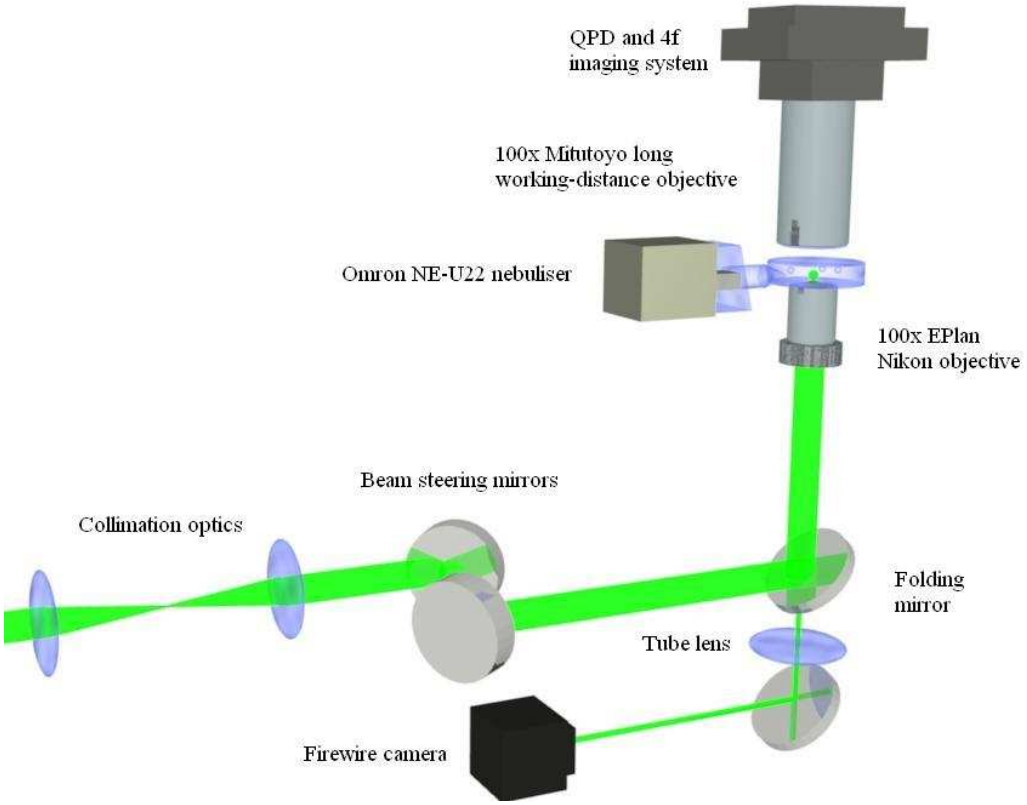

Figure 5.1. Experimental setup for solid particle tweezing. The main feature for this experiment being the addition of the QPD and long-working distance objective. Otherwise, the construction is as described in section 2.2.4.

Our method of generating solid aerosol particles is an extension to our liquid aerosol system, utilizing an Omron MicroAir NE-U22. This model of commercial nebuliser uses a vibrating ultrasonic mesh to generate droplets with a mass median aerodynamic diameter (MMAD) of 4.9 µm. The spacing of the mesh is approximately 3 µm, so passing solid particles of a similar and smaller size range is possible. By suspending silica spheres in ethanol at a suitable concentration, the solid particles can then be nebulised in the ethanol medium. By designing a sample chamber which is relatively open to the environment

(see figure 5.2), the ethanol component of the spray evaporates rapidly and is removed from the silica spheres either by the time they arrive at the trap, or within a few seconds, depending on the quantity of ethanol and design of the cell.

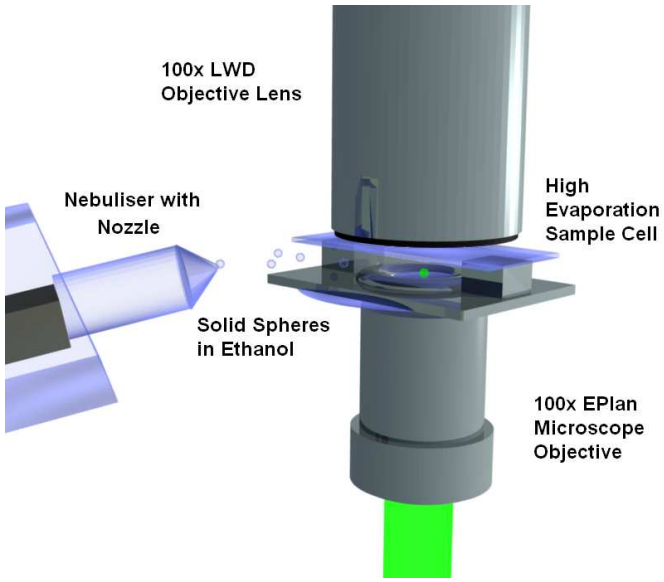

Figure 5.2. Spraying into the high evaporation rate sample cell using the Omron U-22 nebuliser and a cell designed for high evaporation rates.

As has been mentioned, the design of the sample cell is fairly critical to the successful trapping of spheres. It is generally a competition between evaporation rates and isolation from disruptive air currents in the local environment. Our most successful cell design consisted of a well in the centre to shield the region nearest the trapping site. A microscope slide was placed on top of the lower section with 5 mm spacers to provide central vents and also an optical window to allow scattered light from the sample to be collected by the long-working distance condenser objective above.

As with other aerosol trapping experiments [17], the “conditioning” of the aerosol flow is important. We tested a range of nozzle attachments to provide a useful sample flow rate. For our particular nebuliser, the most effective nozzle is shown in detail in figure 3. The solid component of the flow also had to be considered. By testing the number of solid particles deposited on a coverslip over a given time interval, we found that longer tubes or sharp angles

in the flow conditioner restricted the number of solid particles contained in the final aerosol. This is a particular issue in pneumatically driven nebulisers, where the airflow generates a very rapid initial flow. In our preliminary efforts to extend our size range beyond the 3 µm limit set by our handheld nebulisers, pneumatic nebuliser designs seemed to be the most promising for generating larger solid aerosol samples. However, this is essentially an engineering issue and perhaps more suitable options exist.

Another important issue is keeping the solid particles separated in solution. Before each experimental session, the suspended samples were placed in an ultrasonic bath for 5 minutes. This helped to prevent clogging the ultrasonic mesh with the larger particles and gave a higher proportion of individual silica spheres in the resulting aerosol. Although pairs of trapped spheres were trapped for short periods of time, they were not stable.

Silica spheres of 1.86 µm and 3.01 µm diameters were successfully tweezed and held for several minutes in the sample cell at a constant trapping power several times. The axial trapping efficiency, Q, was measured for these sphere sizes (see table 5.3) by first tweezing the spheres, then reducing the optical power until the particles fell out. The trapping powers were measured at the trap site and Q is the axial trapping efficiency, given by

$$Q = \frac{(\rho_s - \rho_m)V_s gc}{n_m} \qquad [5.3]$$

where ρ_s is the density of the sphere, ρ_m is the density of the medium, V_s is the sphere volume, g is the acceleration due to gravity, c is the speed of light and n_m is the refractive index of the medium. The measurement was also made once for 2.47 µm particles, although it could not be repeated. A 0.97 µm particle was trapped for approximately 3 seconds at a power of 200 µW, which was an insufficient time to make a measurement, but the trapping power is included in table 5.3 for completeness. In addition, larger silica spheres of diameter 4.32 µm were trapped for several seconds at a power of 3 mW. However, this size of particle was too large for our small nebuliser, and a pneumatic nebuliser using compressed air (CompAir NE-C28-E) was used.

Unfortunately, the airflow generated by this nebuliser model made trapping unstable and detailed Q measurements impossible.

Diameter (µm)	Initial trapping power (mW)	Minimum trapping power (mW)	Q_{axial}
0.97	0.2 (for 3 seconds)	Unstable	Unstable
1.86	0.6	0.10 ± 0.02	0.19±0.04
2.47	0.8	0.25± 0.06	0.26± 0.06
3.01	1.2	0.29± 0.03	0.28± 0.03
4.32	3 (for 3 seconds)	Unstable	Unstable

Table 5.3. Q_{axial} measurements for aerosolised silica spheres at 1064 nm. Although 0.97 µm and 4.32 µm spheres were observed in the trap, the duration was insufficient to perform the measurement.

With a successful proof of concept, the method was tested on the 532 nm tweezers with a QPD detector system.

5.4 Direct Comparison of Colloidal Solids and Solid Aerosols

5.4.1 Experimental Design

The tweezers were generated using 532 nm light from a c.w. 4 W Laser Quantum Finesse laser. The samples were imaged from below using the same microscope objective and a dichroic mirror which was reflective at 45 degrees at 532 nm and highly transmissive for the white light illumination. Video was captured using a Basler A602f Firewire camera. A Mitutoyo long working distance 100x objective (NA=0.55) was used to image light from the trapping plane onto the QPD via a 4f imaging system. A higher numerical aperture collecting lens would have been desirable [14] but from those available this provided the best compromise between NA and providing enough space

(working distance = 13 mm) for our cell design. The small currents produced by the QPD were sent, via shielded cables to reduce any interference from external sources, to amplification electronics containing a 50 kHz anti-aliasing filter. In order to further still reduce the background noise detected by the QPD the laser was always used at >30% capacity with power control achieved by using a pair of half wave plates with polarizing beam cubes. The first split the beam for two different experiments and the second controlled power for this experiment alone.

The ability to trap and perform measurements on solid aerosols has, up until now, been difficult to achieve. Previous methods of trapping solid aerosol particles [16] used a piezoelectric element to vibrate a microscope slide covered with silica spheres. These particles were observed to bounce and get trapped using conventional non-inverted optical tweezers, focused just above the sample plane.

With our method for tweezing solid particles, the particles often enter the trapping region surrounded by an ethanol shell which quickly evaporates (see figure 5.4). As with liquid aerosols, successful tweezing is dependent on the laser power in the trap. Even once a sphere was trapped, only small increases could be made to the power before it became unstable, typically around 50 %. Once the correct power range was selected, trapping events occurred on an average of once every 15 minutes. This time depended on the concentration of spheres in the sample, the mixing and separation of the spheres by ultrasound and the trajectory and timing of the bursts from the nebuliser to avoid knocking out a trapped particle through the accumulation of further aerosols in the trap. Also, the coverslip requires frequent replacement due to the accumulation of particles on the surface.

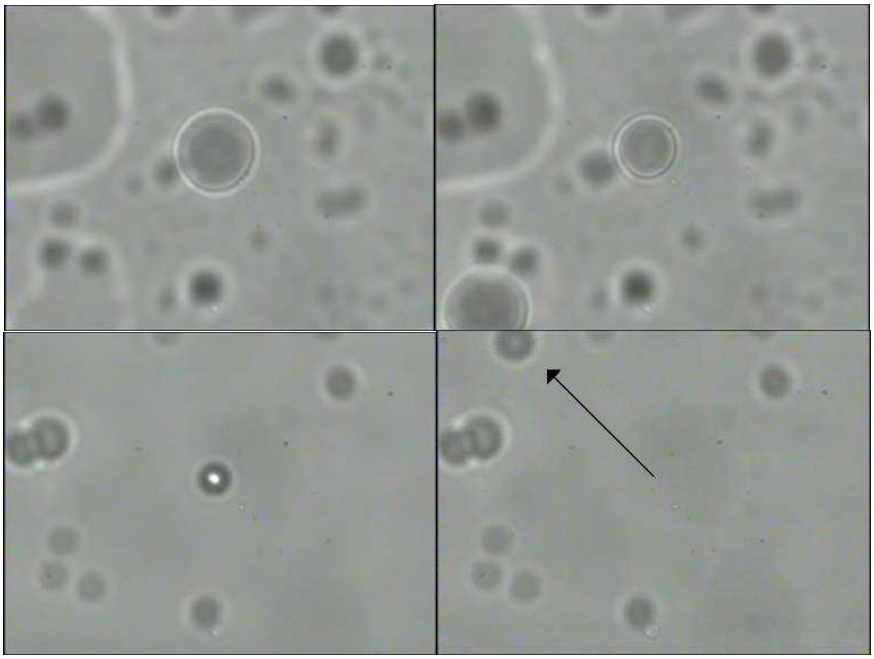

Figure 5.4. Trapping of a 3.01 µm silica sphere in ethanol at 1064 nm. From top left to bottom right: (a) 0 s, the particle is trapped and ethanol can be seen surrounding the particle and on the surface of the slide below; (b) after 0.3 s, the ethanol shell surrounding the sphere has started to evaporate; (c) after 10 s, the liquid has completely evaporated; (d) the particle is deliberately knocked out of the trap after a minute by blocking the beam.

For our comparison study between the trapping behaviour of airborne and colloidal spheres, we chose silica spheres as our solid aerosol. Mathematical modelling suggests that the higher refractive index of polystyrene spheres would make them more difficult to trap in air. We were also limited by the physical design of our nebuliser, so spheres of diameter 1.86 µm and 3.01 µm were used. Silica spheres of diameter 0.97 µm and 2.47 µm were similarly tested, but we were unable to trap these stably in the 532nm trap. The reason for this is unknown to us at present, but may be possible with an improved nebuliser or sample cell design.

For the colloidal measurements, only the sample cell differed. Dilute samples of the spheres in de-ionised water were placed in spacers sandwiched by thickness 1 microscope coverslips. Care was taken to ensure only one particle was being tweezed at a time. For all the following results the diode signal was

sampled at 50 kHz for 4 seconds. When fitting, the data was first binned into units of 50, then, in air we performed the fit between 10 Hz and 10 kHz. When fitting for the water medium data we only fit between 10 Hz and 5 kHz. This is due to the high frequency "tail" not fitting the theoretical Lorentzian profile. For the purposes of our measurements the roll-off frequency was more important and so the fit was made to provide a better match for the lower frequency region of the power spectrum and the data above 5 kHz was omitted. This disagreement between the theoretical and experimental power spectra is due to hydrodynamic friction effects which become significant for small particles at higher frequencies. This hydrodynamic correction will require additional modelling for future work in this area.

Clearly the sensitivity of the position detection system will differ when trapping in an air medium as opposed to a water medium. Therefore to make a comparison between the dynamics of the two systems we must calibrate the detector signals. Conventional methods could be very difficult to implement in an air medium. Moving a fixed bead over a known distance through the laser beam waist is not a good replica of experimental conditions. Oscillation of the sample stage to produce a known drag force on the trapped particle would also be difficult to implement in an air medium [18], and both methods need expensive equipment. There are techniques that use AODs to produce known oscillations of the trapping beam to calibrate the system for the particle currently in the trap, which could be implemented in future airborne trapping systems [19].

In this work we are not concerned with high precision and for simplicity we calculate the detector sensitivity, β, from an uncalibrated voltage power spectrum $S^v(f) = \omega^2 S(f)$ by use of the plateau reached for $\omega >> \omega_c$ in the function $\omega^2 S^v(f)$. For the underdamped case, where inertia is included, it is clear that we must multiply the voltage power spectrum by ω^4 to obtain a similar plateau in $\omega^4 S^v(f)$. We find the detector sensitivity, β_{inert}, to be

$$\beta_{inert} = \sqrt{P_v m / 2 k_B T \Gamma_0} \,. \qquad [5.4]$$

We find β_{inert} and β_{over} for each individual power spectrum allowing us to calibrate the spectrum into units of nm^2Hz^{-1}.

Wishing to make direct comparison, attempts were made to trap in water with the small amount of power needed in air. Although tweezing was possible the corner frequencies were so low they resided in the region of mechanical noise and provided "poor fits". Instead the particles were tweezed with 100 times the power used in air and as shown in table 5.5, κ is given in units of $pN\mu m^{-1}mW^{-1}$.

Medium	Water	Air
Viscosity (Pa.s)	1E-3	1.8E-5
Density (kgm^{-3})	1000	1
Refractive Index	1.33	1.00

Table 5.5. Comparison of the relevant properties of the water and air media, viscosity, density and refractive index.

5.4.2 Experimental Results

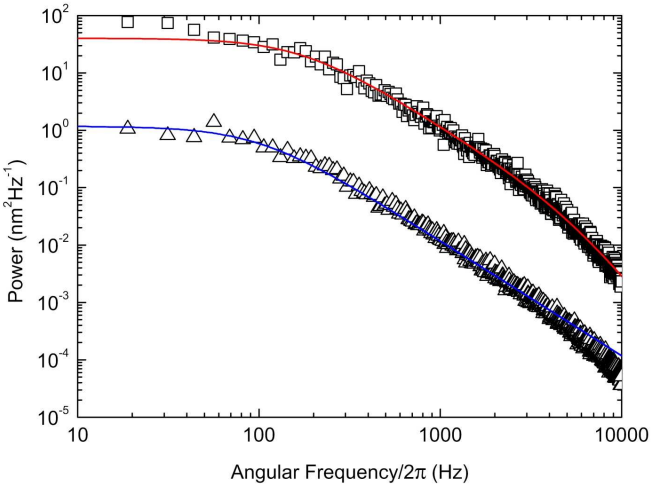

Graph 5.6: Power spectrum for 1.86 µm silica spheres in air (red line) and water (blue line)

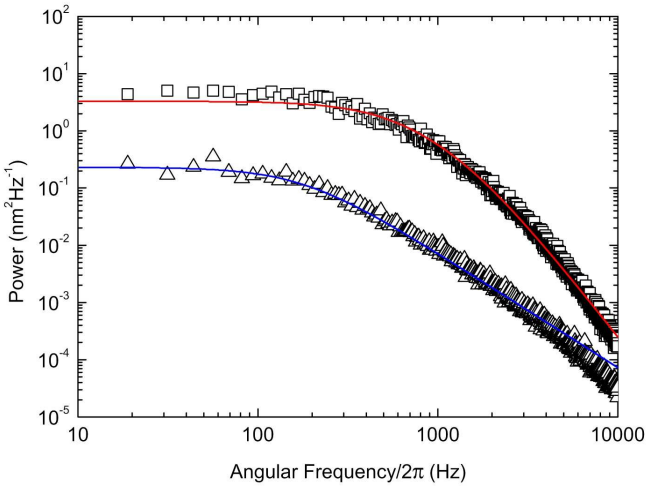

Graph 5.7: Power spectrum for 3.01 µm silica spheres in air (circles) and water (triangles). The red line is a fit to the airborne data using equation X and fitting between 18 and 10000 Hz. The blue line is a fit using equation Y and fitting between 18 and 5000 Hz.

Diameter (µm)	Trapping power in water	Trap stiffness in water ($pN\mu m^{-1}mW^{-1}$)	Trapping power in air	Trap stiffness in air ($pN\mu m^{-1}mW^{-1}$)
1.86	25mW	0.88 ± 0.04	0.25mW	2.02 ± 0.08
3.01	130mW	0.49 ± 0.02	1.3mW	1.50 ± 0.05

Table 5.8: Table of results, displaying trap stiffness for 1.86 µm and 3.01 µm diameter spheres in both water and air.

The first thing to note with the graphs 5.6 and 5.7 above, is the difference in power between the red and blue lines, corresponding to air and water trapping media respectively. A comparison of this power in units of nm^2Hz^{-1}, shows that the magnitude of the lateral movement of optically trapped airborne particles is greater than for identical colloidal samples. This observation makes sense when you consider the density of the media in each case. With only one tenth of the particle density in any one direction, one would expect the mean free path of the silica bead in air to be significantly longer than in water. Likewise, the effect of Brownian motion is stronger for the smaller 1.86 µm

bead. Of course, the optical force acting on the silica bead is the other major factor in the generated power spectrum.

Firstly, the corner frequency is far more obvious in the aerosol case (see table 5.8) and Lorentzian fits could be obtained at much lower optical powers than for the colloidal system. The steeper fall-off beyond the corner frequency [14] seen in previous studies of aerosols is also evident in our spectra, especially in the 3.01 µm case. From our comparison, we found the trap stiffness to be around 3 times greater in air than in water. This is again thought to be due to the increased refractive index contrast provided by aerosol trapping.

5.4.4 Conclusion

Silica spheres of diameter 1.86 µm and 3.01 µm were optically trapped in an optical tweezers setup and power spectra taken using a QPD. The measurements were made using both air and water as a trapping medium and the power spectra compared. This direct comparison between aerosol and colloid samples was made possible by generating a sample consisting of silica spheres suspended in ethanol.

At frequencies greater than 10 kHz it was at times difficult to obtain sufficient signal from the scattered light to bring the spectra above the background level. In the same frequency region there were also spikes in the background signal due to laser noise. At low frequencies mechanical noise can dominate resulting in a non-flat plateau despite using a floating optical bench and where possible working solitarily in the laboratory. For these reasons we only plot between 10 Hz and 10 kHz in our results.

To trap in air the laser power must be carefully selected. Unlike colloidal based tweezers simply increasing the power does not allow aerosols to be ‘caught’ easily. In this case there exists only a small region over which an aerosol can be tweezed from the air, hence the seemingly arbitrary powers shown in table 5.8. To extend the utility of our aerosol traps, we revisited the earlier work of Ashkin [20], looking at the optical guiding of aerosols.

5.6 References

1. Ashkin, A.; Dziedzic, J.M.; Bjorkholm, J.E. and Chu, S., "Observation of a Single-Beam Gradient Force Optical Trap for Dielectric Particles." Opt. Lett. **11** 288 (1986)

2. Svoboda, K.; Schmidt, C.F.; Schnapp, B.J. and Block, S.M., "Direct observation of kinesin trapping by optical trapping interferometry." Nature **365**, 721 (1993)

3. Paterson, L. *et al*, **"**Violet Diode-Assisted Photoporation and Transfection of Cells'- Novel technology offers new directions for automated all-optical cell selection, poration, and imaging in a single system." Opt. Express **13**, 595 (2005).

4. Burnham, D.R. and McGloin, D., "Holographic optical trapping of aerosol droplets." Opt. Express **14**, 4176 (2006)

5. Symes, R. *et al*, "Cavity enhanced droplet spectroscopy: Principles, perspectives and prospects", Phys. Chem. Chem. Phys. **6,** 474 (2004)

6. Jacobson, M.C.; Hansson, H.-C.; Noone, K.J. and R.J. Charlson, "Organic atmospheric aerosols: Review and state of the science," Rev. of Geophys. **38**, 267 (2000)

7. McMurry, P.H., "A review of atmospheric aerosol measurements," Atmospheric Environment **34**, 1858 (2000)

8. Denk, W. and Webb, W.W., "Optical measurement of picometer displacements of transparent microscopic objects," Appl. Opt. **29**, 2382 (1990).

9. Ghislain, L.; Switz, N. and Webb, W., "Measurement of small forces using an optical trap," Rev. Sci. Instrum. **65,** 2762 (1994).

10. Friese, M.E.J.; Rubinsztein-Dunlop, H.; Heckenberg, N.R. and Dearden, E.W., "Determination of the force constant of a single-beam gradient trap by measurement of backscattered light," Appl. Optics **35**, 7112 (1996).

11. Berg-Sørensen, K. and Flyvbjerg, H.K., "Power Spectrum Analysis for Optical Tweezers," Rev. Sci. Instrum. **75**, 594 (2004).

12. Allersma, M.W.; Gittes, F.; deCastro, M.J.; Stewart, R.J. and Schmidt, C.F., "Two-Dimensional Tracking of ncd Motility by Back focal Plane Interferometry, Biophys. J. **74**, 1074 (1998)

13. Kubo, R.; Toda, M. and Hashitsume, N, "Statistical Physics," Vol. 2, Springer (1985)

14. Di Leonardo, R. *et al*, "Parametric Resonance of Optically Trapped Aerosols," Phys. Rev. Lett. **99**, 010601 (2007).

15. Dreyer *et al*, "Improved axial position detection in optical tweezers measurements," Appl. Opt. **43**, 1991 (2004).

16. Omori, R.; Kobayashi, T. and Suzuki, A., "Observation of a single-beam gradient-force optical trap for dielectric particles in air." Optics Letters **22**, 816 (1997).

17. Ashkin, A., "Forces of a single-beam gradient laser trap on a dielectric sphere in the ray optics regime." Biophys. J. **61**, 569 (1992).

18. Vermeulen, K.; Wuite, G.; Stienen, G. and Schmidt, C., "Optical trap stiffness in the presence and absence of spherical aberrations," Appl. Optics **45**, 1812 (2006).

19. Tolic-Norrelykke, S. *et al*., "Calibration of optical tweezers with positional detection in the back focal plane," Rev. Sci. Instrum. **77**, 103106 (2006).

20. Ashkin, A., "Acceleration and Trapping of Particles by Radiation Pressure," Phys. Rev. Lett. **24**, 156 (1970)

Chapter 6

Optical Guiding of Aerosols

6.1 Introduction

While Ashkin's original work studied the acceleration of particles in the horizontal direction, subsequent work would involve optical levitation of both particles and droplets, balancing the gravitational force with the scattering force [1,2,3]. This work was the forerunner of what are now termed *optical tweezers*, which rely on the optical dipole force rather than radiation pressure to trap particles. With a weaker focus, a particle can be held in the transverse plane of the beam and levitated or guided along the direction of propagation. It is the guiding of particles, and specifically liquid droplets, that is the focus of this chapter. In particular, the aim is to produce a system capable of capturing aerosol samples and transport them using optical levitation. Although Gaussian beams could be used, the low diffraction provided by the central spot of a Bessel beam had greater potential. Therefore, these experiments are described in the form of a comparison between beam geometries.

6.2 Guiding with Gaussian Beams

6.2.1 Gaussian beam guiding experiment

With the aim of investigating particle transport in mind, the first task was to design apparatus capable of guiding aerosol particles. Previous work by a summer student, Matt Himsworth, in trapping aerosols with a weakly focussed beam had found some success. It was shown that droplets could be trapped

from a sample cell using a levitating beam focussed loosely into the centre of a tube. The nebuliser used generated an airflow opposing the direction of beam propagation. This resulted in a higher than expected trapping power with droplets trapped with beam powers in the order of 100 mW. There appeared to be differences in the intensity of the scattered light in each case. However, very little in the way of quantitative data was available. In order to take the investigation further, it was necessary to make modifications, leading to the setup shown in figure 6.1, below.

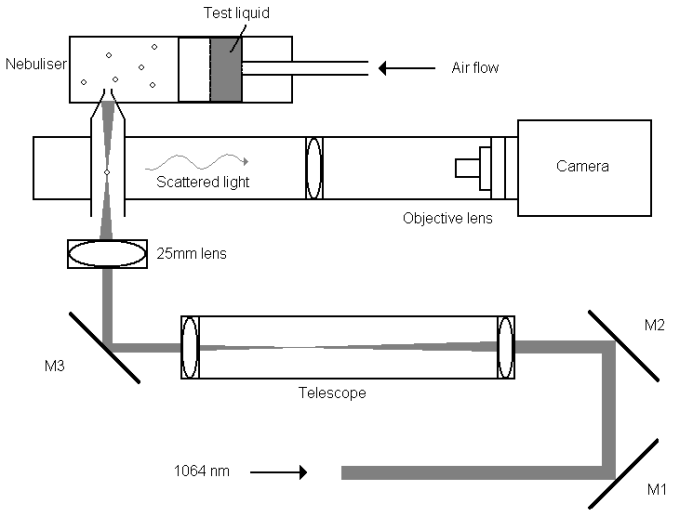

Figure 6.1: Droplet levitation trap. A 2 W laser is weakly focussed into a cell using a 25 mm lens in order to levitate droplets falling from the nebuliser above. Side-scattered light is focussed onto the camera.

The aim was to build on the aerosol guiding work conducted by Ashkin [4]. In order to capture and guide droplets, a standard laser levitation scheme was used. A 2 W CW ytterbium fibre laser at 1064 nm was used to provide a satisfactory range of levitating intensities for particle guiding. For the Gaussian beam experiment the beam is collimated with an appropriate beam waist so as to form the desired spot size after being focused with a final f=25 mm lens. Although microscope objective lenses are used to generate strong gradient forces, the aim in this instance was to create a particle guide confining the droplets in x and y only. Therefore, a 25 mm focal length lens was appropriate for these experiments.

The droplets were generated using a pneumatic nebuliser, filled with a liquid sample driven by a pressurised nitrogen flow. The magnitude of the flow was regulated using a combined flow controller and meter (Omega FMA 5400 Flow Controller) and could be adjusted from 0-2000 cm^3 per minute of gas flow. The trapped droplets had diameters of 7+/-2 µm. This estimate was made using a CCD and microscope objective to image a range of droplets falling on a microscope coverslip above which were in focus. The resulting aerosol was passed into the top of an open-ended glass cell, where in then fell into the guiding laser beam. The upwards force due to the radiation pressure from the laser would then be stably balanced using a combination of both the gravitational force acting on the droplets and the air flow passing through the cell.

Ambient conditions in the laboratory and near the cell were a critical factor in the success rate of the experiment. Any variation in the droplet size would be likely to skew the measurements. The temperature was regulated at 22°C, and the humidity in the cell was kept as high as possible by placing a liquid reservoir in the cell. Care was also taken to minimize air currents around the cell, and the optical bench was floated to prevent any mechanical vibration in the cell. We successfully levitated droplets at 100mW for upwards of 20 minutes with this apparatus.

A Watec 902-DM CCD camera was used to record the intensity profile of the droplets using different microscopes depending on the size of the area to be observed. The imaging lens focussed the scattered light towards the microscope objective and had a focal length of approximately 50.1 mm. The plane being imaged could be adjusted by moving the imaging lens. The distance of the imaging plane from the particle could be calculated using the lens maker's equation and a calibration slide placed in the focal plane to allow the dimensions of the images to be calculated.

The intensity of the beam and hence the balance position where the particle is levitated is a function of the cross-sectional area of the beam. Therefore, the guiding characteristics are dependent on the spot size at the focus and the divergence of the beam. This is given by the equation

$$w(z) = w_0\sqrt{1+\frac{\lambda z}{\pi w_0^{\,2}}}\,, \qquad [6.1]$$

where w(z) is the radius of the beam at a distance, z, from the focus, w_0 is the radius at the beam waist and λ is the wavelength.

6.2.2 Gaussian beam guiding measurements

To test the guiding properties of both the Gaussian aerosol trap, the balance point of a single droplet against the upward scattering force due to the levitating beam was found for a range of laser powers. In addition to the gravitational force acting on the droplets, there was also a down-force due to the airflow which was required to drive the nebuliser generating the droplets. It was found that the precise flow required to generate droplets depended both on the viscosity of the liquid as well as the angle of inclination of the nebuliser. So despite trapping powers of less than 10mW being recorded in Ashkin's previous droplet levitation experiments [5], a much greater power was required initially to offset the nitrogen flow and successfully trap the droplets. The flow could then be reduced in tandem with the laser power to a minimum value for each experiment Thus although this experimental set-up allows for the short-range guiding of droplets, it is more complicated to operate than standard single-beam optical gradient traps which are capable of z-trapping [6].

The equilibrium positions were measured for single droplets at a constant flow rate. This was repeated for samples of three different liquids (water, ethanol and dodecane). Direct imaging of trapped droplets confirms that the droplet sizes for each of the liquids were roughly the same, although there was no means of accurate particle sizing for each individual droplet in the guiding case.

The Gaussian beam had a diameter of 12 µm at the focus. After propagating for 500 mm, the beam diameter expanded to 25 µm. To test the guiding properties of the beam, droplets were generated at a constant flow rate for each of the

three test liquids. Care was taken to ensure that only one droplet was trapped in the beam at any one time. Too great a flow of droplets resulted in up to three droplets being trapped before merging to become larger droplets than originally intended (see figure 6.2).

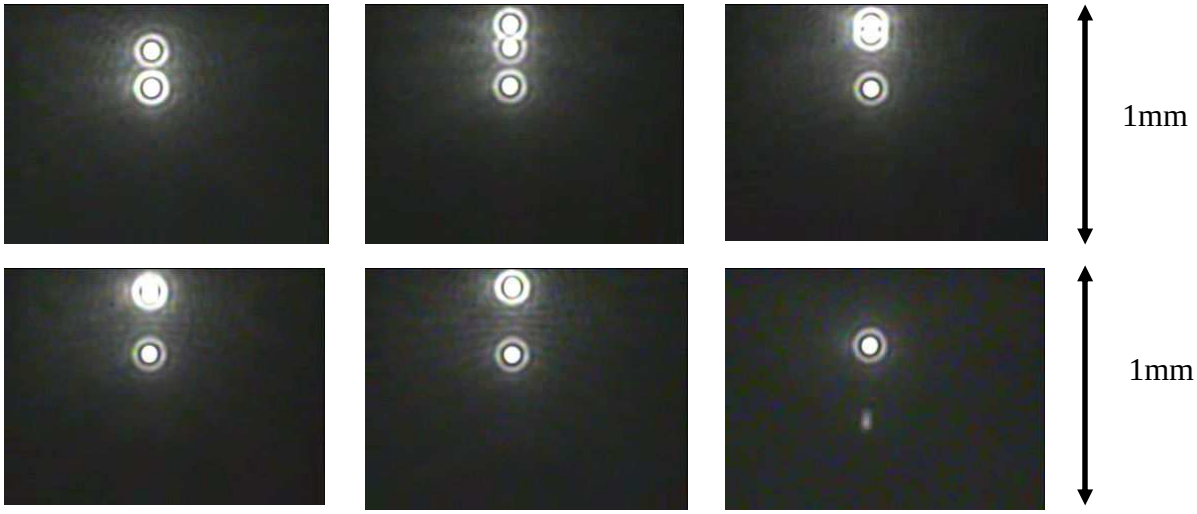

Figure 6.2: The formation of a stacked array of water droplets from left to right trapped in a Gaussian beam. After the third particle was trapped (top-centre), the top two particles merged and fell out of the trap as the power was decreased (bottom-centre and right).

6.2.3 Gaussian beam guiding results

Using the Gaussian beam, both water and ethanol trapped in a stable manner and could be made to move up and down with adjustment of the output power. Although dodecane droplets were trapped at lower intensities than water and ethanol, they were found to be less stable in the beam, as result of the higher refractive index and hence scattering of the dodecane. Despite the increase in vibrational motion observed, the maximum guiding distance was found to be significantly greater for dodecane. The, maximum guiding distances were found to be 250 µm for water (graph 6.3) and 275 µm for ethanol (graph 6.4).

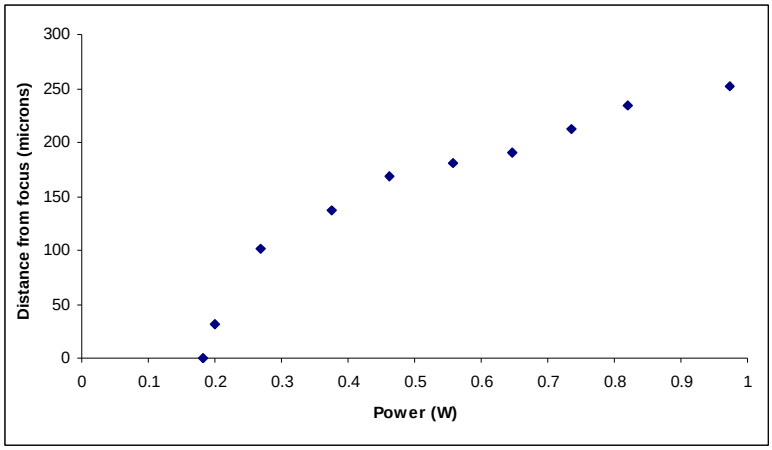

Graph 6.3: Water droplet height against laser power (W) for water for a constant flow rate of 0.58 litres/min levitated in a Gaussian laser beam.

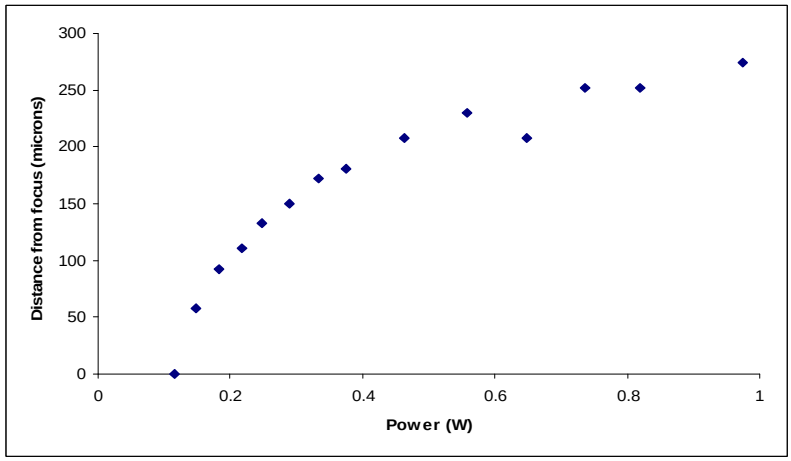

Graph 6.4: Particle height against laser power (W) for ethanol for a constant flow rate of 0.5 litres/min levitated in a Gaussian laser beam.

Figure 6.5: Guiding of a dodecane droplet over a distance of approximately 800 µm levitated in a Gaussian beam. The increased scatter of the laser on the sample can be compared to figure 6.4 above.

The maximum guiding distance of 800 µm for dodecane (see figure 6.5) could not be repeated consistently and was observed in a single experimental run.

This non-repeatability is due to a combination of instability once trapped and the increased chance of additional droplets entering the trap during the course of each run of the experiment. However, the total guiding distance can be found easily by rapidly adjusting the power. The increased guiding distance compared with water and ethanol may be due in part to an increased scattering force.

The scattering force (F_z) in the axial direction can be calculated using the ROT model for spherical particles illuminated by a uniform field [7].

$$F_z = -\int_0^{\frac{\pi}{2}} d\theta \int_0^{2\pi} d\phi \frac{E^2 \cos i a^2 \sin\theta n_m^2}{2\mu_0 c^2} \times \left(\cos(i-\theta) + R\cos(i+\theta) - \frac{T^2(\cos(i+\theta-2\tau) + R\cos(i+\theta))}{1+R^2+2R\cos 2\tau} \right) \quad [6.2]$$

where R and T are the Fresnel coefficients, μ_0 the permeability of free space, and i and τ are the incident and refracted angles of our rays (and are equal to zero in our case of the scattering force opposing the gravitational force). Using the ROT model, the refractive index difference between water (n=1.33) and dodecane (n=1.42) only amounts to a difference of around 1% in the axial scattering force, F_z.

6.3 Guiding with Bessel Beams

6.3.1 Bessel beam guiding theory

For particle guiding applications, Bessel beams [8,9] offer advantages over Gaussian laser modes. This stems from the pseudo-nondiffracting nature of the central maximum of the profile. The distance over which the beam is considered non-diffracting is termed the propagation distance in our experiment. This can be as great as a hundred times the Rayleigh range of a Gaussian beam with a beam diameter equivalent to the Bessel beam core size. The ‘advantages’ of the Bessel beam always come at a price, however. For a

given core size the beam propagation distance is a function of the Gaussian beam waist used to create the beam. However for a long propagation distance the number of rings in the Bessel beam increases and as such the power is distributed across the entire beam profile. Therefore a balance must be found between propagation distance and the fraction of the overall power present in the core.

Durnin showed that there was a propagation-invariant solution for the free space wave equation

$$\left(\nabla^2 - \frac{1}{c^2}\frac{\partial^2}{\partial t^2}\right)E(x,y,z,t) = 0\,. \qquad [6.3]$$

For a zeroth order (n=0) Bessel beam [10] generated by illuminating the axicon with a simple Gaussian beam (of diameter w_0), the phase factor $\exp(\pm in\varphi)$ simply becomes equal to 1 and the intensity can be expressed as

$$I(r,z) = 2\pi k_r w_0 \frac{2P_0 z}{\pi w_0^2 z_{\max}} J_0^2(k_r r)\exp\left(\frac{-2z^2}{z_{\max}^2}\right), \qquad [6.4]$$

where P_0 is the power incident on the axicon (z=0), $k_r=k(n-1)\gamma$ where γ is the opening angle of the axicon with refractive index n in the paraxial approximation and

$$z_{\max} = \frac{kw_0}{k_r}\,. \qquad [6.5]$$

The on-axis (r=0) intensity of the beam with z can be easily plotted from the experimental parameters (see figure 6.6). In our experimental case, we have an additional double telescope arrangement which reduces the dimensions of the beam by a factor of 32, so this must be taken into account. n=1.507 (BK7 at 1060 nm) [11], w_0=0.001, γ=1.5 degrees (0.026 radians) and λ=1064 nm.

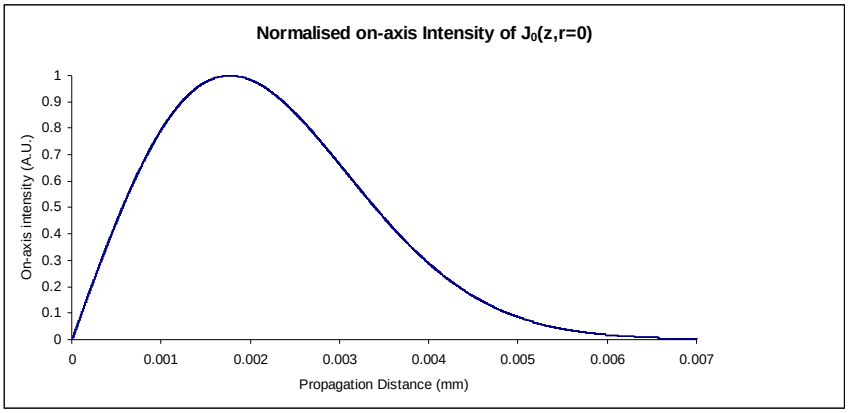

Figure 6.6: Plot of Bessel beam intensity along the centre (r=0) with z, with the intensity normalized to the maximum, which occurs 1.76 mm from the focal point of the final lens.

If we assume the minimum guiding height occurs at the point of maximum intensity in the beam as with the Gaussian case then the advantage of the Bessel beam becomes obvious. If we assume, to a first approximation, that the maximum on-axis intensity is the same in our Gaussian case as with the Bessel beam then we can plot the following (figure 6.7).

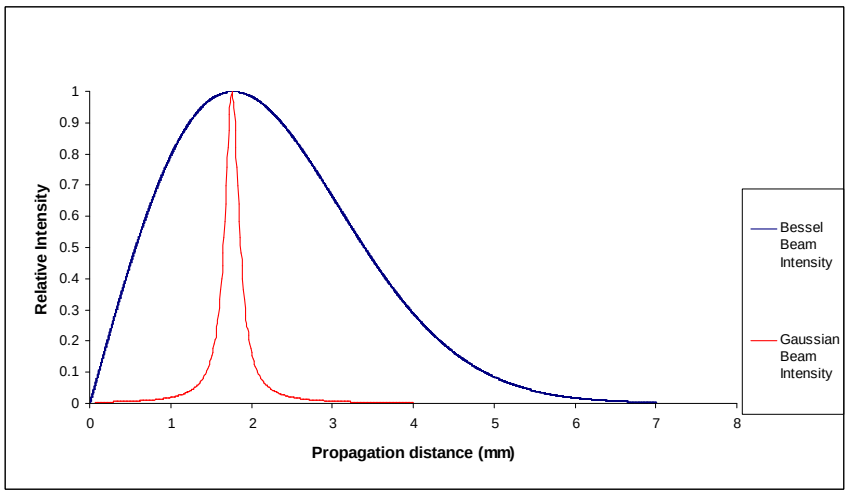

Figure 6.7: Plot of Bessel and Gaussian beam intensities along the centre (r=0) with z, assuming the same maximum on-axis intensity.

The Gaussian intensity varies according to the diffraction of the beam based on the beam waist of 6 μm used in the previous experiment and an expansion of the beam cross-section of the form

$$A(z) = \pi w(z)^2 \qquad [6.6]$$

and

$$z_0 = \frac{\pi w_0^2}{\lambda}. \qquad [6.7]$$

Of course, the radial distribution of the light fields must be taken into account. Most obviously, the light in the Bessel beam is distributed across multiple rings. In our experimental case, a Bessel beam consisting of 10 rings and a centre spot was used. Assuming the power is distributed evenly across each of these regions and the droplet is guided using the light from the core only, then over 90 % of the light in the Bessel beam is wasted. The comparison of Bessel and Gaussian beams was detailed by Durnin in 1988 [12]. This demonstrates that the Bessel range is approximately N times the Gaussian range where N is the number of rings in the Bessel beam. This would appear to be confirmed in this experiment.

We know experimentally that the minimum power required to levitate a typical 7 µm droplet in a Gaussian beam with a diameter of 12 µm using our setup is 0.18 W. This is 18 % of the 1 W available for levitation. This becomes our threshold point for the Gaussian beam. We can further refine the model by taking into account the axial profile of the levitating light in each case. By integrating across the beam cross-section and setting the limits to the diameter of a typical droplet (diameter of 7 µm), we can get an estimate of how much of the power was incident on the droplet in each case. The Bessel beam is the easiest to examine, as the core diameter is smaller than the droplet diameter. Therefore light from across the entire core of the Bessel beam makes a contribution to the scattering force acting to levitate the particle. In the Gaussian case the droplet is smaller than the beam diameter, even at the beam waist. Therefore, only the proportion of light incident on the particle should be considered (see figure 6.8).

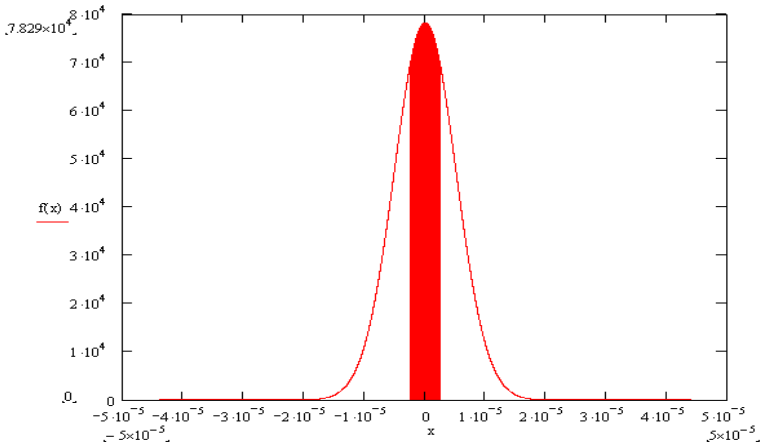

Figure 6.8: Normalised Gaussian profile with the droplet diameter shaded indicating the light in the beam focus with contributes to the forces acting on the particle.

For our Bessel beam, we must take this factor into account. Of the 180 mW in the Gaussian focus, only 14 % was used to levitate the droplet at the focus and the remainder was wasted. This gives us a threshold levitation power of approximately 30 mW for our Gaussian levitation experiment, or 3 % of the available laser power. If we assume that this levitation power is the same for the Bessel beam case, then we can redraw our Gaussian versus Bessel beam propagation graph with the new levitation threshold value of 3 %, as well as adjusting the relative beam powers to exclude light which is not incident on our droplet (see figure 6.9).

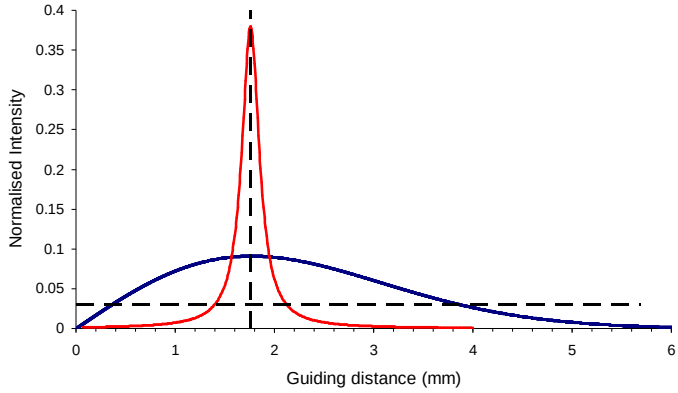

Figure 6.9: Plot of normalized Bessel and Gaussian beam intensities along the centre (r=0) with a threshold levitation power of 3 % of the maximum (horizontal dotted

line). The theoretical droplet guiding distances are shown in the x-axis by the part of the curves above and to the right of the dotted lines.

This graph demonstrates our experimental guiding distance of around 300 µm for water in a Gaussian beam in our experiment. It suggests that we can achieve guiding distances for water droplets of around 2mm for a Bessel beam using the same laser source. Of course, this is only an estimate, as there are a number of other factors involved such as the airflow from the nebuliser, the uncertainty in the droplet sizes generated and the refractive index of the liquid sample. These could significantly alter the threshold intensity required to levitate droplets at the focus. However, expecting an increase in guiding distance of 10 times was not unreasonable.

6.3.2 Bessel beam guiding experiment

A single vertical Bessel beam was used to levitate and guide droplets balanced against gravity and an opposing air flow. As with the previous Gaussian guiding experiments, the balance points of droplets at different levitating powers were found to get a sense of the beam parameters. The airflow against the beam meant that laser powers in excess of 1 W were required to initially capture the samples. Again, the flow rate and laser power were decreased in tandem to the most stable range.

As far as possible, guiding in the Bessel beam was compared to that achieved with a Gaussian beam for the same liquids. However, in this case a CCD camera with a long working distance 10x microscope objective lens was used to image the droplets through a flat window in the cell. The camera was mounted to an *xyz* translation stage to allow the droplets to be observed along their entire guiding distances. The method of analysing the divergence of the side-scatter used in the previous Gaussian guiding experiment wasn't going to provide any increase in sizing accuracy and would limit the distance that the

detector could traverse below the mm distances we anticipated could be achieved with the Bessel beam.

The Bessel beam is made using an axicon with an opening angle of 1.5 degrees in a double telescope arrangement [13] resulting in a beam with ten rings and a core diameter of approximately one-tenth of a Gaussian beam. The first telescope expands the beam to allow adjustment of the propagation distance of the beam, while the second telescope is used to adjust the central core size of the beam (to match the spot size of the Gaussian beam). The experimental arrangement for the Bessel beam is shown in figure 6.10.

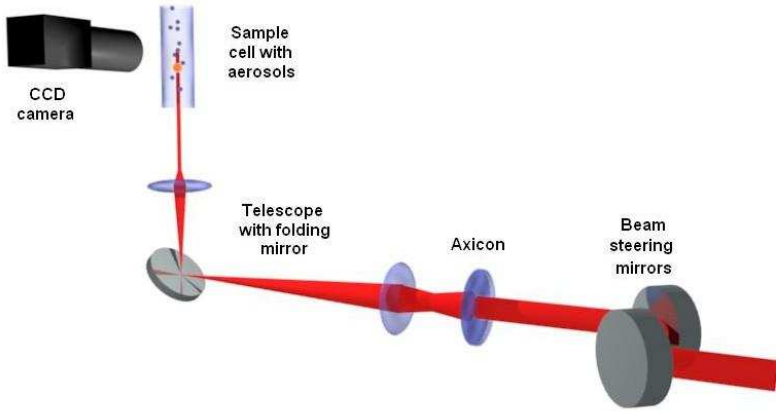

Figure 6.10: Experimental setup for optical levitation using a Bessel beam. The camera is mounted on a translation stage to allow it to travel along the direction of beam propagation.

The maximum guiding distances achieved were with a Bessel beam with a minimum core diameter of 4 µm and a core propagation distance (the distance over which it can be considered non-diffracting) of 4 mm. A detailed profile was made of the beam along its direction of propagation at 250 nm intervals (see figure 6.11). The core was found to expand to 25 µm at the end of the 4 mm propagation distance, at which the 2nd ring became indistinct and the central spot became irregular.

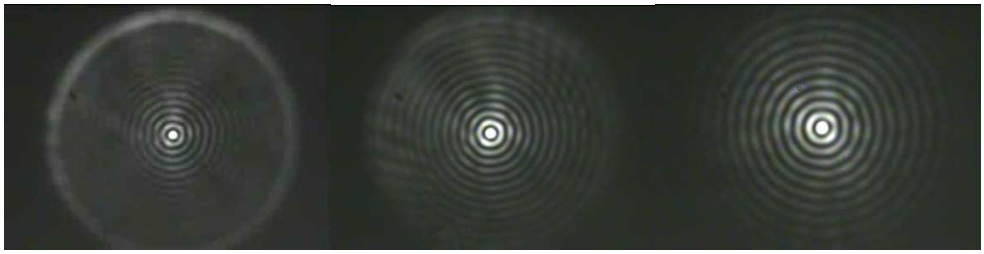

Figure 6.11: From left (z=1 mm) to right (z=2 mm): Propagation of the Bessel beam at 500 µm intervals, imaged using a 100x microscope objective lens. The centre image corresponds to the highest on-axis intensity (r=0). The central core is saturated to allow the rings to be counted accurately.

6.3.3 Bessel beam guiding results

As with the Gaussian beam experiments, dodecane was found to be more easily trapped than the other sample liquids. In addition, the problem of trapping multiple droplets was a greater issue for the Bessel beam trap. Isolating single droplets was particularly difficult and the flow rate had to be carefully selected to avoid trapping multiple droplets. In some cases, droplets were trapped over a significant portion of the beam, forming extended arrays of particles. This was possible due to the relatively large vertical trapping region presented by the core over the large propagation distance. Another factor may have been the documented self-healing effect of Bessel beams which we have shown to form similar arrays in colloidal solutions [14].

For water droplets, the Bessel beam allowed guiding to occur over 1.2 mm. This is approximately five times the distance achieved in the Gaussian beam. There was less improvement in the ethanol case, with only an approximate fourfold increase observed. Similar improvements were evident in the case of dodecane, where we observed maximum guiding distances of approximately 2.75 mm; 3 times the distance achieved with the Gaussian beam trap. In addition, the guiding was more controllable in the Bessel case, due to the smaller changes in intensity as the particle moved in the beam, and the increased stability allowed more precise measurements to be made. We note

that the increases in guiding distances are in accordance with the relative refractive indexes of the liquids which is proportional to the scattering force. We also note that while we have restricted the comparison in this paper to powers of 1 W, the maximum guiding distances observed in the Bessel beam were 2 mm for water, 1 mm for ethanol and 3.5 mm for dodecane using 2.25 W of power in the beam.

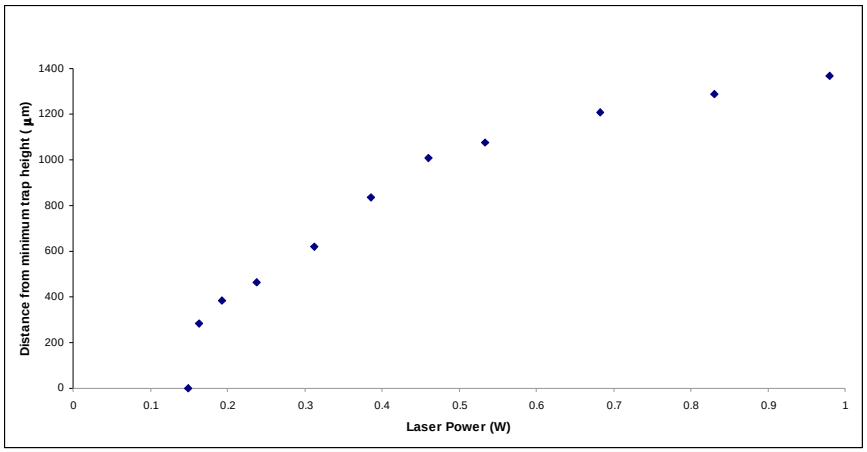

(a)

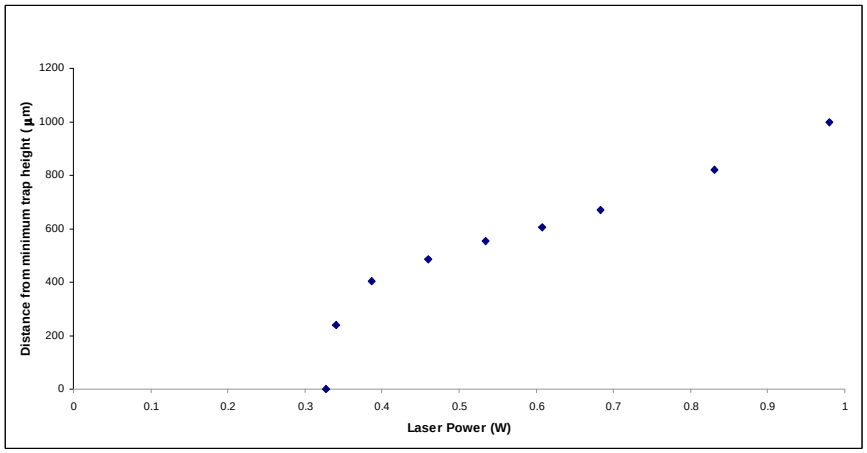

(b)

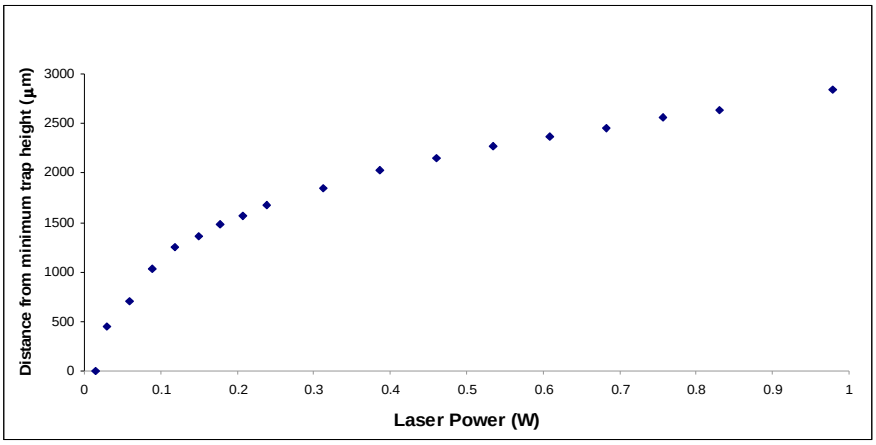

(c)

Graph. 6.12: Particle height against laser power (W) for (a) water, (b) ethanol and (c) dodecane at a constant flow rate in a Bessel beam. The particle displacement is relative to the displacement for the minimum trapping power.

The longer propagation distances achieved for the dodecane samples suggest a lower threshold levitation power. Although the scattering force is a small factor, the dodecane was more easily trapped in the beam at lower powers and so the nebuliser flow could be decreased more than with the other liquids. From graphs 6.12(a-c) above, a modest reduction in threshold power provides a large increase in guiding distance in both the Gaussian and Bessel cases. Indeed, the minimum levitating power achieved for the dodecane droplet in a Bessel beam was of the order of 10 mW, or less than 1 mW in the core (see graph 6.13).

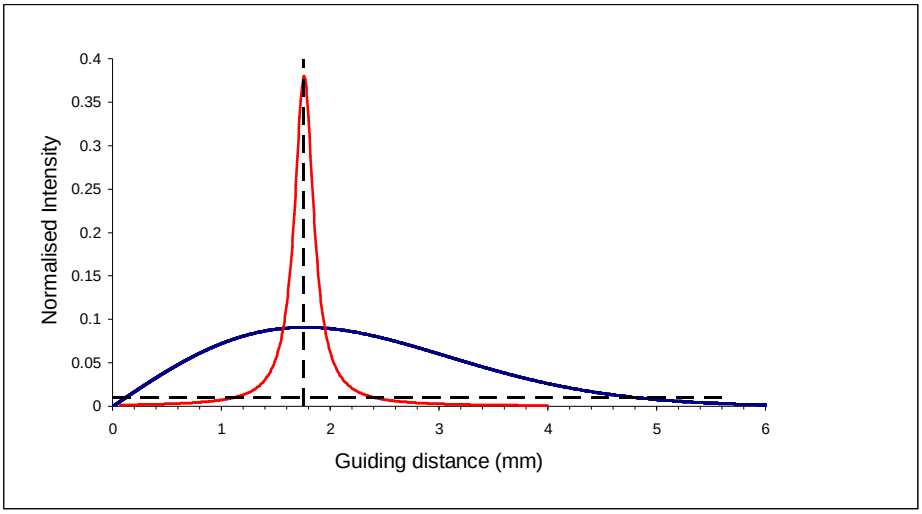

Fig. 6.13: Plot of normalized Bessel and Gaussian beam intensities along the centre (r=0) for dodecane, with a threshold levitation power of 1 % of the maximum (horizontal dotted line). The theoretical droplet guiding distances are shown in the x-axis by the part of the curves above and to the right of the dotted lines.

From this, it is clear that the effect of the nebuliser airflow makes a significant difference to the guiding distances possible. Unfortunately, having an increased threshold trapping power improves the stability of the system, making it less sensitive to changes in the laser and the environment. Greater guiding distances could be achieved for the other liquids if the experimental design used a laser with excellent power stability and was extremely isolated from the surrounding environment. However, this is an engineering problem which would require an alternative means of aerosol generation and a drastic redesign of the system in order to remove the airflow.

However, we can use the ROT model again to estimate a theoretical minimum threshold levitation power in the absence of airflow. By setting F_z equal to the gravitational force acting on our droplet, we can obtain a value for E^2, allowing us to estimate the threshold levitation power in the absence of airflow. The value of 1.42 nW obtained is significantly lower than those achieved experimentally and would provide an additional increase in the theoretical guiding distance.

6.3.4 Other measurements of interest

One effect which was observed while attempting to capture droplets at high power with the Gaussian beam was the accumulation of multiple droplets in the trap. At sufficiently high powers (>300 mW), up to 3 droplets could be levitated, one above the other. As the power was decreased, the uppermost droplets would begin to fall into one another. An indication of the type of effect that is observed is illustrated in figure 2. The screenshots shows an array of three water droplets being trapped. The upper two droplets merge with each other and the then the new coagulated drop is too heavy for the beam to support and falls out of the beam. The merged droplet does not fall directly down to hit the lower droplet, as a result of air currents in the sample chamber.

Although we successfully trapped up to 3 droplets simultaneously at high powers in the Gaussian trap, the "self-healing" characteristics of the Bessel beam have been shown in previous experiments [14] to allow the trapping of regularly spaced 1-D arrays. While the increased trapping volume and array formation was problematic when conducting single-particle measurements, large numbers of droplets could be levitated at higher laser powers and nebuliser flow rates (see figure 6.14 below). Unfortunately, due to the nature of the experiment in this case, controlled array formation as in the colloidal experiments was extremely difficult. In addition to the airflows and the somewhat random nature of the droplet loading, the liquid droplets merged in collisions. When a larger droplet formed in this way, it fell down through the other droplets in the chain.

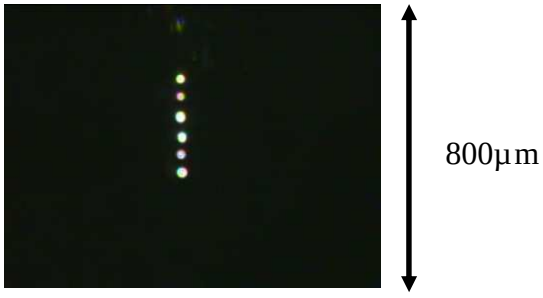

Figure 6.14: Screenshot of dodecane droplets in a Bessel beam forming a linear vertical array.

Although we are interested in analysing the properties of Bessel beams, the possibility of optical binding and the nature of the scattered light; this was not an ideal system for the task. With a more advanced sealed cell with no airflow and controlled droplet loading, this may be an interesting future experiment.

6.4 Droplet Guiding Comparisons

The guiding of the droplets is a simple consequence of radiation pressure and the ability of the Bessel beam to guide further than the Gaussian, for a similar beam core size similar to the Gaussian beam diameter, is a consequence of the quasi-non-diffracting nature of such beams. One of the consequences of the way in which the Bessel beam is formed is an effective larger depth of focus than a Gaussian beam, and hence a less rapidly diverging intensity profile than a tightly focused Gaussian.

In this comparison we must of course choose some sort of basis on which to compare. The droplets were always at a point of equal beam intensity, with an increase in power compensating for the expansion in the cross-sectional area of the beam. It was therefore decided that that the minimum vertical point was the most sensible place to make a measurement of these guiding distances. In the Gaussian case, the minimum point was taken to be at the focus of the beam, where the droplet would be located at the lowest levitating power. Similarly, the Bessel guiding distances were measured from the point where the intensity of the core was highest.

We note that the increased and controlled guiding distances achieved by the Bessel beam are a result of the non-ideal nature of our experimental beam. For the case of an ideal beam we would not be able to guide by adjusting the power, as provided we could find a power which resulted in an equilibrium position, every point in the beam core would be an equilibrium point. Any increase in power would result in an increase in power along the whole of the beam, and no point in the beam would now be an equilibrium point. We make

use of the fact that our quasi-Bessel beam has a varying intensity profile along the beam propagation distance.

We demonstrated the successful levitation and guiding of aerosol droplets of water, ethanol and dodecane in vertical optical radiation pressure traps. The guiding characteristics of both Gaussian and Bessel beam geometries were compared. For a minimum core diameter of 4 µm, droplets were captured and guided up to 2.75mm in the Bessel beam using adjustments in the output power only. For a comparable Gaussian beam we achieved guiding distances of 800 µm (see table 6.15, below).

Liquid	Gaussian Beam Guiding Distance	Bessel Beam Guiding Distance
Water	250 µm	2 mm
Ethanol	275 µm	1 mm
Dodecane	800 µm	3.5 mm

Table 6.15: Table of maximum guiding distances achieved for each sample in both Gaussian and Bessel beams

The Bessel beam trap design showed potential for applications in "lab-in-a-box" concepts. The ability to capture aerosol samples and guide them through a number of sensors appeared to be particularly feasible using a Bessel beam for droplet guiding and was therefore the intended future direction of this work. Improving single droplet sampling and detection techniques is of particular importance to applications in atmospheric chemistry, and so my colleagues in Bristol asked for a similar system to be built for their studies. This would allow multiple measurements to be made on a single trapped particle, guided through various sensors used there for analysis.

6.5 References

1. Ashkin, A. and Dziedzic, J.M., "Observation of Resonances in the Radiation Pressure on Dielectric Spheres" Phys. Rev. Lett. **38**, 1351 (1977).

2. Ashkin, A. and Dziedzic, J.M., "Optical levitation of liquid drops by radiation pressure", Science **187** 1073 (1975)

3. Ashkin, A. and Dziedzic, J.M., "Feedback Stablization of optically levitated particles", Appl. Phys. Lett. **30**, 202 (1977).

4. Magome, N.; Kohira, M.I.; Hayata, E.; Mukai, S. and Yoshikawa, K., "Optical Trapping of a Growing Water Droplet in Air" J. Phys. Chem. B **107**, 3988 (2003).

5. Ashkin, A. and Dziedzic, J.M., "Feedback Stablization of optically levitated particles", Appl. Phys. Lett. **30**, 202 (1977).

6. Ashkin, A.; Dziedzic, J.M.; Bjorkholm, J.E. and Chu, S., "Observation of a Single-Beam Gradient Force Optical Trap for Dielectric Particles." Opt. Lett. **11** 288 (1986).

7. Roosen, G. and Imbert, C., "Optical levitation by means of two horizontal laser beams: a theoretical and experimental study," Phys Lett **59,** 6 (1976)

8. Durnin, J.; Meceli, J.J. and Eberly, J.H., "Diffraction-Free Beams", Phys. Rev. Lett. **58**, 1499 (1987).

9. McGloin, D. and Dholakia, K., "Bessel Beams: Diffraction in a New Light", Contemp. Phys. **46** 15 (2005)

10. Arlt, J. and Dholakia, K., "Generation of high-order Bessel beams by use of an axicon," Optics Communications **177**, 297 (2000)

11. Manufacturers literature gives dispersion coefficients: B_1 = 1.03961212, B_2 = 2.31792344x10^{-1}, B_3 = 1.01046945, C_1 = 6.00069867x10^{-3}, C_2 = 2.00179144x10^{-2}, C_3 = 1.03560653x10^{2}.

12. Durnin, J.; Miceli, J.J. and Eberly, J.H., "Comparison of Bessel and Gaussian beams," Optics Lett., **13**, 79 (1988)

13. Arlt, J.; Garces-Chavez, V; Sibbett, W. and Dholakia, K., "Optical micro-manipulation using a Bessel light beam", Opt. Commun. **197**, 239 (2001)

14. Garcés-Chávez, V.; Roskey, D.; Summers, M.D.; Melville, H.; McGloin, D.; Wright, E.M. and Dholakia, K., "Optical Levitation in a Bessel Light Beam," Appl. Phys. Lett. **85**, 4001 (2004)

Chapter 7

Towards a Lab-in-a-box and Optically Trapped Lasing Droplets

7.1 Introduction

With the necessary tools developed for the capture, sizing and manipulation of aerosol samples developed, the next task was to integrate these with spectroscopic techniques to make practical measurements useful to physical chemistry. Such "lab-in-a-box" concepts, combining optical trapping methods with chemical detection techniques, are one of the main motivations behind the work in aerosol trapping. To this end, two experimental setups were designed. One experiment was designed to optically trap and pump a droplet of laser dye and view the emission spectrum. The second experiment was constructed to capture and guide droplet samples through optical sensors and probe beams, providing a means to compare the accuracy of different droplet sizing techniques on a single aerosol sample and to build on the work detailed in the previous chapter.

7.2 Trapping of Laser Droplets

7.2.1 Introduction

Building on work by Ashkin [1] on the optical trapping of liquid droplets, many recent studies have involved the use of cavity enhancement in Whispering Gallery Modes (WGMs) [2] The high quality of the microcavites formed by typical droplets allow accurate sizing and spectroscopic measurements to be made [3]. By doping the liquid with a suitable laser dye, lasing can even be achieved in these WGMs. A number of methods have been explored to control the droplet generation and optical pumping of the laser dye. These range from exciting falling droplets [4], to ultrasonic levitation [5] and are detailed in Chapter 3 of this thesis. Work with droplets includes both fluorescence [6] and Raman [3] spectroscopy. Earlier experiments described in this thesis demonstrate that liquid droplets in the 2µm-10µm range have been trapped using optical tweezers. This is a smaller size regime than the majority of previous trapped laser droplet experiments and the corresponding free spectral range of these modes would be larger than in other droplet experiments. The lasing of small droplets was achieved by Tona and Kimura [7,8] using a Paul trap to confine droplets with a diameter of around 12µm. In our experiment, Coumarin 4 was selected as the laser dye due to its low toxicity. The dye was dissolved in ethanol and absorbed pump light from 300-370 nm [9] and emitted at around 430 nm and a suitable pump laser at 355 nm was used.

7.2.2 Experimental Designs

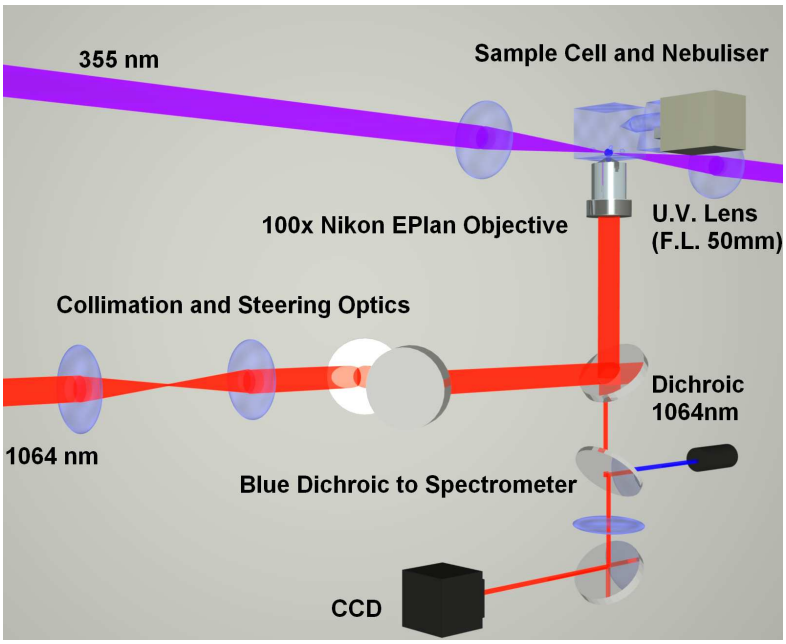

Figure 7.1: Apparatus for laser droplet tweezers. The 355 nm source is split with a 50:50 beamsplitter cube and focussed into the cell using u.v. optics. Blue light (around 430 nm) from the objective is directed with a dichroic mirror onto the fiber coupler for the spectrometer.

The optical trapping was conducted using an inverted single beam gradient force tweezers arrangement [10] with a 1064 nm (IPG 2W cw) laser source (see figure 7.1). An infinity-corrected 100x Nikon E Plan oil-immersion microscope objective (NA=1.25) was used to generate the trap and a thickness 1 coverslip was placed on top. The back aperture of the objective was slightly overfilled [11] to maximize the gradient trapping forces. As with other experiments involving the optical trapping of droplets, a sample cell was placed over the coverslip and saturated with the sample liquid to reduce evaporation effects. The droplet sample itself consisted of solution of Coumarin-4 laser dye dissolved in ethanol.

Coumarin-4 was selected for a number of reasons. Coumarin-4 is used as a food additive and is poses less of a health risk than many common laser dyes, which are often toxic or carcinogenic. Using a more harmful dye, especially in

an aerosolised form, would require special safety measures and an airtight chamber. Due to constraints in time, space and money, a simple system using Coumarin-4 was desirable. Although Coumarin could be dissolved in both ethanol and di-methyl sulfoxide (DMSO), ethanol was chosen for safety reasons. Although DMSO would have a lower rate of evaporation [12], it would also potentially increase the concentration of coumarin-4 reaching the organs of anyone exposed to the dye solution. Although DMSO itself is non-toxic and has an excellent solvating power [13], it also penetrates human skin very easily, potentially carrying anything dissolved in it directly to the bloodstream.

A 355 nm frequency tripled Nd:YAG pulsed system was used as the pump source. The cell consisted of a Petri dish modified with UV quartz glass windows to allow the pump light to reach the droplet sample. Given that the efficiency of coumarin-4 as a laser dye in our system was unknown, saturated solutions of laser dye were used. Saturation occurred at a concentration of 1.5 % mpv in an ethanol solution.

A means of detecting the emission spectra and droplet size of the trapped droplets was the next consideration. A visual measurement of the droplet diameters were made using a white-light Kohler style system [14] to illuminate the sample from above, with imaging taking place from below with the same objective lens used for the trap. The mirror was dichroic and designed to reflect the trapping wavelength at 45 degrees but transmit visible wavelengths. The remaining visible light was the passed to a Watec CCD (WAT-DM2S) for direct observation of the droplet and visual measurement of the diameter.

A second dichroic mirror was inserted to reflect the expected emission wavelengths in the blue region of the spectrum to a spectrometer [Andor]. The reflected light was collected by a lens and coupled into the optical fibre collector for the spectrometer. The collection optics were mounted on an xy-translation stage. Crude alignment of the spectrometer was achieved using an iris aperture placed above the mirror to only allow rays from the centre of the objective field of view (i.e. the trap site) to reach the detectors. The

spectrometer collector head was then translated to achieve the maximum signal. Later, small adjustments to the spectrometer alignment were made to increase the fluorescence signal from a droplet sample in the tweezers trap itself.

As with the previous aerosol tweezing experiments, care had to be taken to manage the evaporation of droplets within the cell. Although the addition of the dye (a salt) reduced the vapour pressure of the ethanol, the evaporation rate of the samples was still too fast to make any meaningful spectroscopic measurement. To prevent broadening of resonance peaks, the circumference of the droplet (cavity length) had to remain relatively constant. The evaporation of water/ethanol mixtures have been examined by Jonathan Reid's group in Bristol [15].

Firstly, care was taken to ensure the sample cells tested were flat enough so as to be airtight in contact with the coverslip below. The hole for the injection of the sample aerosol was placed pointing slightly away from the trap site. This reduced the disturbance to the trapping region when the aerosol flow was stopped. It was also crucial that the environment within the cell was oversaturated with ethanol, so reservoirs were placed within the cell. These were typically a combination of ethanol-soaked tissue paper and a small cup filled with ethanol. This ensured that the flow of ethanol towards and from the droplet surface was balanced, hence eliminating evaporation.

After testing, two general sample cell designs were used in the experiments. The first, which was more suited to trapping small droplets, consisted of a modified Petri dish. Flat sections were cut on opposite sides using a hot wire and quartz glass plates were glued on and a hole drilled in another part of the cell for the injection of samples. The small volume of the cell should also have helped to reduce convection currents in the air and increased stability. However, this also meant that a limited ethanol reservoir could be used, reducing the sample droplet lifetime. Droplets also sank to the bottom of the cell more rapidly, reducing the time available for the droplets to coagulate, hence providing smaller droplets.

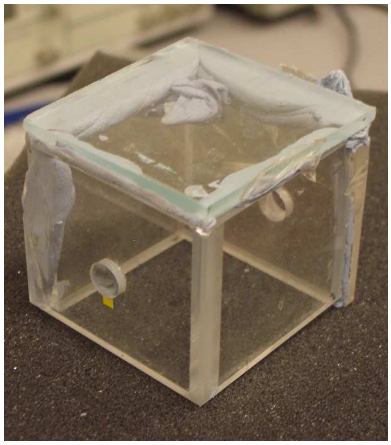

Figure 7.2: Large cubic sample cell used in the trapping of fluorescent droplets under UV excitation.

The production of larger droplets was achieved using a larger cubic cell with 2 UV transparent sides (see figure 7.2 above). The section towards the back of the cell (relative to the hole) could be filled with ethanol, maintaining an ethanol saturated environment for longer. By placing the inlet hole 2 cm above the coverslip, aerosol clouds sink slowly to the bottom of the cell, resulting in larger droplets at the bottom of the cell, above the coverslip.

Another feature of this experiment worth mentioning is the formation of crystals on the surface of the coverslip. These were an unforeseen difficulty and required routine changing of the coverslips. Trapping of droplets was found to be easier after forming a layer of liquid sample above the coverslip, as with previous experiments. If the surface ethanol evaporates, the concentration of dye in the liquid layer increases. If the concentration of dye is close to saturation, the excess dye quickly forms crystals on the surface. This is another reason to reduce the rate of evaporation of ethanol near the bottom of the cell.

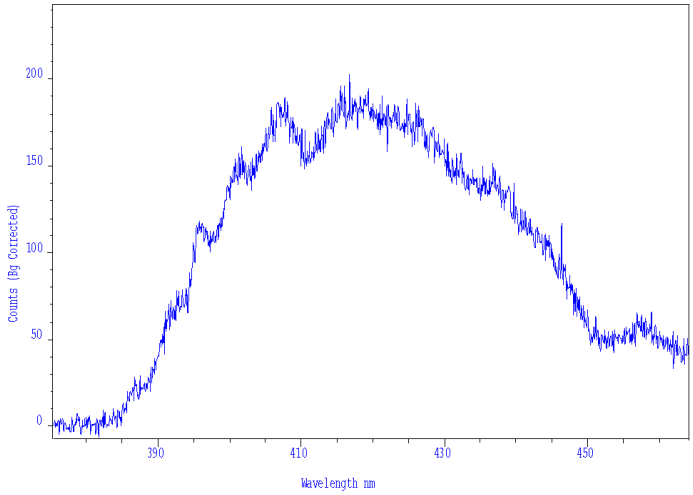

Graph 7.3: Spectrum of 1.5% Coumarin-4 dye sample on the surface of the slide (bulk spectrum) illuminated by 4µJ pulses with a repetition rate of 200Hz at 355nm. Sampling time of 0.2s.

Once the trapping and evaporation of droplets in the sample cells was investigated, the pumping of the samples was optimised. Any focussing optics had to be located outside the sample cell and transparent to UV, so 25 mm fused silica plano-convex lenses were used. The pump intensity was varied using a graded filter. Initial attempts to pump the dye droplets from one side were unsuccessful (see graph 7.3). The force provided by the pump beam was in the order of pNs and droplets were pushed out of the trap by the pump beam before reaching lasing threshold. However, there was evidence of cavity modes from some of the spectra (graph 7.5).

In an effort to balance the momentum acting on the droplets, a lens and mirror were added to reflect some of the UV light back into the sample (figure 7.4 and graphs 7.8 and 7.9 below). This provided very limited improvement so to increase the stability pump light was focused into the sample from two opposing directions. No suitable half wave-plate was available, so a non-polarising beam splitting cube was used with filters to balance the power going to each side. This allowed a greater pump power to be used while minimizing the risk of knocking the droplet out of the trap.

Care was also taken to ensure the focus of each lens was located at the trapping region. This could be checked by creating a layer of dye solution on the coverslip and moving the lenses to maximise the count on the spectrometer. Using the colour camera, the fluorescence produced by the beam could also be used as a guide for alignment. The UV mirrors used to get the pump to the sample cell could be used for rough alignment. The focussing lenses were mounted on 2-axis kinematic mirror mounts to provide finer control, using off-axis shift due to refraction at the lens surfaces to redirect the pump beam. For similar reasons, the cell walls had to be perpendicular to the pump beam at all times to avoid altering the pump alignment.

Figure 7.4: Images of a 1.5 % Coumarin-4 dye droplet in the optical trap illuminated by 1 µJ pulses at 355 nm with a repetition rate of 200 Hz; (Left) under white light illumination, (Right) fluorescence only.

7.2.3 Results

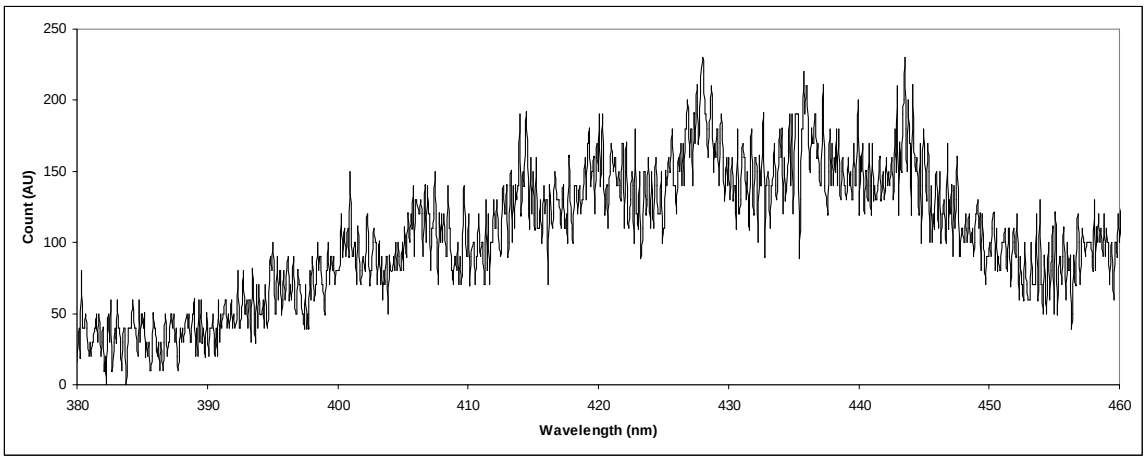

Graph 7.5: Spectrum of a 1.5 % Coumarin-4 dye droplet in the optical trap illuminated by 1 µJ pulses with a repetition rate of 200 Hz at 355 nm. Sampling time of 0.2 s.

Graph 7.5 was produced by increasing the energy of the pump pulses using a graded index filter to 20 % of the maximum. The pump pulse energy was increased gradually to this point and any further increase led to observed instability in the trap. This is the best spectrum achieved with a droplet which was still stable in the tweezers with an external pump source incident from one direction. Cavity resonances are visible, but the spectrum has a low signal to noise ratio and significant broadening on the peaks. Some of this broadening is likely due to evaporation of the droplet reducing the resonance cavity length and the fact that the droplet is relatively small.

Despite the poorly defined peaks, some analysis is still possible for this optically trapped droplet. The mode spacing for 8 of these peaks can still be estimated (see table 7.6, below). From the equation 3.5 described in Chapter 3 [16], the mode separation S(a) can be used to obtain the droplet diameter a, where

$$a = \frac{\lambda^2 \tan^{-1}\sqrt{(m^2 - 1)}}{S(a)2\pi\sqrt{(m^2 - 1)}}, \qquad [7.1]$$

and m=1.4 (for our sample liquid)

Peak Number	Wavelength (nm)	Mode Spacing (nm)	Droplet Diameter (µm)
1	395.4	-	
2	400.7	5.3	3.8
3	406.6	5.9	3.5
4	414.4	7.8	2.8
5	420.4	6.0	3.7
6	428.0	7.6	3.0
7	435.8	7.8	3.1
8	443.6	7.8	3.2

Table 7.6: Calculated mode spacings from fluorescent spectrum (7.4) of trapped 2 % Coumarin 4 in ethanol droplet.

However, one would expect the presence of both TE and TM modes in such a spectrum but it is difficult to distinguish these in graph 7.5, so each peak is assumed to correspond to a combination of the TE and TM mode for each peak. Given that these droplet diameters are relatively small (on the order of 20 to 25 wavelengths in circumference), the poor quality of the spectrum is not surprising.

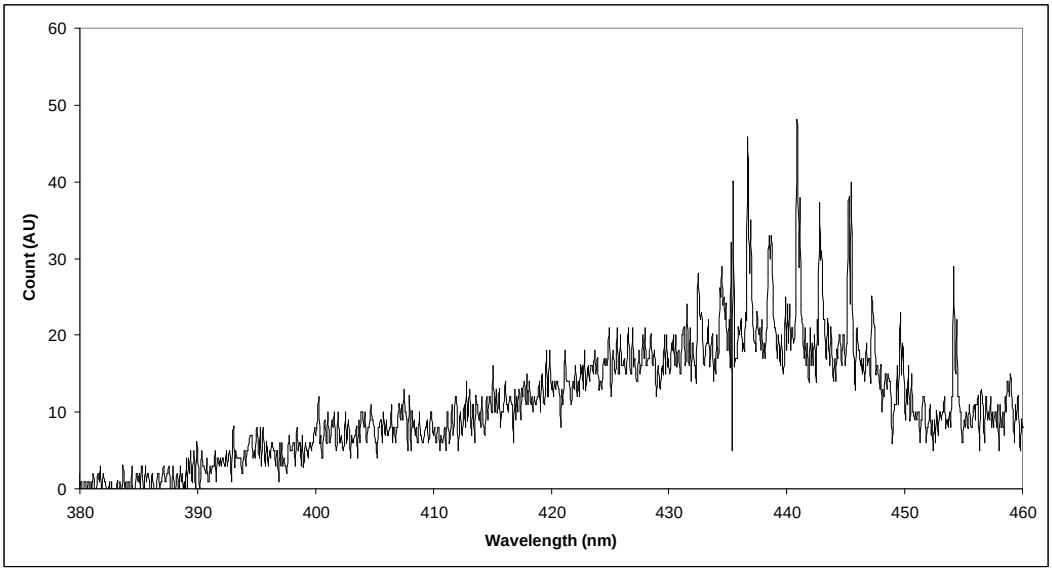

Graph 7.7: Spectrum of a 1.5 % Coumarin-4 in ethanol droplet, passing through the pump beam (3 µJ, 200 Hz), but not held securely in the tweezers. Sampling time of 0.2 s; although the exposure time may be shorter because the droplet wasn't stationary.

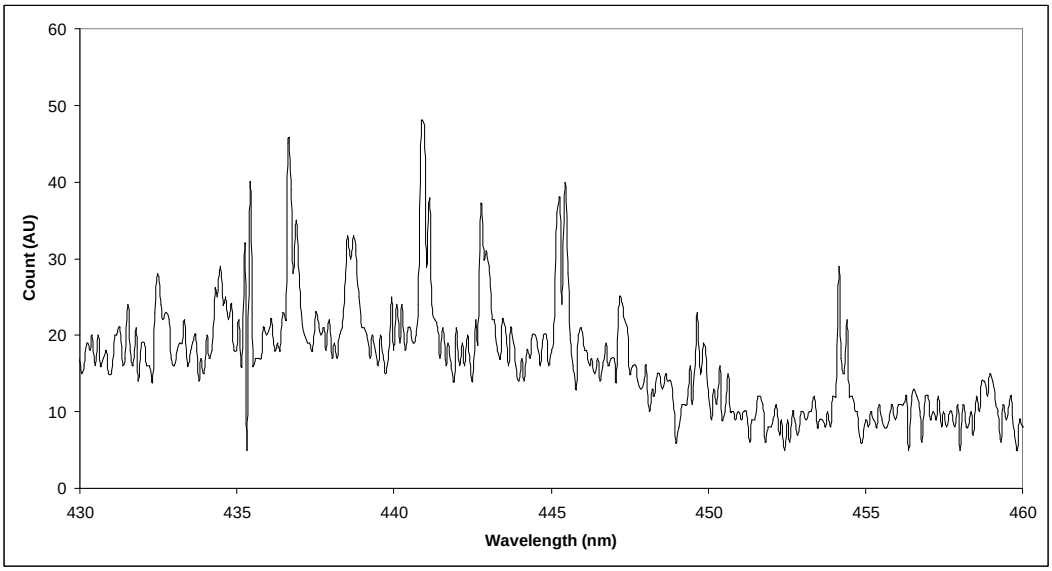

Graph 7.8: Close-up of the region of interest for Graph 7.6. Some evidence of mode degeneracy in the stronger peaks. However, low signal-to-noise ratio makes this difficult to confirm. The peak at 435.4 nm is spurious (cosmic ray event).

Peak Number	Wavelength (nm)	Mode Spacing (nm)	Droplet Diameter (µm)
1	432.6	-	
2	434.6	2	
3	436.8	2.2	5.61
4	438.6	1.8	5.95
5	441.0	2.4	5.72
6	442.9	1.9	5.63
7	445.4	2.5	5.57
8	447.3	1.9	5.61

Table 7.9: Calculated mode spacings from fluorescent spectrum (7.6) of 2 % Coumarin 4 in ethanol droplet. The mode spacings suggest that these are alternating TE and TM modes, so the droplet diameter estimates are made using two mode spacings, corresponding to the free spectral range of the microcavity under this assumption.

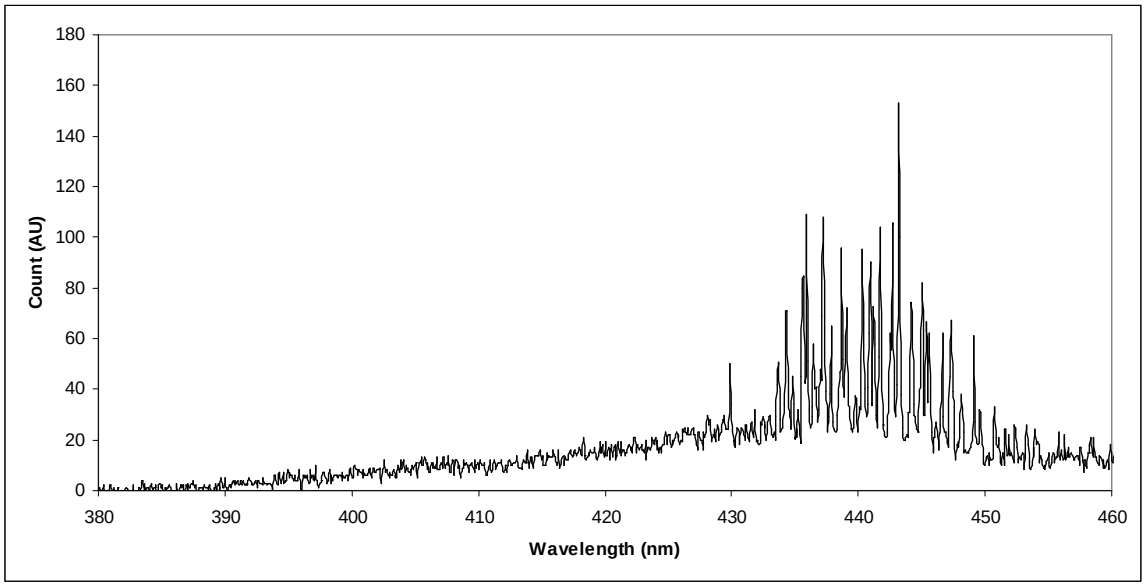

Graph 7.10: Spectrum of a 1.5 % Coumarin-4 in ethanol droplet, passing through the reflected pump beam (4.5 µJ, 200 Hz) region, but not held securely in the tweezers. Sampling time of 0.2 s, but the droplet was moving, so the exposure time may be shorter.

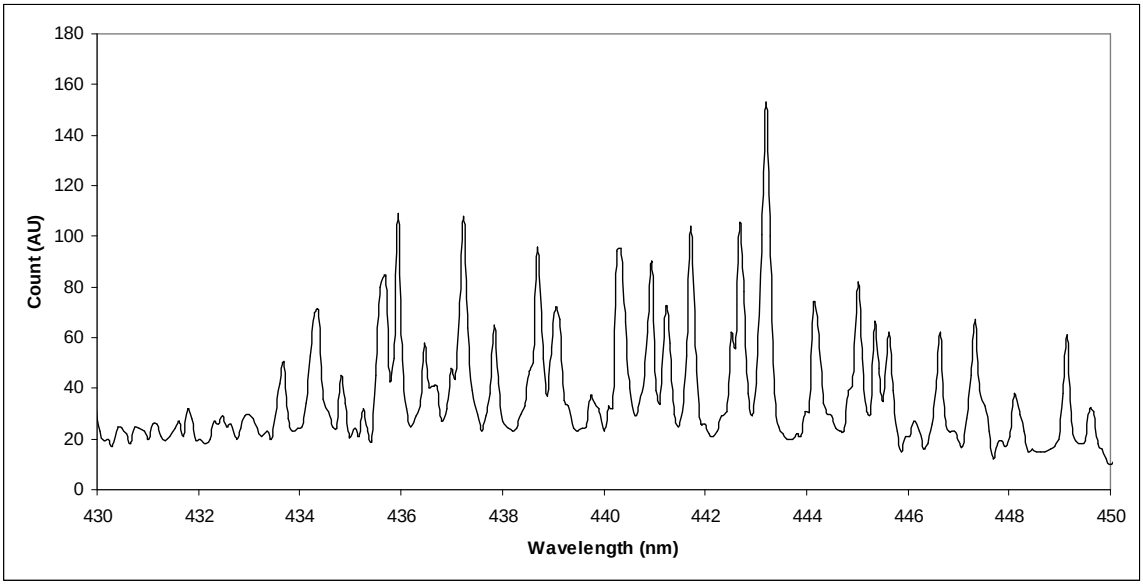

Graph 7.11: Close-up of region of interest for graph 7.8. This mix of modes is similar to those found in the lasing regime as described by [7,8] and the described red-shift of the fluorescent spectrum is also seen. The photon count is relatively low, suggesting poor alignment of the spectrometer.

Graphs 7.10 and 7.11 (above) were produced when droplets passed through the pump beam near the trapping site. The strong peaks present at a longer wavelength than the bulk spectrum match similar spectra produced in the "lasing" regime in similar microcavity experiments where gain takes place. These improved spectra are due to these being larger droplets which hadn't had the opportunity to evaporate much before being excited by the UV pump, and the fact that their motion through the trap led to a shorter exposure time on the spectrometer. However, these droplets were not held in the tweezers for a significant period, if at all, so there is little confidence that these were optically trapped lasing droplets, and that these graphs don't really improve on the lasing droplet experiments conducted using similar falling droplet methods [17,18].

After attempts to improve the stability of the trap in the presence of strong pump pulses, the signal strength was still insufficient to provide conclusive evidence that gain was taking place within the droplet while simultaneously being trapped. Perhaps with additional time, the dual pumping regime may

have been successful, but an alternative experimental design is likely more desirable.

7.2.4 Conclusions and Discussion

Work was conducted to test the feasibility of optically trapping a dye droplet and producing gain in a WGM with an appropriate pumping regime. For our experiment, constraints meant the pump beam was focused onto the droplet sample from outside the cell. Although spectra were obtained from the Coumarin 4 dye samples used in these studies, droplets were knocked out of the tweezers at higher pump energies. Cavity modes could be seen in the trapped droplets but strong Raman signals could not using this pump regime. Strong signals were only detected on droplets in the process of passing through the trap or being knocked out of the trap when exposed to strong pump pulses.

Ideally, a more conventional laser dye with a visible absorption band, such as Rhodamine 6G would have been used, but as mentioned preciously, aerosolizing such a toxic dye safely would require the engineering of a more complex sample cell and an alternative method of aerosol generation. An airtight sample cell with droplet injectors to generate droplet samples would be one such solution. In that case, the trapping beam itself could be used to excite the cavity modes in the droplet without requiring a UV transparent microscope objective. Another alternative to our pumping regime could use an objective built from UV optics to trap and excite the Coumarin dye droplets.

7.3 Further Development in Bessel Guiding (Towards a Lab-in-a-box)

7.3.1 Introduction

After the demonstration of controlled optical guiding of droplet samples (Chapter 6), the next goal was to integrate this with chemical analysis techniques. Of particular interest was the ability to directly compare different droplet sizing techniques on the same sample. The basic scheme for the experiment was to use a single Bessel beam to capture and levitate droplet samples over millimetre distances, passing the droplet through probe beams and chemical sensors. This required the optical trap to be constructed in a chemistry laboratory at the University of Bristol.

7.3.2 Experimental Design

The optical system used for the system at Bristol was very similar to the one used in the previous guiding experiments at St Andrews. A 532 nm (Coherent Verdi V5) was used due to availability and convenience. Light of this wavelength was used for many of the previous spectroscopy experiments conducted at Bristol. The axicon used to generate the Bessel beam was the same one used for the previous droplet guiding work, with an opening angle of 1.5 degrees. The telescope system for demagnifying the beam consisted of a 400 mm and a 25 mm lens, providing 16 times demagnification.

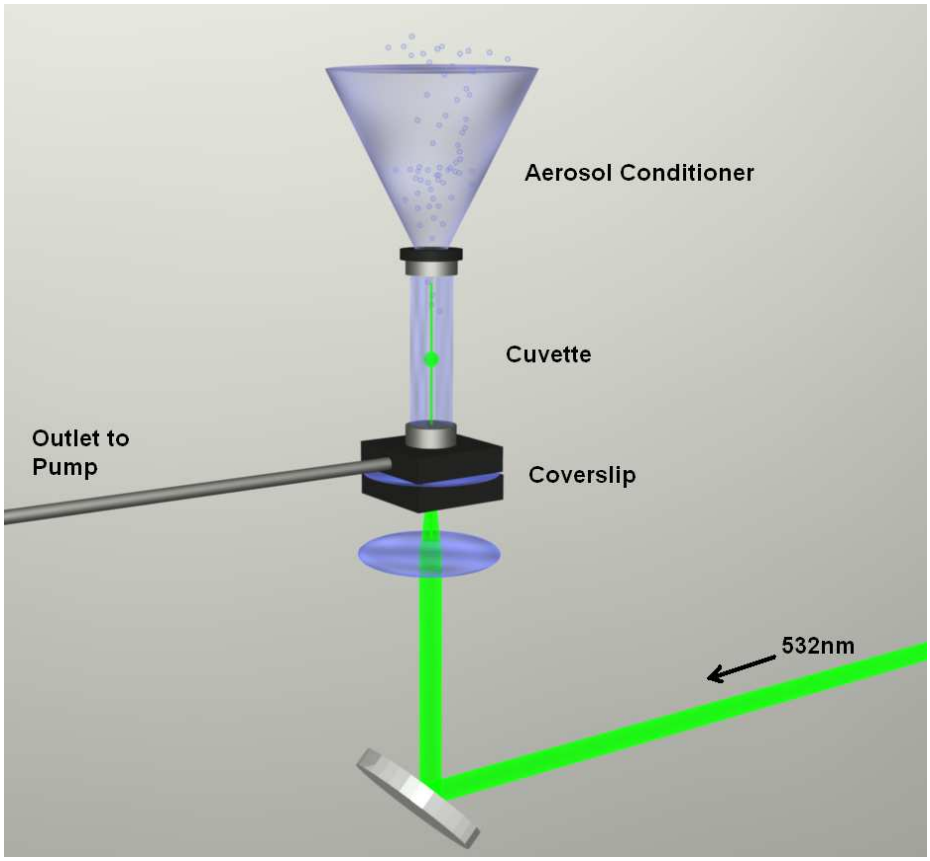

Figure 7.12: Sample cell design for the droplet guiding lab-in-a-box concept. The laser input from below the cell is generated in the same way as in Figure 6.10.

Given the additional complexity and airflow problems produced by using a pneumatic nebuliser, a new approach for the sample delivery was desirable. For this work, a new cell design was constructed (see figure 7.12), combining several of the features previously designed into sample cells. The basis of the new cell was a 5 cm long cuvette with 2 optical windows. This was the main sample chamber, where the measurements were to take place. The main chamber was placed in a rubber insert with a square section cut out which matched the shape of the bottom of the cuvette. The hole was slightly smaller than the cuvette, but the rubber could deform slightly, providing a good seal.

The rubber insert was stuck into a standard cage plate so the bottom of the cell was aligned to the optics below. This allowed the Bessel beam to travel up through the centre of the cell and eliminated much of the difficulty of aligning the droplet flow with the levitating beam. To prevent the aerosol flow from

falling through the bottom and onto the optics below, another cage plate was positioned below the cell with a microscope coverslip sandwiched between. This way, if there was a build up of sample on the bottom of the cell interfering with the beam quality, the lower plate could slide down the cage and the coverslip replaced quickly and easily.

The cage plate used to hold the bottom of the cell also contained a small tapped hole for M4 screws as part of its design. This seemed ideal for drawing the aerosol out of the bottom of the cell, just above the coverslip on the bottom and preventing the sample from pooling there. A small extraction unit was available and was connected to the cage plate hole with a long hose. The operation of the pump in the extractor could be varied via a power supply, providing a means to regulate the flow of aerosol through the cell.

With a means to generate a consistent flow through the cell, the delivery of aerosol into the top of the cell was simplified. A funnel was placed at the top of the cell, with a variable iris aperture at the bottom to restrict the flow. The funnel could be filled with aerosol from any nebuliser (an Omron Aerosonic was used) and the sample would flow through the cell at a rate determined by the pump at the other end.

This system provided a very smooth aerosol flow with no disturbance from the nebuliser. The flow rate was controllable and once aligned, the aerosol passed through the centre of the Bessel beam. The sample cell was well sealed and evaporation wasn't an issue until the reservoir of aerosol at the top was depleted, which took many minutes. Although the previous Bessel beam work was successful with the previous cell design, this experiment was much more consistent. It is hoped that Bristol can use this new design to further extend our knowledge of aerosols and the way in which these individual particles interact within the large scale systems commonly studied in atmospheric chemistry.

7.4 References

1. Ashkin, A., “Acceleration and trapping of particles by radiation pressure”, Phys. Rev. Lett. **24**, 156 (1970)

2. Symes, R. *et al*, “Cavity enhanced droplet spectroscopy: Principles, perspectives and prospects”, Phys. Chem. Chem. Phys. **6**, 474 (2004)

3. Hopkins, R.J.; Symes, R.; Sayer, R.M. and Reid, J.P., “Determination of the size and composition of multicomponent ethanol/water droplets by cavity-enhanced Raman scattering,” Chem Phys. Lett. **380**, 665 (2003)

4. Qian, S.X.; Snow, J.B.; Tzeng, H.M. and Chang R.K., “Lasing Droplets: Highlighting the Liquid-Air Interface by Laser Emission Science,” Science, **231**, 486 (1986)

5. Mason, N.J.; Drage, E.A.; Webb, S.M.; Dawes, A; McPheat, R. and Hayes, G., “The spectroscopy and chemical dynamics of microparticles explored using an ultrasonic trap,” Faraday Discuss. **137**, 367 (2008)

6. Preda, A.M.; Cristescu, C.P.; Popescu, I.M. and Toma, A.G., “The fluorescence of liquid micro spheres induced by laser irradiation,” Applied Surface Science **106**, 517 (1996)

7. Tona, M. and Kimura, M., “Polarization Effects in both Emission Spectra and Microscopic Images of Lasing Microdroplets Levitated in an Ion Trap,” J. Phys. Soc. Jpn. **71**, 425 (2002)

8. Tona, M. and Kimura, M., “Dependence of Lasing Modes of Microdroplets on Dye Concentration,” Journal J. Phys. Soc. Jpn. **72**, 1238 (2003)

9. Kauffman, J.M., "Laser dye structures and synonyms," Appl. Opt. **19**, 3431 (1980)

10. Ashkin, A., J.M. Dziedzic, J.E. Bjorkholm and S. Chu. "Observation of a Single-Beam Gradient Force Optical Trap for Dielectric Particles." Opt. Lett. **11**, 288 (1986)

11. Neuman, K.C. and Block, S.M., “Optical trapping review,” Review of Scientific Instruments **75**, 2787 (2004)

12. DMSO data at Chemspider http://www.chemspider.com/659

13. Stoughton, R.B. and Fritsch, W., “Influence of Dimethylsulfoxide (DMSO) on human percutaneous absorption,” Arch Dermatol. **90**, 512 (1964)

14. Schulz, G.; Schwider, J.; Hiller, C. and Kicker, B., "Establishing an Optical Flatness Standard," Appl. Opt. **10**, 929 (1971)

15. Hopkins, R.J. *et al*, “Determination of the size and composition of multicomponent ethanol/water droplets by enhanced raman scattering”, Chemical Physics Letters **380**, 665. (2003)

16. Chylek, P. *et al*, “Simultaneous determination of refractive index and size of spherical dielectric particles from light scattering data.” Applied Optics **22**, 2302. (1983)

17. H Tzeng, H.M., Wall, K.F., Long, M.B. and Chang, R.K., “Laser emission from individual droplets at wavelengths corresponding to morphology-dependent resonances,” Opt. Lett., **9**, 499 (1984)

18. Magome, N.; Kohira, M.I.; Hayata, E.; Mukai, S. and Yoshikawa, K., “Optical trapping of a growing water droplet in air,” J. Phys. Chem. B **107**, 3988 (2003)

Chapter 8

Conclusion

The main part of this thesis began with an overview of optical trapping and the use of optical techniques in the study of aerosols. Many of the general techniques were described in detail and a review of the state of the art was provided for the reader. Initial studies demonstrating the optical trapping of aerosol droplets were described in Chapter 4, along with characterisation studies performed on tweezed droplet samples. Some of this data was published in "Optical manipulation of airborne particles: techniques and applications" [Appendix A-3].

Chapter 5 detailed work on the optical trapping of solid aerosol particles. A practical method for solid aerosol delivery was developed and basic characterisation of the trap axial efficiency at 1064nm was obtained. The tweezing of solid silica microspheres allowed a direct comparison of tweezers dynamics air and a liquid medium to take place using a position detector based on a quadrant photodiode (QPD). This forms the basis of the paper "Trapping solid aerosols with optical tweezers: A comparison between gas and liquid phase optical traps" [Appendix A-4].

With the goal of aerosol analysis in mind, Chapter 6 moved away from optical tweezing and into optical guiding of aerosols. The first task was to reproduce one of Ashkin's early experiments involving the optical levitation of liquid droplets in air. The task was then to optimise the technique to provide a means of capturing and transporting trapped aerosol samples. Using a Bessel beam profile, mm guiding distances were achieved, as documented in the papers "Optical guiding of aerosol droplets" [Appendix A-2] and "Optical guiding of aerosols" [Appendix A-1]. This would allow one droplet to be trapped and guided through a number of optical sensors, allowing numerous scattering, imaging and spectroscopic measurements to be conducted on the same sample. This "lab-in-a-box" arrangement may be useful for our colleagues in Bristol and provide a means for calibrating the various techniques used to characterise

aerosol samples.

Chapter 7 describes some of the work conducted with Jonathan Reid's group at Bristol in designing and building the prototype resulting from the work of the previous chapter. As this work was somewhat preliminary, it has been combined with other chemistry-related experiments which were conducted at St Andrews. Droplets consisting of laser dye dissolved in ethanol were used to examine Whispering Gallery Modes in the fluorescent spectrum produced when the droplets were excited by a UV source. Due to the high degree of cavity enhancement provided by droplets, it was hoped that the droplets could be pumped above laser threshold. Although similar experiments had been conducted previously on larger droplets, lasing had not been previously observed in optically tweezed droplets. This success of this experiment was promising, but not conclusive. It is my hope that the study can be completed following a few refinements to the experimental design. Likewise, I hope that Bristol achieve some degree of success with their new aerosol analyser. Indeed, I am sure there are still a great many opportunities in the underdeveloped field of aerosol particle studies and I wish my colleagues at the University of Dundee and the University of Bristol every success in their future work in this fascinating area of applied optics.

Appendix A

Publications Arising from this Thesis

1 **Optical guiding of aerosols**
Michael D. Summers, Jonathan Reid, and David McGloin, Proc. SPIE Vol. 6326, 63261E (2006)

2 **Optical guiding of aerosol droplets**
M. D. Summers, J.P. Reid and D. McGloin, Opt. Express 14, 6373-6380 (2006)

3 **Optical manipulation of airborne particles: techniques and applications,**
D. McGloin, D. R. Burnham, M. D. Summers, D. Rudd, N. Dewar and S. Anand, *Faraday Discuss.*, (2008), DOI: 10.1039/b702153d

4 **Trapping solid aerosols with optical tweezers: A comparison between gas and liquid phase optical traps**
M. D. Summers, D. R. Burnham, and D. McGloin, Opt. Express 16, 7739-7747 (2008)

5 **Fiber based Optical Trapping of Aerosols**
D. Rudd, C. López-Mariscal, M. Summers, A. Shahvisi, J. C. Gutiérrez-Vega, D. McGloin, Opt. Express 16, 14550-14560 (2008)

Appendix B

Optical Constants of Water in the 200 nm to 200 µm Region

Hale, G.M., Querry, M.R., "Optical constants of water in the 200 nm to 200 µm wavelength region," Appl. Opt. **12**, 555 (1973)

lambda (nm)	abs (1/cm)	920.00	0.10927	1600.0	6.7200
200.00	0.069000	925.00	0.14400	1620.0	5.8200
225.00	0.027400	930.00	0.17296	1640.0	4.9800
250.00	0.016800	940.00	0.26737	1660.0	4.5400
275.00	0.010700	950.00	0.39000	1680.0	4.4900
300.00	0.0067000	960.00	0.42000	1700.0	4.4400
325.00	0.0041800	970.00	0.45000	1720.0	5.1100
350.00	0.0023300	975.00	0.45000	1740.0	6.1400
375.00	0.0011700	980.00	0.43000	1760.0	7.1400
400.00	0.0005800	990.00	0.41000	1780.0	8.1200
425.00	0.0003800	1000.0	0.36000	1800.0	8.0300
450.00	0.0002800	1020.0	0.27000	1820.0	8.9800
475.00	0.0002470	1040.0	0.16000	1840.0	10.240
500.00	0.0002500	1060.0	0.12000	1860.0	14.190
525.00	0.0003200	1080.0	0.13000	1880.0	31.080
550.00	0.0004500	1100.0	0.17000	1900.0	66.140
575.00	0.0007900	1120.0	0.52000	1920.0	114.54
600.00	0.0023000	1140.0	0.66000	1940.0	119.83
625.00	0.0028000	1160.0	0.89000	1960.0	105.79
650.00	0.0032000	1180.0	1.0400	1980.0	92.030
675.00	0.0041500	1200.0	1.0400	2000.0	69.120
700.00	0.0060000	1220.0	0.95000	2020.0	55.990
725.00	0.015900	1240.0	0.88000	2040.0	44.970
750.00	0.026000	1260.0	0.89000	2060.0	39.040
775.00	0.024000	1280.0	0.98000	2080.0	31.420
800.00	0.020000	1300.0	1.1100	2100.0	26.930
810.00	0.019858	1320.0	1.3800	2120.0	24.010
820.00	0.023907	1340.0	1.8300	2140.0	20.550
825.00	0.028000	1360.0	2.7700	2160.0	18.620
830.00	0.029069	1380.0	6.1000	2180.0	17.290
840.00	0.034707	1400.0	12.390	2200.0	16.510
850.00	0.043000	1420.0	22.120	2220.0	16.130
860.00	0.046759	1440.0	28.800	2240.0	16.550
870.00	0.051999	1460.0	28.400	2260.0	17.240
875.00	0.056000	1480.0	21.230	2280.0	19.840
880.00	0.055978	1500.0	17.590	2300.0	22.400
890.00	0.060432	1520.0	14.050	2320.0	26.810
900.00	0.068000	1540.0	11.830	2340.0	31.950
910.00	0.072913	1560.0	9.6700	2360.0	37.270
		1580.0	7.9500	2380.0	43.300

2400.0	50.060	4500.0	374.00	8600.0	453.00
2420.0	59.720	4600.0	402.00	8800.0	550.00
2440.0	66.950	4700.0	420.00	9000.0	557.00
2460.0	76.620	4800.0	393.00	9200.0	567.00
2480.0	86.140	4900.0	351.00	9400.0	579.00
2500.0	90.480	5000.0	312.00	9600.0	594.00
2520.0	102.23	5100.0	274.00	9800.0	614.00
2540.0	108.84	5200.0	244.00	10000	638.00
2560.0	115.36	5300.0	232.00	10500	792.00
2580.0	131.51	5400.0	240.00	11000	1106.0
2600.0	153.21	5500.0	265.00	11500	1552.0
2650.0	317.72	5600.0	319.00	12000	2084.0
2700.0	884.30	5700.0	448.00	12500	2604.0
2750.0	2696.1	5800.0	715.00	13000	2948.0
2800.0	5161.2	5900.0	1325.0	13500	3193.0
2850.0	8157.1	6000.0	2241.0	14000	3321.0
2900.0	11613	6100.0	2699.0	14500	3363.0
2950.0	12694	6200.0	1784.0	15000	3368.0
3000.0	11394	6300.0	1137.0	15500	3356.0
3050.0	9888.3	6400.0	881.00	16000	3314.0
3100.0	7783.1	6500.0	758.00	16500	3260.0
3150.0	5385.6	6600.0	678.00	17000	3171.0
3200.0	3628.6	6700.0	632.00	17500	3081.0
3250.0	2358.6	6800.0	604.00	18000	2974.0
3300.0	1401.3	6900.0	586.00	18500	2860.0
3350.0	979.05	7000.0	574.00	19000	2738.0
3400.0	720.72	7100.0	566.00	19500	2604.0
3450.0	480.80	7200.0	560.00	20000	2469.0
3500.0	337.50	7300.0	554.00	30000	1374.0
3600.0	179.77	7400.0	550.00	38000	1194.0
3700.0	122.27	7500.0	546.00	50000	1292.0
3800.0	112.44	7600.0	542.00	60000	1229.0
3900.0	122.44	7700.0	540.00	70000	1034.0
4000.0	144.51	7800.0	540.00	80000	859.00
4100.0	172.00	7900.0	539.00	90000	748.00
4200.0	206.00	8000.0	539.00	100000	669.00
4300.0	247.00	8200.0	538.00	200000	317.00
4400.0	294.00	8400.0	540.00		

Querry, M.R.; Wieliczka, D.M. and Segelstein, D.J., "Water (H_2O),"Handbook of Optical Constants of Solids II," 1059 (1991)

lambda (nm)	absorption (1/cm)	535	0.000676
418.6	0.000466	536.6	0.000667
421.9	0.000447	538.2	0.000677
425.2	0.000442	539.7	0.000724
428.4	0.000449	541.2	0.000696
431.7	0.000465	542.8	0.000711
434.9	0.000455	544.3	0.000709
438.2	0.000452	545.8	0.000701
441.5	0.000464	547.8	0.000737
444.7	0.000466	550.1	0.000762
448	0.000443	552.4	0.000784
450.4	0.000374	554.5	0.000798
453.5	0.000399	556.8	0.000807
455.9	0.000412	559	0.000816
458.3	0.00037	561.2	0.000828
460.6	0.00035	563.4	0.000843
463	0.000342	565.6	0.00086
465.4	0.000337	567.7	0.000879
468.3	0.000376	570	0.000892
470.7	0.000375	580.3	0.001072
473	0.000392	582.5	0.001126
475	0.000359	584.6	0.001209
477.3	0.000371	586.8	0.001311
479.6	0.000372	588.3	0.001422
481.8	0.00037	591	0.00155
484.2	0.000366	593.2	0.001686
486.6	0.000367	595.4	0.001852
489	0.000366	597.5	0.002074
491.4	0.000367	599.7	0.002361
493.8	0.000373	601.9	0.002628
495.7	0.000413	604	0.002787
497.9	0.000437	606.2	0.002854
500.3	0.000452	609.1	0.002902
502.5	0.00048	611.2	0.002929
504.8	0.000481	613.3	0.002949
507.2	0.000519	615.5	0.002975
509.5	0.000544	617.6	0.003
511.8	0.000587	619.7	0.003018
514.2	0.000599	621.8	0.003041
516.6	0.000649	623.9	0.003067
518.9	0.000643	626.1	0.003101
521.2	0.000646	628.2	0.00313
523.6	0.000652	630.3	0.003154
525.9	0.000621	632.4	0.003191
528.2	0.000632	634.5	0.003215
530.4	0.000636	636.7	0.003254
532.8	0.000647	638.9	0.003274
		640.3	0.003302